Supplementary Information (SI) for Catalysis Science & Technology.

Supporting Information

Automation Accelerated screening of H-Bond Rich Iridium Photosensitisers for Hydrogen Generation

T. Harri Jones,[a] Christopher F. Bradshaw John W. Ward*[b] and Barry A. Blight*[a]

[a]University of New Brunswick, Department of Chemistry,
Fredericton, New Brunswick, Canada, E3B 5A3
[b]University of Liverpool, Department of Chemistry and Materials Innovation Factory,
Liverpool, U.K, L69 7ZD

Table of Contents

SI. Materials and Techniques

Materials. All starting materials were purchased from commercial sources (Sigma Aldrich, Fisher Scientific and TCI) and used without further purification. Analytical thin layer chromatography (TLC) was carried out on precoated TLC plates Alugram Sil G/ UV254. Column chromatography purifications were done with silica gel (ultrapure, 60-200 µm (60 Å)). Experiments were performed as follows:

(i) A conventional hotplate (IKA™ RCT Basic magnetic hot plate stirrer (Stirring range: 50 to 1500 rpm; Size: 5.3 in. dia; Supplier: IKA™ 3810001) – fume hood), under a dry N_2 atmosphere using standard Schlenk Line techniques when specified.

(ii) Microwave reactor – Anton Paar-Monowave 400 (max. temp. 300°C, power 850 W and pressure of 30 bar) with 10- and 30-mL borosilicate glass vials with a cap material of PEEK. The seal material is made from Teflon-coated silicone. Supplier: Anton Paar.

Nuclear Magnetic Resonance (NMR). ^1H (400 MHz) and ^{13}C (101 MHz) NMR spectra were recorded on an Agilent 400 NMR spectrometer in deuterated solvents, namely chloroform-*d* ($CDCl_3$) and dimethyl sulfoxide-d_6 (DMSO-d_6), which were purchased from Fisher Scientific. All chemical shifts are reported in δ (ppm) referenced to tetramethylsilane ($Si(CH_3)_4$) and the peak multiplicities are referred to as singlet (s), doublet (d), triplet(t), quartet (q), multiplet (m). Spin-spin coupling effect is quantify with the coupling constants, which is abbreviated with the capital letter J.

Mass Spectrometry. High-resolution mass spectral data measurements were performed by Xiao Feng at the Mass Spectrometry Laboratory (Dalhousie University, Halifax, Canada). High-resolution mass spectra were recorded on Bruker Daltonics MicrOTOF instrument. The ionization method used for low/high-resolution analysis was positive electrospray ionization (ESI+). The sample was introduced by a syringe pump at a flow rate of 2 μL/min and the spray voltage applied to the ESI needle was 4.5 kV. The dry gas flow rate was 4 L/min with a pressure of 1 Bar and a temperature of 180°C. For the analysis, samples sizes were between 1-2.5 mg and the experiment was replicated 2-3 times to ensure the viability of the results (sample sizes of 5-7 mg were sent).

UV-Vis Spectroscopy. UV-Vis spectra for the cyclometalated Ir(III) complexes **1**-**5** were recorded with a Cary Series UV-Vis Spectrophotometer (Agilent Technologies). Chloroform – HPLC grade (C606-1, LOT 214513) was used as the blank solution and the solvent to prepare the solutions of the several Ir(III) complexes **1**-**5**. Two standard Q macro cuvettes with an optical path length of 10 millimetres which are made of fused quartz glass were used to measure the absorbance of these compounds. UV-Vis spectra were collected with a concentration of the cyclometalated Ir(III) complexes **1-5** of 1.10^{-4} M.

Photoluminescence Emission Spectroscopy. Emission and excitation spectra, PLQY, and decay lifetime measurements were recorded with a FS5 Spectrofluorometer (Edinburgh Instruments).

- Excitation and emission spectra for the cyclometalated Ir(III) complexes **1-5** were recorded with a FS5 Spectrofluorometer (Edinburgh Instruments) and a SC-05 (Standard Cuvette Holder) at 298 K. A Hellma Fluorescence Cuvette (Suprasil 6 Quartz, spectral range 200-2,500 nm, pathlength 10x4 mm and chamber volume 3,500 μL) was used to measure the excitation and emission spectra of **1-5**. The sample solutions were prepared in chloroform – HPLC grade (C606-1, LOT 214513), which was used as a blank solution and the solvent to prepare the solutions of **1-5** (concentrations specified in **Table S1**).

- Measurements of the quantum yield were carried out with use of an FS5 SC-30 integrating sphere module and a Xenon lamp at 298 K in argon degassed $CHCl_3$. Excitation wavelengths will be specified with figures as compounds have significant variation in excitation.

$$PLQY = \frac{\#\ emitted\ photons}{\#\ absorbed\ photons}$$

Number of absorbed photons was inferred by comparing the difference in the excitation light scattering of the blank and the sample (Ex_{blank} and Ex_{sample}) – whereas the number of emitted photons can be inferred by comparing the difference between the sample and the blank (Em_{sample} and Em_{blank})

$$PLQY = \frac{Em_{sample} - Em_{blank}}{Ex_{blank} - Ex_{sample}}$$

- Decay lifetime measurements were recorded with a FS5 Spectrofluorometer (Edinburgh Instruments) and a SC-05 (Standard Cuvette Holder). All solutions of **1-5** were prepared to a concentration of ~$1\cdot10^{-5}$ M using chloroform – HPLC grade (C606-1, LOT 214513) that was degassed in a cuvette for 20 minutes (Ar) before each measurement at 298 K.

A QF2001 – 10 mm Lightpath Spectrophotometer Screw Cap Cuvette (Threaded – Quartz 3.5 mL) was used to measure the excitation spectra of each Ir(III) complexes (**1-5**). The excited state lifetimes were measured by the time correlated single photon counting spectra (TCSPC) technique using an EPLED-365 (Edinburgh Instruments) laser with emission detection at 520 nm for all complexes. Each lifetime measurement was calculated through an Exponential Fit Time Scan that follows the formula:

$$\text{Fit: } B_1 e^{(-t/\tau_1)} + B_2 e^{(-t/\tau_2)} + B_3 e^{(-t/\tau_3)} + B_4 e^{(-t/\tau_4)}$$

A chi-squared (χ^2) of values between 1-1.3 were found suitable. These complexes showed either monoexponential decay or biexponential decay.

Hydrogen Evolution Studies. The accelerated screening hydrogen studies were conducted Chemspeed Technologies Sweigher platform, operating with a constant N_2 purge at the University of Liverpool. Samples were prepped in vials and thoroughly degassed with N_2. From here vials were moved to the Chemspeed platform to perform a further degas and cap operation. From the degas and cap, sample vials were transferred to an Oriel Solar Simulator 94123A (IEC/JIS/ASTM, 1600 W Xenon) for high energy photo-irradiation rated at 1.0 sun. After a reaction specific amount of time (between 0-5 hours) samples were removed and placed on the carousel of a Shimadzu GC-2010 Plus GC with HS-20 Headspace Sampler. From here an aliquot of the gasses in the vials were taken up and relative volumes of the gasses calculated from the data.

Cyclic Voltammetry. CV was carried out in an argon filled glovebox using a potentiostat/galvanostat (BioLogic SP-150) with a cell consisting of a working electrode (platinum disk, 0.07 cm^2), counter electrode (platinum wire, 5 cm) and Ag/Ag$^+$ reference electrode (0.01M $AgNO_3$ in 0.1 M NBu_4PF_6 in anhydrous chloroform). All E_{ox} and E_{red} values were referenced to a ferrocene standard. The electrode was washed thoroughly with the electrolyte solution before each sample run. Each sample concentration was measured to be 2mM.

DFT methodology. DFT calculations were performed using the Gaussian16 revision c.01 [2] software package provided by the University of Waterloo (University of Waterloo) through the Digital Research Alliance of Canada (alliancecan.ca). The ground state geometries were optimised at the B3LYP [3] level using LANL2DZ [4] basis set for iridium and the 6-31G** basis set for all other atoms. [4] The energy minima were confirmed using frequency analysis and the absence of any imaginary frequencies. The butyl chains on the ‘guanidine’ ligand were truncated to methyl groups to reduce disorder and computational costs. Time-dependant DFT (TD-DFT) was also undertaken to calculate the singlet and triplet excited energetic states. All relevant orbital and geometries are given in section S8.

All initial input structures were created using and optimised Avogadro2 1.91.0 [5]

Orbital plots were generated using Avogadro2 1.91.0 [5]

UV-vis plots were generated using GaussSum 3.0.2 [6]

SII. Synthetic Routes of Ir(III) complexes 1-5

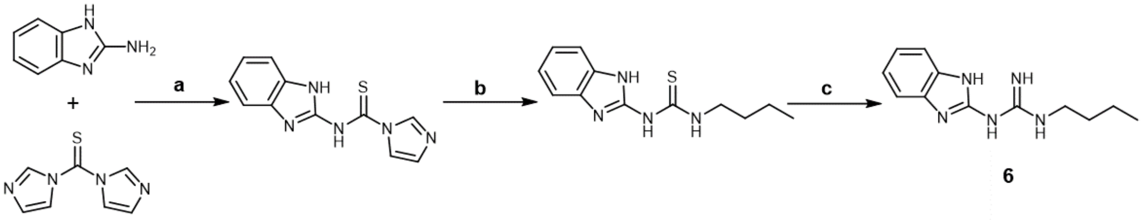

Scheme S1. General procedure for the synthesis of the 1-(1H-benzo[d]imidazole-2-yl)-3-butylguanidine ligand (**6**) is as follows. Reagents and conditions: a) MeCN, 50°C, 20 hours; b) *n*-butyl amine, catalytic DMAP, DMF, 100°C, 18 hours; c) HgO, (NH_3/MeOH (2M)), $CHCl_3$, room temperature, 3 hours. [7]

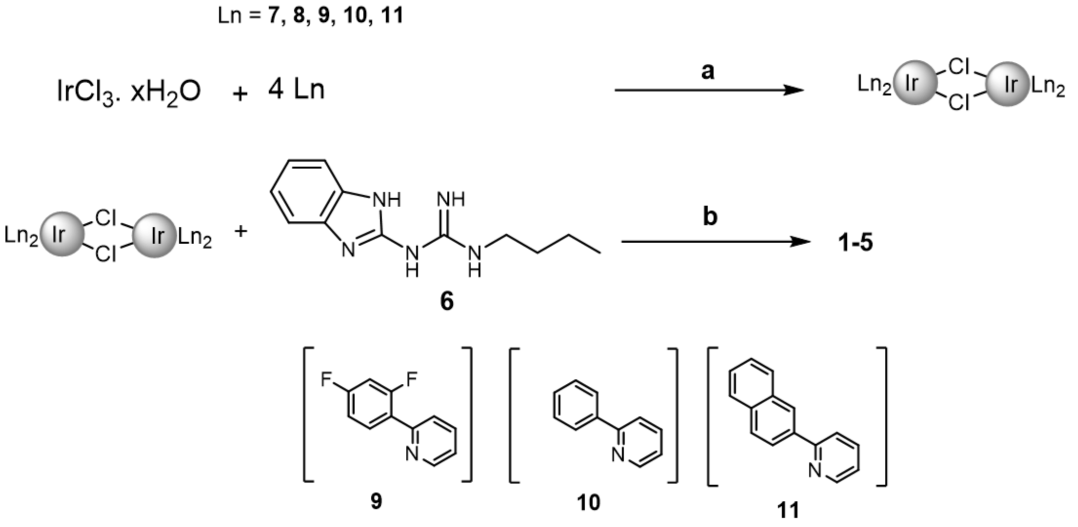

Scheme S2. The general synthetic route of all iridium complexes herein. Reagents and conditions: a) 2- ethoxyethanol: water (3:1), 130°C, 19 hours; b) K_2CO_3, toluene, N_2, 110°C, 16 hours. Ligands 9-11 were all synthesised using previously established procedures in the literature.[8]

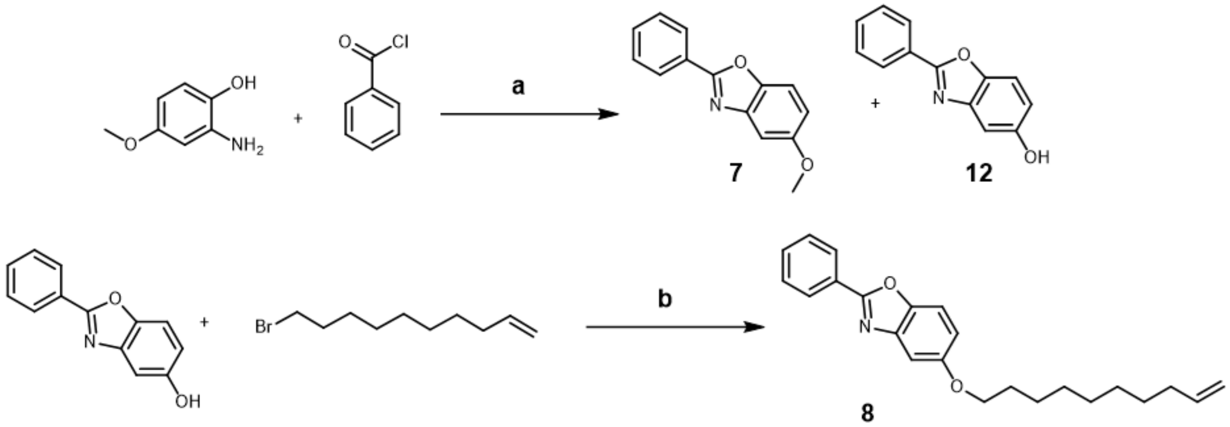

Scheme S3. The routes for the preparation of the ligands **7** and **8**. Reagents and conditions: a) NMP, pyridine, N_2, 202°C, 5 hours; b) MeCN, K_2CO_3, N_2, 90°C, 12 hours.

Iridium dimers

All iridium μ-chloro bridged dimers were synthesized following Nonoyama's procedure.[] Iridium chloride hydrate (1 equivalent) and 2 equivalents of appropriate ligand were added into a mixture of 2-ethoxyethanol: water (3:1) and refluxed for 19-24 hours under nitrogen atmosphere. After cooling to room temperature, a precipitate was formed and filtered off. The solid was washed with water (5 mL), ethanol (5 mL) and acetone (5 mL) and dried on Schlenk line for 48 hours.

SIII. Synthetic Procedures

Iridium complex 1 – procedure following previous protocol established in the group.[8] Combine $[Ir(dFppy)_2Cl]_2$ chloro-briged dimer (100 mg, 0.082 mmol, 1.0 eq) with 2 equivalents of ligand **6** (38 mg, 0.164 mmol) and 10 equivalents of potassium carbonate (72 mg, 0.822 mmol), then add to 10 mL of dry degassed toluene and reflux under nitrogen atmosphere for 16 hours. Next the reaction was cooled to room temperature and solvent was removed under reduced pressure. The solid was then redissolved in DCM and extracted with water, the organic phase was dried again and was then purified by silica gel column chromatography (DCM: MeOH, 10: 0.5). Product **1** was obtained in 80% yield (132 mg).

^{1}H NMR (400 MHz, $CDCl_3$, 298 K) δ 8.64 (dd, *J* = 5.9, 0.9 Hz, 1H), 8.30 (d, *J* = 8.4 Hz, 1H), 8.21 (d, *J* = 8.4 Hz, 1H), 8.09 (d, *J* = 5.8 Hz, 1H), 7.80 (td, *J* = 7.6, 1.7 Hz, 1H), 7.73 (td, *J* = 7.7, 1.8 Hz, 1H), 7.22 (d, *J* = 7.9 Hz, 1H), 7.13 (ddd, *J* = 7.4, 5.8, 1.4 Hz, 1H), 7.02 (q, *J* = 7.3 Hz, 2H), 6.76 (t, *J* = 7.8 Hz, 1H), 6.47 (dddd, *J* = 15.0, 12.5, 9.1, 2.4 Hz, 2H), 6.19 (d, *J* = 8.3 Hz, 1H), 5.84 (dd, *J* = 8.6, 2.4 Hz, 1H), 5.61 (dd, *J* = 8.5, 2.4 Hz, 1H), 4.85 (s, 2H), 4.45 (s, 1H), 3.08 – 2.91 (m, 2H), 1.47 – 1.39 (m, 2H), 1.25 (h, *J* = 7.6 Hz, 2H), 0.81 (t, *J* = 7.4 Hz, 3H). ^{13}C NMR (101 MHz, $CDCl_3$) δ 165.64, 164.68, 156.93, 156.10, 154.45, 151.24, 149.91, 148.80, 145.86, 140.20, 138.13, 138.04, 128.64, 128.22, 123.29, 123.07, 122.74, 122.33, 120.57, 116.57, 114.90, 114.76, 114.19, 113.99, 111.13, 98.47, 98.22, 97.83, 41.07, 30.70, 20.07, 13.75. HMRS [ESI+] ion $[C_{34}H_{29}F_4IrN_7]^+$ m/z calculated: 804.2044 Found: 804.2034 [M+].

Iridium complex 2 – procedure following previous protocol established in the group.[7] Iridium chloro-bridged dimer $[Ir(ppy)_2Cl]_2$ made from ligand **10** (500 mg, 0.684 mmol) was combined with ligand **6** (316 mg, 1.368 mmol) and 10 equivalents of K_2CO_3 (945 mg, 6.841 mmol), the mixture then had 20 mL of dry toluene added and was heated to reflux under nitrogen. After 16 hours, the reaction was cooled to r.t, toluene was removed under reduced pressure and the crude was extracted between DCM and water. DCM was removed under reduced pressure and the product was columned between DCM and methanol (1:99). 850 mg of the final product was obtained, an 85% yield.

^{1}H NMR (400 MHz, $CDCl_3$, 298 K) δ 11.87 (s, 1H), 11.14 (s, 1H), 8.66 (dd, *J* = 5.8, 0.8 Hz, 1H), 8.09 (dd, *J* = 5.8, 0.8 Hz, 1H), 7.89 (d, *J* = 7.9 Hz, 1H), 7.82 – 7.71 (m, 2H), 7.68 (td, *J* = 7.8, 1.6 Hz, 1H), 7.60 (dd, *J* = 7.8, 1.3 Hz, 2H), 7.23 (d, *J* = 7.8 Hz, 1H), 7.11 (ddd, *J* = 7.4, 5.8, 1.4 Hz, 1H), 7.05 – 6.88 (m, 5H), 6.82 (td, *J* = 7.4, 1.4 Hz, 2H), 6.77 (td, *J* = 7.4, 1.4 Hz, 1H), 6.68 (ddd, *J* = 8.5, 7.4, 1.3 Hz, 1H), 6.45 – 6.36 (m, 2H), 6.21 (dd, *J* = 7.6, 1.4 Hz, 1H), 6.10 (d, *J* = 8.3 Hz, 1H), 4.60 (s, 1H), 3.03 – 2.83 (m, 2H), 1.44 (pd, *J* = 7.4, 3.1 Hz, 2H), 1.22 (dq, *J* = 14.9, 7.4 Hz, 2H), 0.79 (t, *J* = 7.3 Hz, 3H). ^{13}C NMR (101 MHz, $CDCl_3$) δ 169.08, 168.11, 152.35, 150.43, 150.20, 149.89, 148.73, 145.03, 144.61, 144.35, 140.19, 137.15, 137.04, 133.02, 132.01, 131.43, 129.90, 124.65, 124.15, 122.81, 122.72, 122.32, 122.08, 121.92, 121.42, 118.97, 117.42, 110.64, 41.01, 30.68, 20.04, 13.78. HMRS [ESI+] ion $[C_{34}H_{33}IrN_7]^+$ m/z calculated: 732.2421 Found: 732.2434 [M+].

Iridium complex 3 – procedure following previous protocol established in the group.[8] Iridium chloro-bridged dimer made from ligand **11** (120 mg, 0.094 mmol) was combined with ligand **6** (44 mg, 0.189 mmol) and 10 equivalents of potassium carbonate (125 mg, 0.943 mmol), this was added to 10 mL of dry toluene and refluxed under nitrogen atmosphere for 16 hours. After the reaction was completed, it was cooled to room temperature and solvent was removed under reduced pressure. The solid was re-dissolved in dichloromethane and extracted with water, combined organic phases were then purified through column chromatography (DCM: MeOH, 10:0.5). The product was dried in vacuo (Schlenk line) for 48 h. The final product **3** was obtained as a dark yellow powder in 70 % yield (110 mg).

^{1}H NMR (400 MHz, CDCl$_3$, 298 K) δ 11.84 (s, 1H), 11.29 (s, 1H), 8.79 (d, *J* = 5.9 Hz, 1H), 8.26 (d, *J* = 5.9 Hz, 1H), 8.15 (d, *J* = 4.0 Hz, 2H), 8.13 – 8.06 (m, 3H), 7.89 (t, *J* = 7.8 Hz, 1H), 7.82 (t, *J* = 7.8 Hz, 1H), 7.70 (t, *J* = 6.8 Hz, 2H), 7.21 (t, *J* = 7.3 Hz, 7H), 7.13 (t, *J* = 6.6 Hz, 2H), 6.93 (t, *J* = 7.8 Hz, 1H), 6.73 (s, 1H), 6.52 (s, 1H), 6.47 (t, *J* = 7.9 Hz, 1H), 6.41 (s, 1H), 6.15 (d, *J* = 8.4 Hz, 1H), 4.69 (s, 1H), 2.86 (ddd, *J* = 50.9, 12.9, 6.3 Hz, 3H), 1.46 – 1.36 (m, 2H), 1.17 (q, *J* = 7.7 Hz, 2H), 0.75 (t, *J* = 7.3 Hz, 3H). ^{13}C NMR (101 MHz, CD$_2$Cl$_2$) δ 168.31, 167.33, 150.59, 150.20, 149.05, 145.53, 145.44, 145.07, 144.57, 144.09, 143.78, 140.46, 137.16, 137.00, 135.25, 131.45, 131.32, 130.20, 129.91, 129.75, 129.00, 128.93, 128.78, 126.74, 126.66, 125.96, 124.17, 123.63, 123.55, 123.14, 123.01, 122.70, 122.35, 119.85, 117.41, 110.66, 41.05, 30.63, 20.00, 13.77. HMRS [ESI+] ion $[C_{42}H_{37}IrN_7]^+$ m/z calculated: 832.2732. Found: 832.2734 [M+].

Iridium complex 4 – Iridium chloro-bridged dimer made from ligand **7** (200 mg, 0.148 mmol) was combined with ligand **6** (68.4 mg, 0.296 mmol) and 10 equivalents of potassium carbonate (205 mg, 1.48 mmol). This solid mixture was degassed and, 15 mL of dry toluene was added, this solution was then refluxed at 110°C for 16 hours. The mixture was then cooled to room temperature, solvent was removed under reduced pressure and the crude was redissolved in DCM, then extracted with water. The combined organic phases were then purified through column chromatography (DCM: MeOH, 99:1). The final product was a dark yellow powder 63 % yield (162 mg).

^{1}H NMR (400 MHz, $CDCl_3$) δ 12.04 (br, 1H), δ 11.44 (br, 1H), δ 7.74 – 7.67 (m, 2H), 7.50 (dd, *J* = 8.9, 1.3 Hz, 2H), 7.23 (d, *J* = 7.6 Hz, 1H), 7.05 – 6.97 (m, 5H), 6.93 – 6.84 (m, 3H), 6.73 (ddd, *J* = 8.5, 7.4, 1.3 Hz, 1H), 6.67 (d, *J* = 7.5 Hz, 1H), 6.53 (d, *J* = 7.4 Hz, 2H), 6.26 (d, *J* = 8.4 Hz, 1H), 5.70 (d, *J* = 2.5 Hz, 1H), 4.76 (s, 1H), 3.84 (s, 3H), 3.13 – 2.93 (m, 2H), 2.85 (s, 3H), 1.60 – 1.48 (m, 2H), 1.37 – 1.26 (m, 3H), 0.84 (t, *J* = 7.4 Hz, 3H). ^{13}C NMR (101 MHz, $CDCl_3$) δ 178.86, 177.88, 158.59, 151.02, 150.89, 148.64, 145.55, 144.77, 144.54, 141.60, 139.64, 139.00, 134.18, 133.43, 132.08, 131.29, 130.23, 130.15, 126.44, 125.78, 123.01, 122.56, 122.43, 121.89, 118.19, 115.14, 113.10, 112.19, 110.67, 99.70, 98.02, 55.99, 54. 73, 41.24, 30.76, 20.16, 13.73. HMRS [ESI+] ion $[C_{40}H_{37}IrN_7O_4]^+$ m/z calculated: 872.2546 Found: 872.2546 [M+].

Iridium complex 5 – Iridium chloro-bridged dimer made from ligand **8** (250 mg, 0.135 mmol), ligand **6** (31.3 mg, 0.270 mmol) and 10 equivalents of potassium carbonate (187 mg, 1.35 mmol) was degassed and dissolved in dry toluene (15 mL). The mixture was refluxed for 16 hours at 110°C, after this it was cooled, the solvent was removed under reduced pressure and the crude was redissolved in DCM before being extracted with water. The combined organic phases were then purified by column chromatography (DCM), the final product was a orange-yellow solid (50 %, 151 mg).

^{1}H NMR (400 MHz, $CDCl_3$, 298K) δ 7.70 (dd, *J* = 6.4, 4.5 Hz, 2H), 7.48 (dd, *J* = 9.3, 2.4 Hz, 2H), 7.20 (d, *J* = 7.6 Hz, 1H), 7.04 – 6.94 (m, 5H), 6.93 – 6.82 (m, 3H), 6.73 – 6.64 (m, 2H), 6.53 (d, *J* = 7.5 Hz, 1H), 6.21 (d, *J* = 8.3 Hz, 1H), 6.16 (s, 1H), 5.70 (s, 1H), 5.51 – 5.28 (m, 4H), 4.70 (s, 1H), 3.95 (dd, *J* = 36.6, 6.8 Hz, 2H), 3.10 – 2.90 (m, 2H), 2.57 – 2.46 (m, 2H), 1.98 (m, 7H), 1.32 (dd, *J* = 30.3, 21.4 Hz, 21H), 0.93 – 0.79 (m, 7H). ^{13}C

NMR (101 MHz, $CDCl_3$) δ 178.80, 177.77, 158.07, 144.66, 144.38, 141.99, 139.70, 139.05, 134.28, 133.45, 131.89, 130.29, 126.35, 125.63, 124.78, 122.23, 122.09, 121.68, 119.74, 117.92, 115.38, 113.47, 112.00, 110.42, 105.88, 100.37, 98.62, 91.62, 68.76, 67.51, 62.02, 52.93, 48.93, 41.26, 34.85, 32.62, 31.91, 31.52, 30.92, 29.39, 29.13, 25.74, 22.88, 22.35, 20.22, 18.07, 14.11, 13.79. HMRS [ESI+] ion $[C_{58}H_{69}IrN_7O_4]^+$ m/z calculated: 1120.5036 Found: 1120.5036 [M+].

Ligand 7 – 2-Amino-4-methoxyphenol (5.00 g, 35.9 mmol) was dissolved in the minimum amount of degassed, dry NMP (40 mL) and cooled to 0°C. The cooled mixture then had dropwise additions of benzoyl chloride (4.17 ml, 35.9 mmol) over 30 minutes before being allowed to warm to room temperature over an hour. Next 12 ml of pyridine was added, and the mixture was heated to reflux at 202°C under nitrogen. After 5 hours, the mixture was cooled to room temperature and extracted between DCM (6x30mL) and water 50 mL. Combined organic phases were dried over $MgSO_4$, filtered then dry loaded onto silica for purification by column chromatography (gradient, Hexanes:EtOAc, 95:5 → 80:20). The column yields two products ligand **7** 35% %, 2.83 g (crystalline white solid) and compound **12** 37 %, 2.81 g (an off-white powder).

^1H NMR (400 MHz, $CDCl_3$, 298 K) δ 8.22 (dd, *J* = 6.9, 2.9 Hz, 2H), 7.51 (dd, *J* = 5.2, 1.8 Hz, 3H), 7.45 (d, *J* = 8.9 Hz, 1H), 7.25 (s, 1H), 6.95 (s, 1H), 3.86 (s, 3H). ^{13}C NMR (101 MHz, $CDCl_3$) δ 163.84, 157.43, 145.44, 142.92, 133.68, 131.44, 130.20, 128.92, 127.52, 127.27, 113.76, 110.74, 102.91, 55.97. HMRS [ESI+] ion $[C_{14}H_{11}NO_2Na]^+$ m/z calculated: 248.0688 Found: 248.0682 [M+].

Ligand 8 – 647 mg, 3.06 mmol of compound **12** [2-Phenyl-5-benzoxazolol] was added to a 50 mL Schlenk flask with 1 eq. of 10-bromodecene (0.63 ml, 3.06 mmol) and 5 eq. potassium carbonate (2g, 6.12 mmol). The flask was degassed, then 15 mL of dry acetonitrile was added, and the mixture was refluxed at 90°C under nitrogen. After 12 hours the solvent was removed under reduced pressure, the mixture was redissolved in DCM (20 mL), extracted with water and dried over $MgSO_4$. The product was then purified by column chromatography, (EtOAc:Hexanes, 5:95). The final pure product is a very pale-yellow oil and was acquired as a 75 % yield (800 mg).

^1H NMR (400 MHz, $CDCl_3$, 298 K) δ 8.23 (dd, *J* = 6.8, 3.0 Hz, 2H), 7.54 – 7.49 (m, 3H), 7.45 (d, *J* = 8.8 Hz, 1H), 7.25 (d, *J* = 2.4 Hz, 1H), 6.95 (dd, *J* = 8.9, 2.5 Hz, 1H), 5.82 (ddt, *J* = 16.9, 10.2, 6.7 Hz, 1H), 5.05 – 4.89 (m, 2H), 4.01 (t, *J* = 6.6 Hz, 2H), 2.05 (qt, *J* = 6.7, 1.5 Hz, 2H), 1.82 (dq, *J* = 8.0, 6.6 Hz, 2H), 1.55 – 1.25 (m, 11H). ^{13}C NMR (101 MHz, $CDCl_3$) δ 163.73, 156.91, 145.35, 142.93, 139.21, 131.37, 128.90, 127.49, 127.35, 114.32, 114.17, 110.66, 103.69, 68.87, 33.81, 29.43, 29.38, 29.28, 29.08, 28.93, 26.08. HMRS [ESI+] ion $[C_{23}H_{28}NO_2]^+$ m/z calculated: 350.2115 Found: 350.2115 [M+].

SIV. ^{1}H and ^{13}C NMR Spectra, Mass Spectra

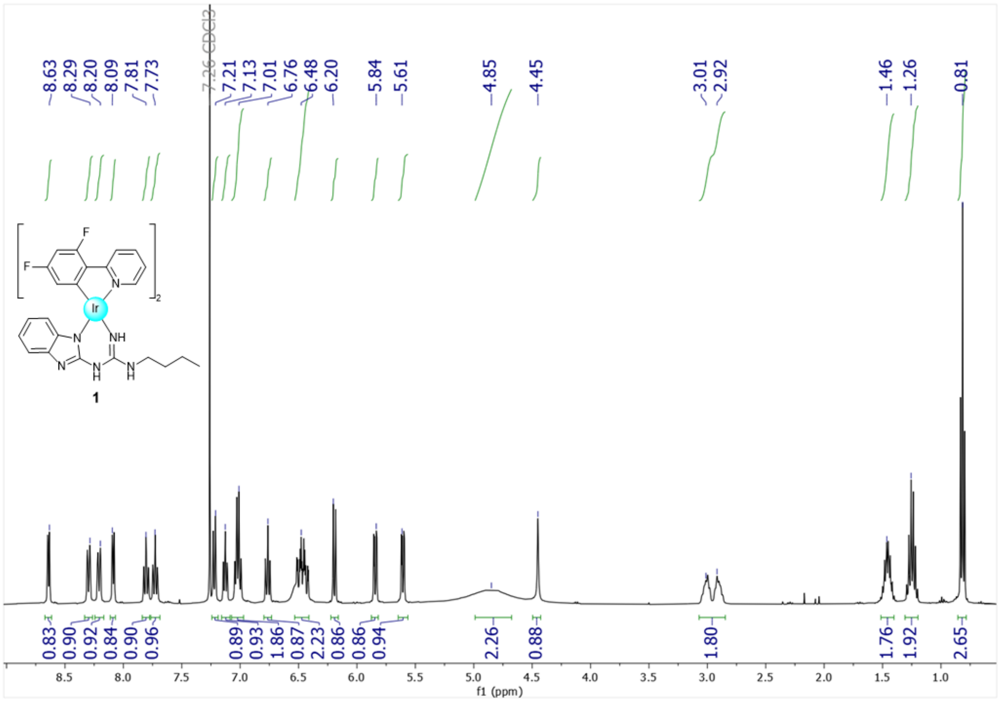

Figure S1. ^{1}H NMR spectrum of iridium complex **1**, $CDCl_3$, 400 MHz, 298 K.

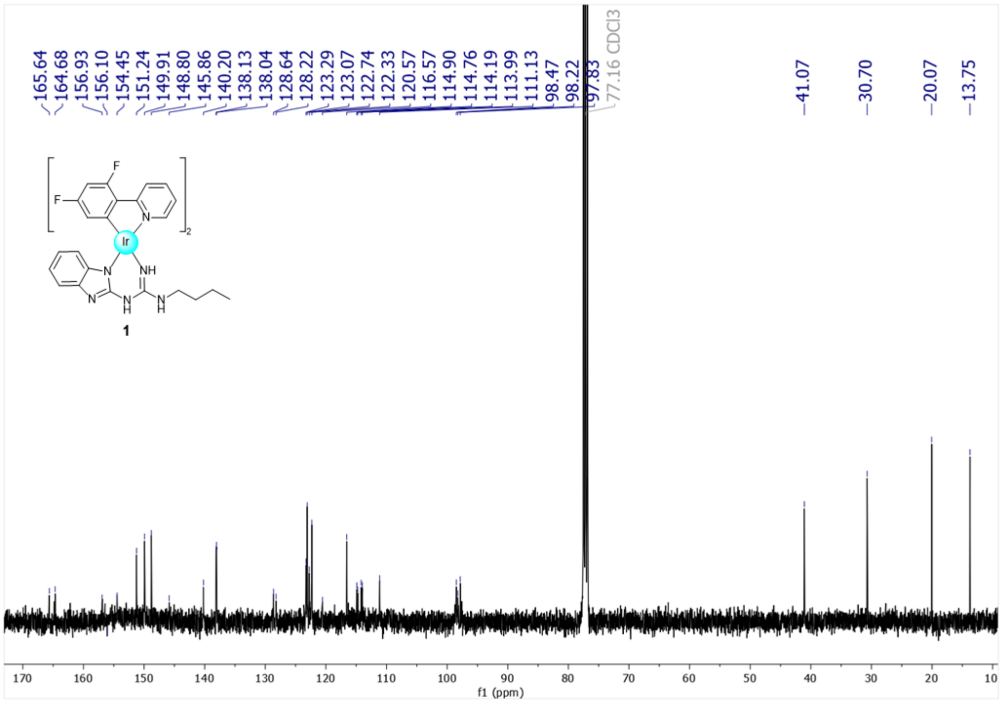

Figure S2. ^{13}C NMR spectrum of iridium complex **1,** $CDCl_3$, 101 MHz, 298 K.

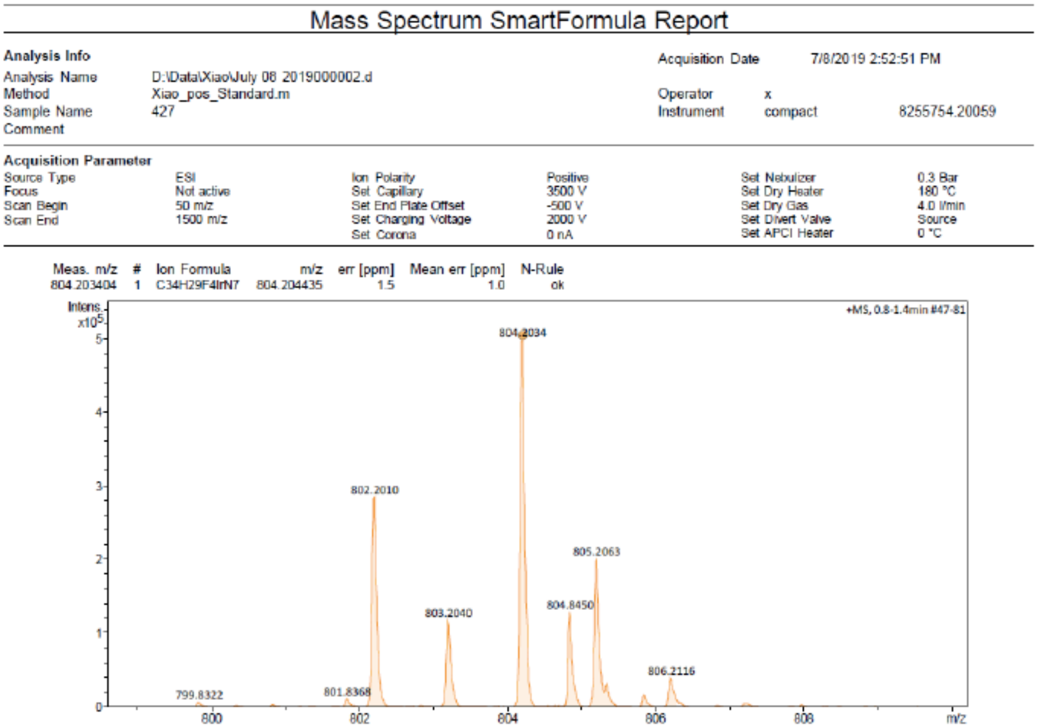

Mass Spectrum SmartFormula Report

Analysis Info

Analysis Name	D:\Data\Xiao\July 08 2019000002.d	Acquisition Date	7/8/2019 2:52:51 PM	
Method	Xiao_pos_Standard.m	Operator	x	
Sample Name	427	Instrument	compact	8255754.20059
Comment				

Acquisition Parameter

Source Type	ESI	Ion Polarity	Positive	Set Nebulizer	0.3 Bar
Focus	Not active	Set Capillary	3500 V	Set Dry Heater	180 °C
Scan Begin	50 m/z	Set End Plate Offset	-500 V	Set Dry Gas	4.0 l/min
Scan End	1500 m/z	Set Charging Voltage	2000 V	Set Divert Valve	Source
		Set Corona	0 nA	Set APCI Heater	0 °C

Meas. m/z	#	Ion Formula	m/z	err [ppm]	Mean err [ppm]	N-Rule
804.203404	1	C34H29F4IrN7	804.204435	1.5	1.0	ok

Figure S3. Mass spectrum of iridium complex **1**. HMRS [ESI+] ion $[C_{34}H_{29}F_4IrN_7]^+$ m/z calculated: 804.2044 Found: 804.2034 [M+].

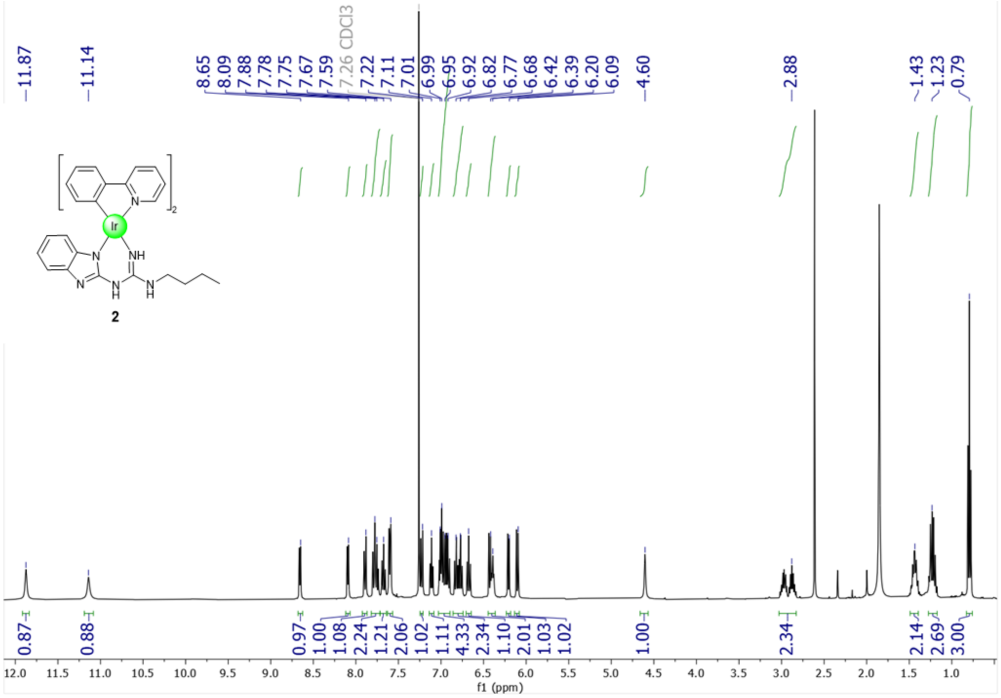

Figure S4. ^{1}H NMR spectrum of iridium complex **2**, $CDCl_3$, 400 MHz, 298 K.

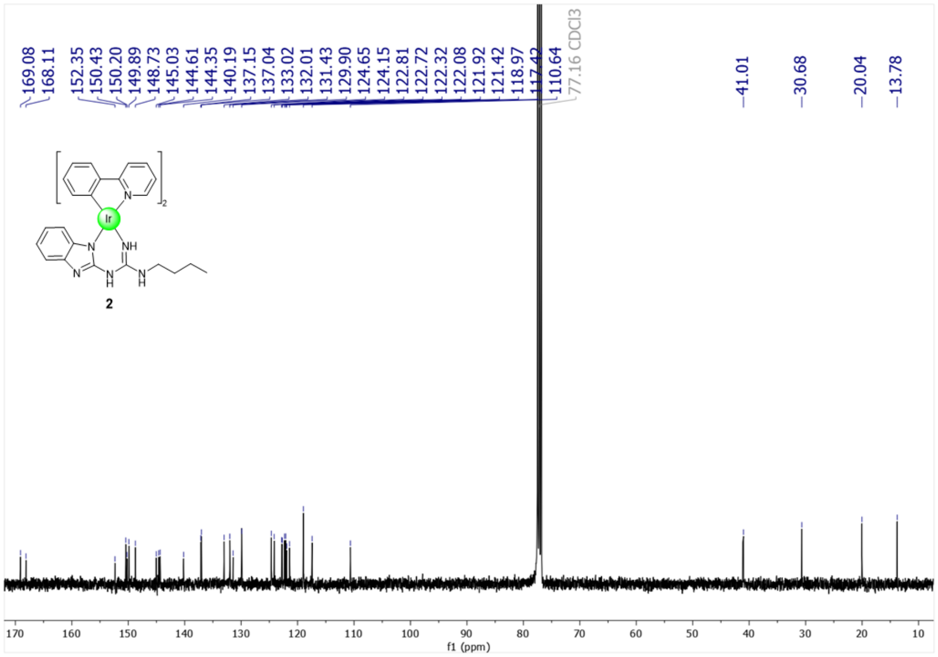

Figure S5. ^{13}C NMR spectrum of iridium complex **2,** $CDCl_3$, 101 MHz, 298 K.

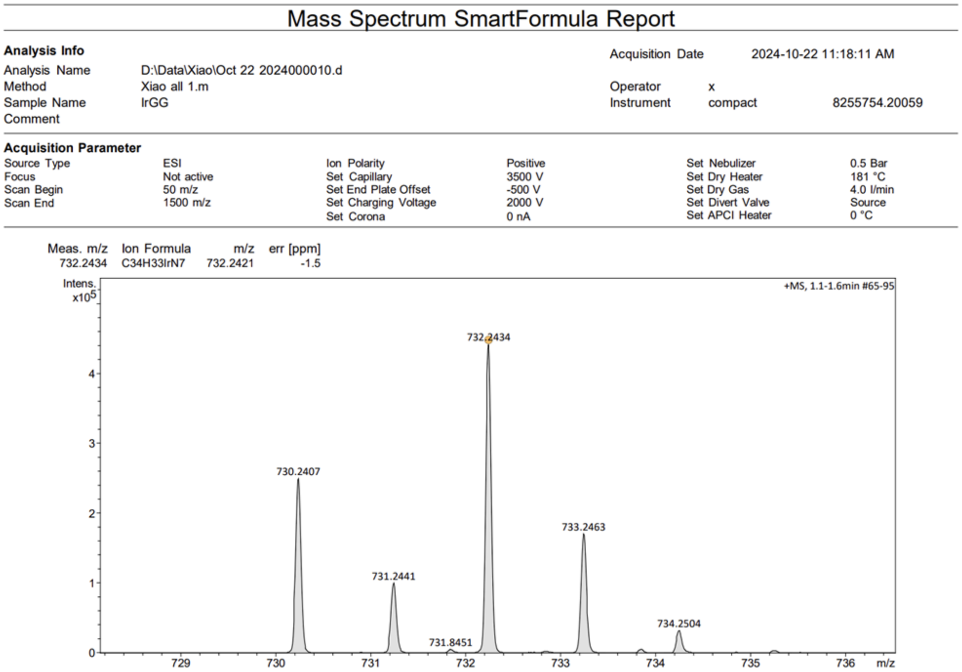

Mass Spectrum SmartFormula Report

Analysis Info

Analysis Name	D:\Data\Xiao\Oct 22 2024000010.d	Acquisition Date	2024-10-22 11:18:11 AM
Method	Xiao all 1.m	Operator	x
Sample Name	IrGG	Instrument	compact 8255754.20059
Comment			

Acquisition Parameter

Source Type	ESI	Ion Polarity	Positive	Set Nebulizer	0.5 Bar
Focus	Not active	Set Capillary	3500 V	Set Dry Heater	181 °C
Scan Begin	50 m/z	Set End Plate Offset	-500 V	Set Dry Gas	4.0 l/min
Scan End	1500 m/z	Set Charging Voltage	2000 V	Set Divert Valve	Source
		Set Corona	0 nA	Set APCI Heater	0 °C

Meas. m/z	Ion Formula	m/z	err [ppm]
732.2434	C34H33IrN7	732.2421	-1.5

Figure S6. Mass spectrum of complex **2**. HMRS [ESI+] ion $[C_{34}H_{33}IrN_7]^+$ m/z calculated: 732.2421 Found: 732.2434 [M+].

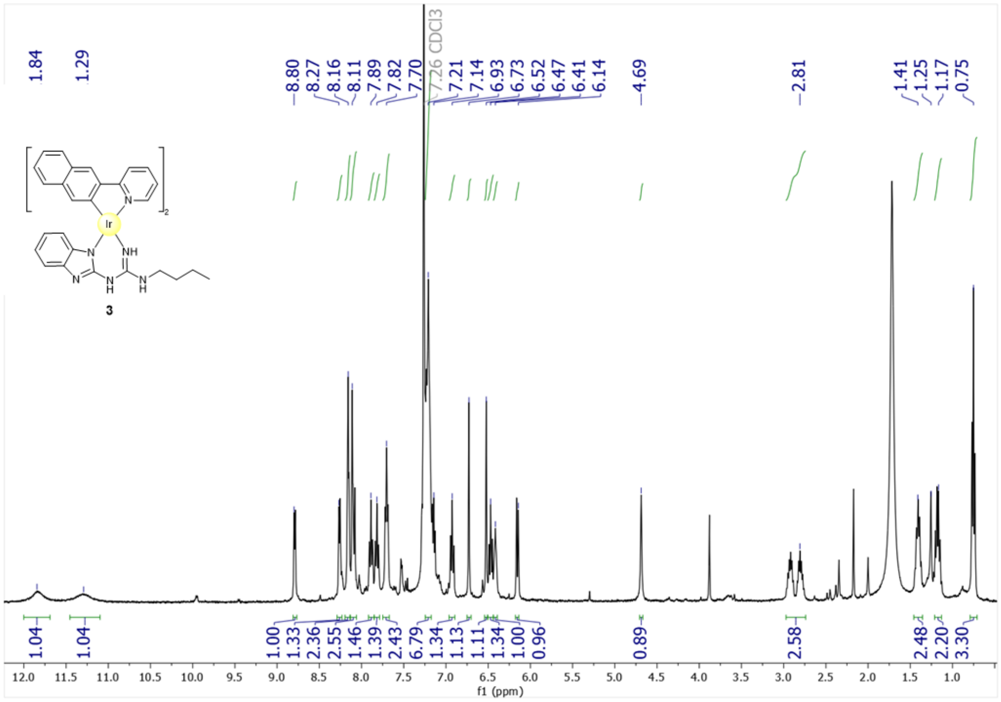

Figure S7. ^{1}H NMR spectrum of iridium complex **3**, $CDCl_3$, 400 MHz, 298 K.

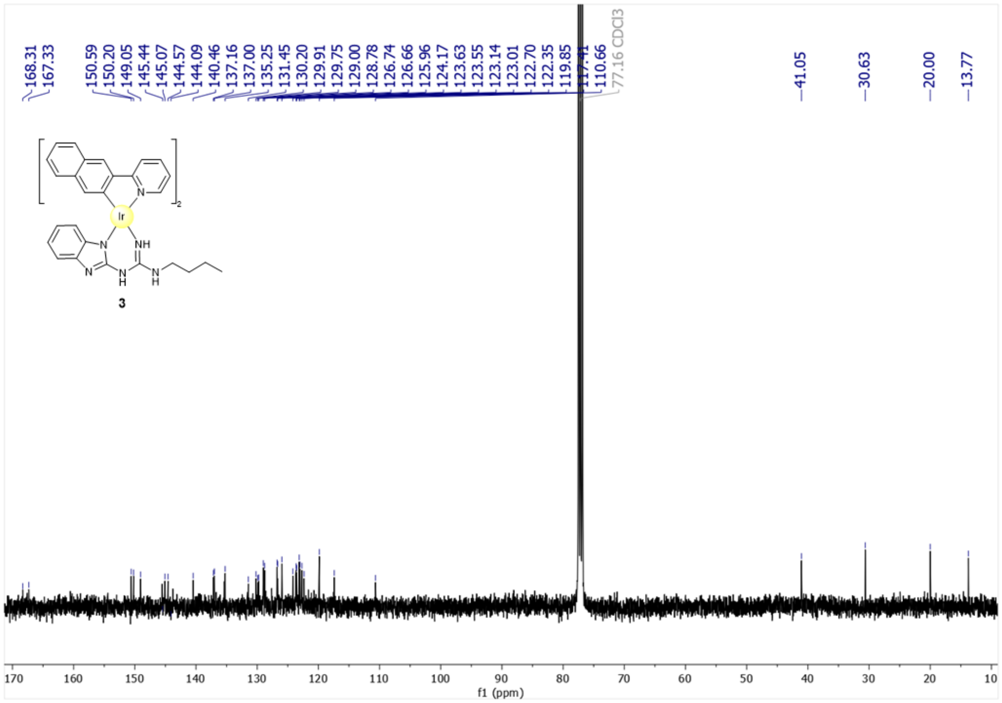

Figure S8. ^{13}C NMR spectrum of iridium complex **3,** $CDCl_3$, 101 MHz, 298 K.

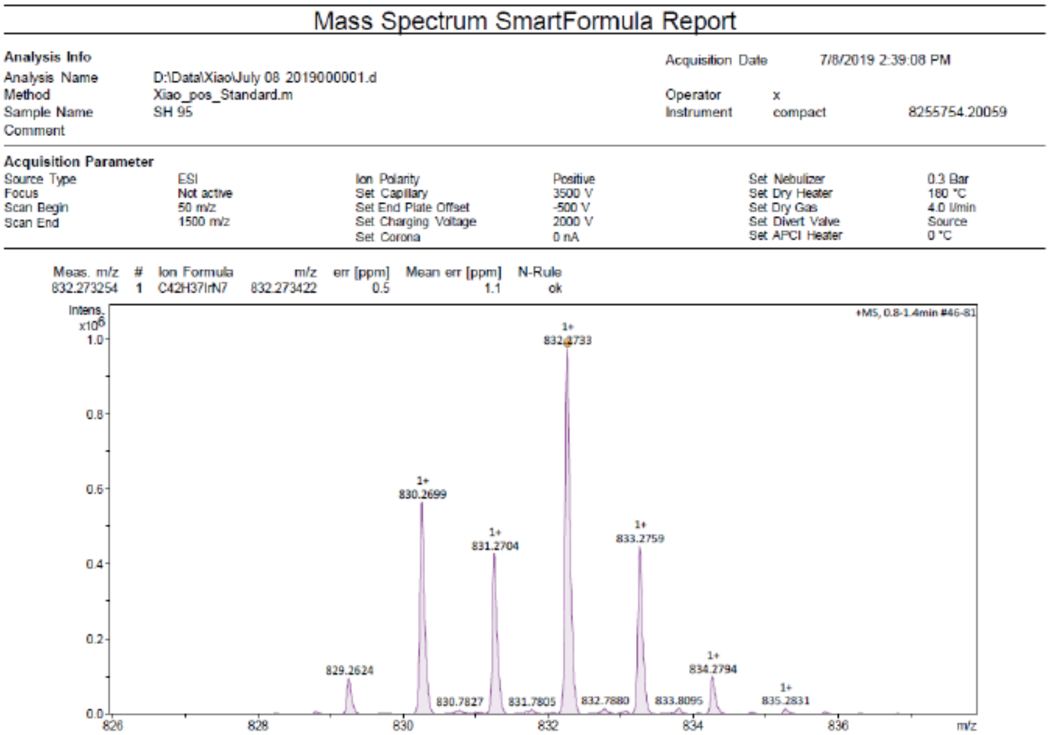

Mass Spectrum SmartFormula Report

Analysis Info			Acquisition Date	7/8/2019 2:39:08 PM	
Analysis Name	D:\Data\Xiao\July 08 2019000001.d				
Method	Xiao_pos_Standard.m		Operator	x	
Sample Name	SH 95		Instrument	compact	8255754.20059
Comment					

Acquisition Parameter					
Source Type	ESI	Ion Polarity	Positive	Set Nebulizer	0.3 Bar
Focus	Not active	Set Capillary	3500 V	Set Dry Heater	180 °C
Scan Begin	50 m/z	Set End Plate Offset	-500 V	Set Dry Gas	4.0 l/min
Scan End	1500 m/z	Set Charging Voltage	2000 V	Set Divert Valve	Source
		Set Corona	0 nA	Set APCI Heater	0 °C

Meas. m/z	#	Ion Formula	m/z	err [ppm]	Mean err [ppm]	N-Rule
832.273254	1	C42H37IrN7	832.273422	0.5	1.1	ok

Figure S9. Mass spectrum of iridium complex **3**. HMRS [ESI+] ion $[C_{42}H_{37}IrN_7]^+$ m/z calculated: 832.2732. Found: 832.2734 [M+].

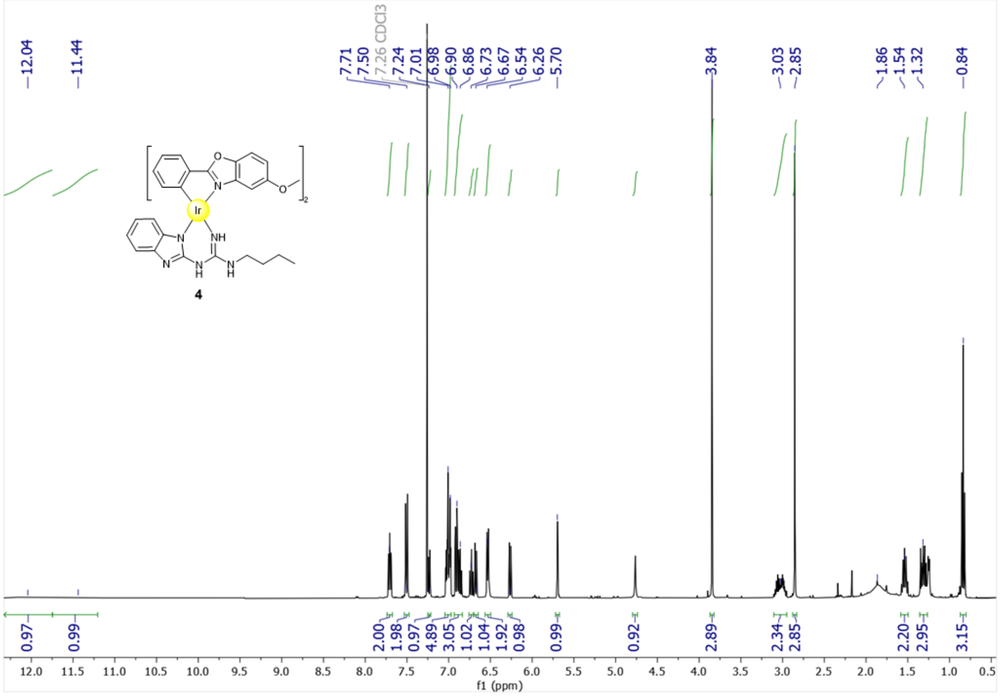

Figure S10. ^1H NMR spectrum of iridium complex **4**, $CDCl_3$, 400 MHz, 298 K.

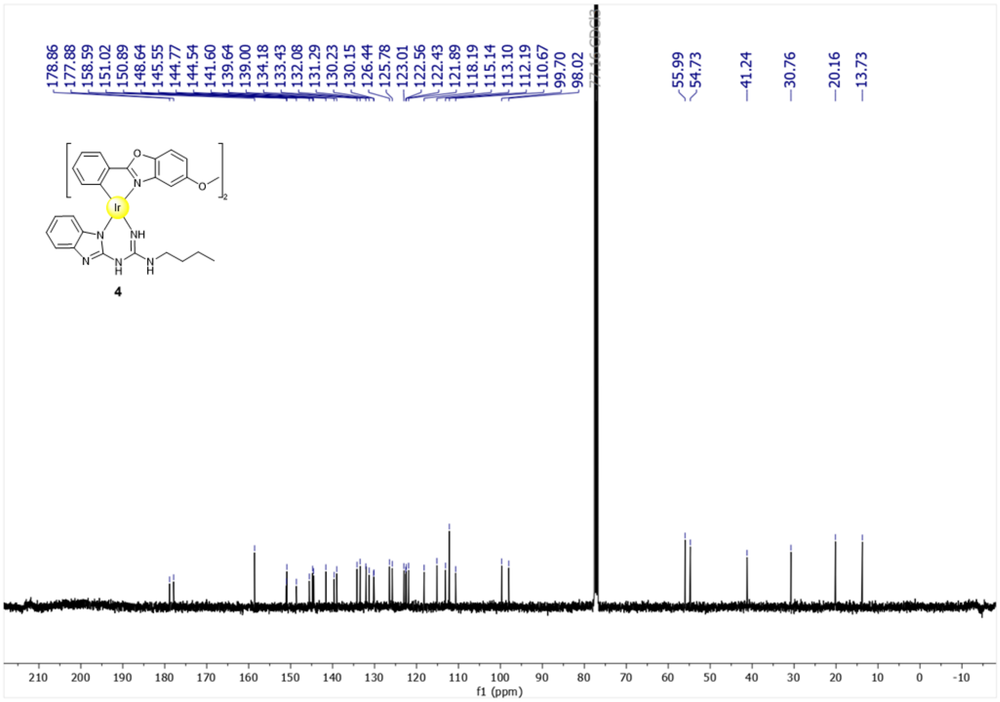

Figure S11. ^{13}C NMR spectrum of iridium complex **4,** $CDCl_3$, 101 MHz, 298 K.

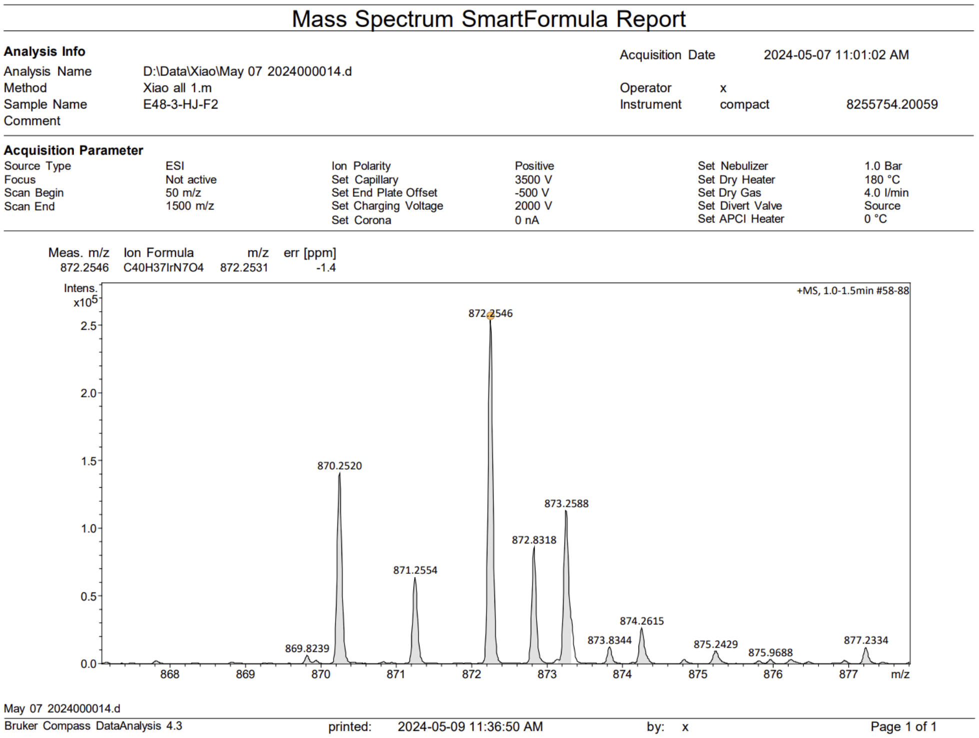

Mass Spectrum SmartFormula Report

Analysis Info

Analysis Name	D:\Data\Xiao\May 07 2024000014.d	Acquisition Date	2024-05-07 11:01:02 AM	
Method	Xiao all 1.m	Operator	x	
Sample Name	E48-3-HJ-F2	Instrument	compact	8255754.20059
Comment				

Acquisition Parameter

Source Type	ESI	Ion Polarity	Positive	Set Nebulizer	1.0 Bar
Focus	Not active	Set Capillary	3500 V	Set Dry Heater	180 °C
Scan Begin	50 m/z	Set End Plate Offset	-500 V	Set Dry Gas	4.0 l/min
Scan End	1500 m/z	Set Charging Voltage	2000 V	Set Divert Valve	Source
		Set Corona	0 nA	Set APCI Heater	0 °C

Meas. m/z	Ion Formula	m/z	err [ppm]
872.2546	C40H37IrN7O4	872.2531	-1.4

May 07 2024000014.d

Bruker Compass DataAnalysis 4.3 printed: 2024-05-09 11:36:50 AM by: x Page 1 of 1

Figure S12. Mass spectrum of iridium complex **4**. HMRS [ESI+] ion $[C_{40}H_{37}IrN_7O_4]^+$ m/z calculated: 872.2546 Found: 872.2546 [M+].

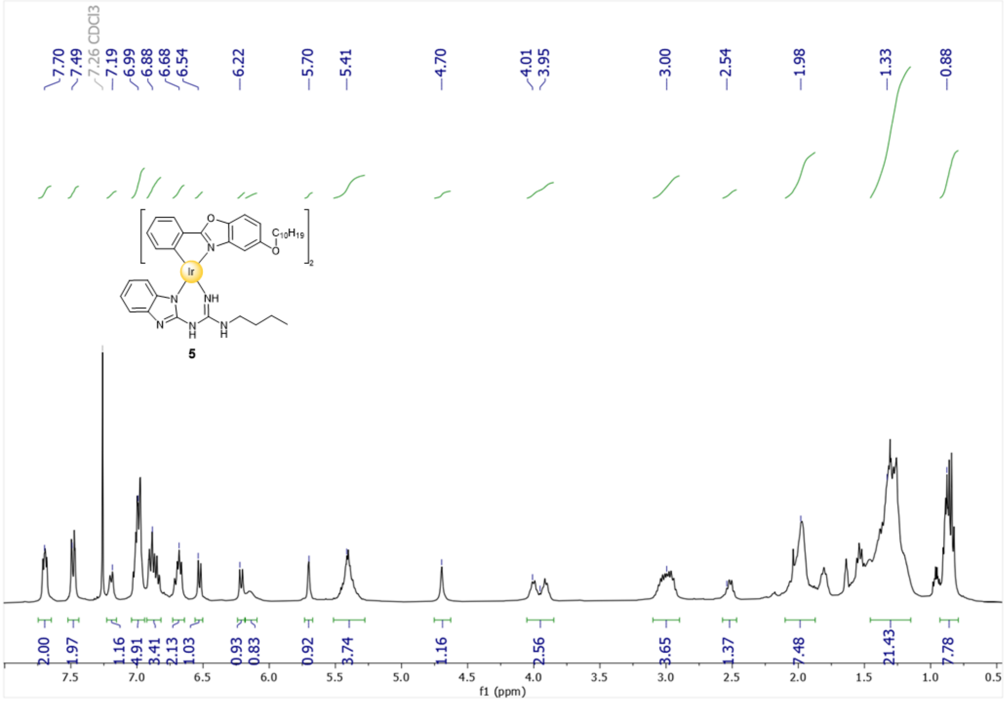

Figure S13. ^{1}H NMR spectrum of iridium complex **5**, CDCl$_3$, 400 MHz, 298 K.

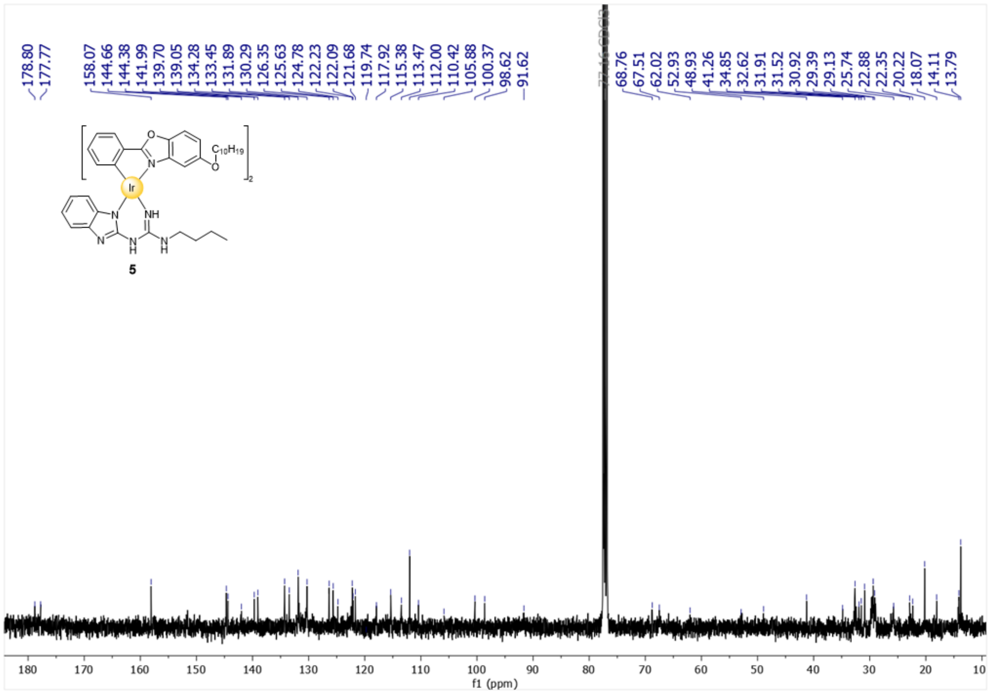

Figure S14. ^{13}C NMR spectrum of iridium complex **5,** CDCl$_3$, 101 MHz, 298 K.

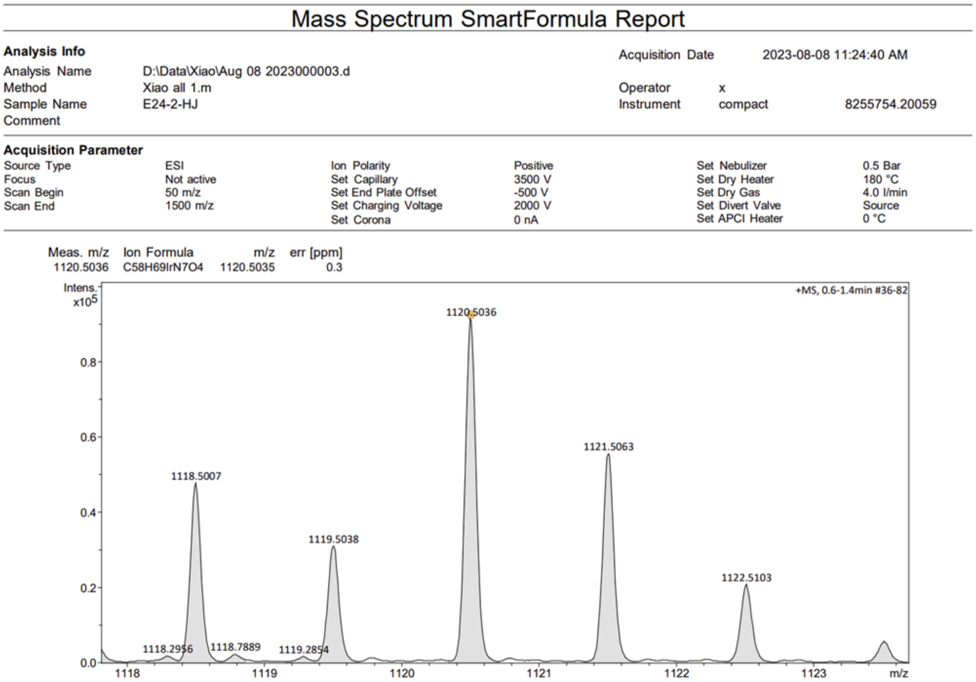

Mass Spectrum SmartFormula Report

Analysis Info

Analysis Name	D:\Data\Xiao\Aug 08 2023000003.d	Acquisition Date	2023-08-08 11:24:40 AM	
Method	Xiao all 1.m	Operator	x	
Sample Name	E24-2-HJ	Instrument	compact	8255754.20059
Comment				

Acquisition Parameter

Source Type	ESI	Ion Polarity	Positive	Set Nebulizer	0.5 Bar
Focus	Not active	Set Capillary	3500 V	Set Dry Heater	180 °C
Scan Begin	50 m/z	Set End Plate Offset	-500 V	Set Dry Gas	4.0 l/min
Scan End	1500 m/z	Set Charging Voltage	2000 V	Set Divert Valve	Source
		Set Corona	0 nA	Set APCI Heater	0 °C

Meas. m/z	Ion Formula	m/z	err [ppm]
1120.5036	C58H69IrN7O4	1120.5035	0.3

Figure S15. Mass spectrum of iridium complex **5**. HMRS [ESI+] ion $[C_{58}H_{69}IrN_7O_4]^+$ m/z calculated: 1120.5036 Found: 1120.5036 [M+].

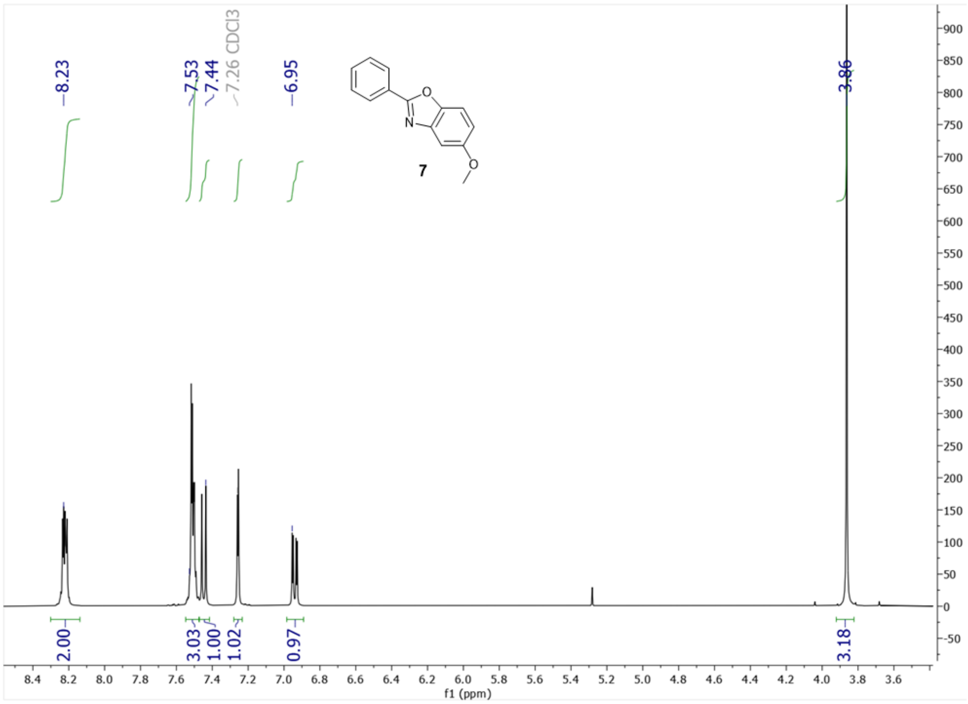

Figure S16. ^{1}H NMR spectrum of ligand **7**, $CDCl_3$, 400 MHz, 298 K.

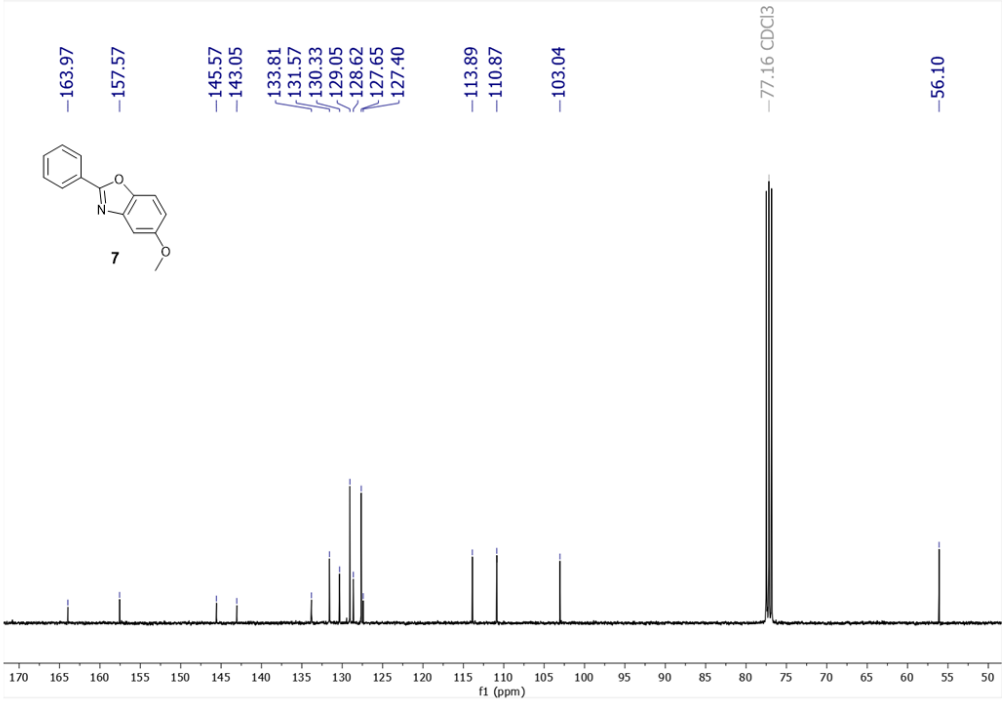

Figure S17. ^{13}C NMR spectrum of ligand **7,** $CDCl_3$, 101 MHz, 298 K.

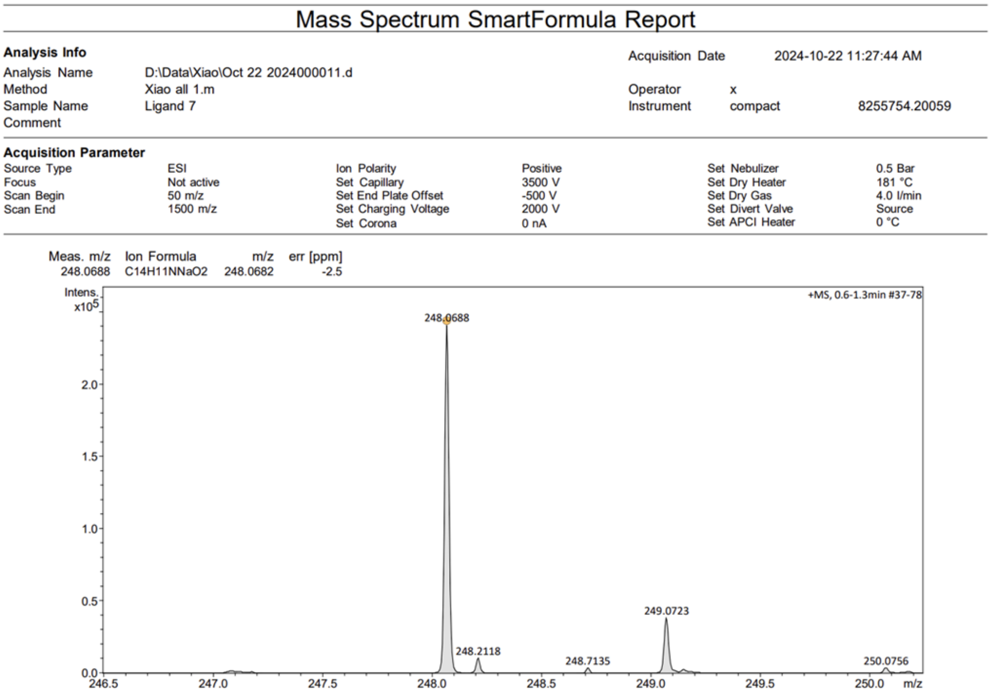

Mass Spectrum SmartFormula Report

Analysis Info

Analysis Name	D:\Data\Xiao\Oct 22 2024000011.d	Acquisition Date	2024-10-22 11:27:44 AM	
Method	Xiao all 1.m	Operator	x	
Sample Name	Ligand 7	Instrument	compact	8255754.20059
Comment				

Acquisition Parameter

Source Type	ESI	Ion Polarity	Positive	Set Nebulizer	0.5 Bar
Focus	Not active	Set Capillary	3500 V	Set Dry Heater	181 °C
Scan Begin	50 m/z	Set End Plate Offset	-500 V	Set Dry Gas	4.0 l/min
Scan End	1500 m/z	Set Charging Voltage	2000 V	Set Divert Valve	Source
		Set Corona	0 nA	Set APCI Heater	0 °C

Meas. m/z	Ion Formula	m/z	err [ppm]
248.0688	C14H11NNaO2	248.0682	-2.5

Figure S18. Mass spectrum of ligand **7**. HMRS [ESI+] ion $[C_{14}H_{11}NO_2Na]^+$ m/z calculated: 248.0688 Found: 248.0682 [M+].

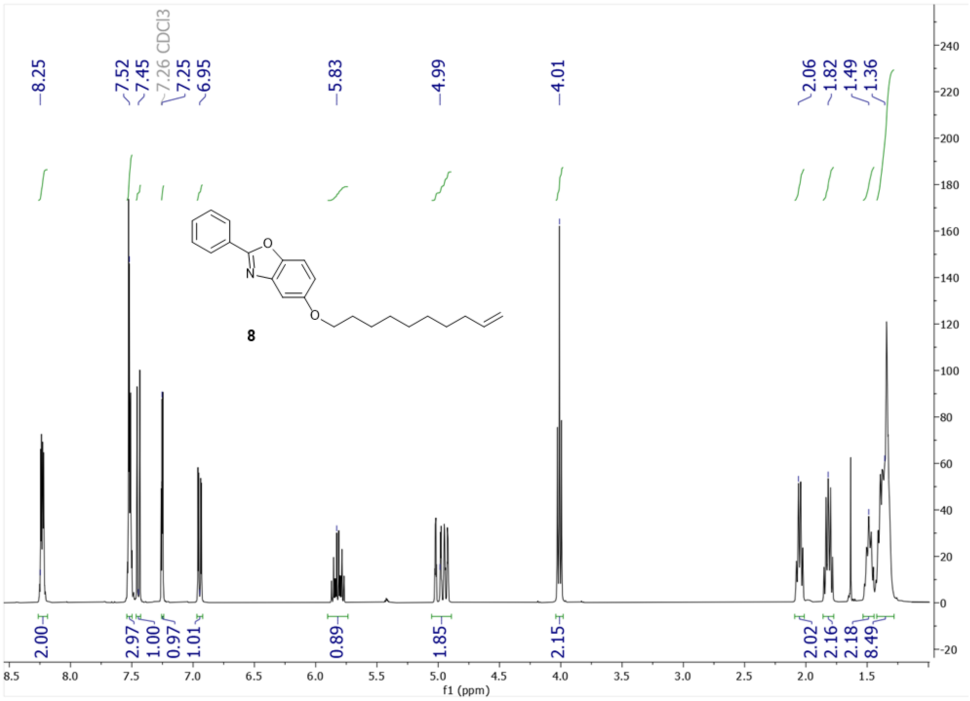

Figure S19. ^{1}H NMR spectrum of ligand **8**, $CDCl_3$, 400 MHz, 298 K.

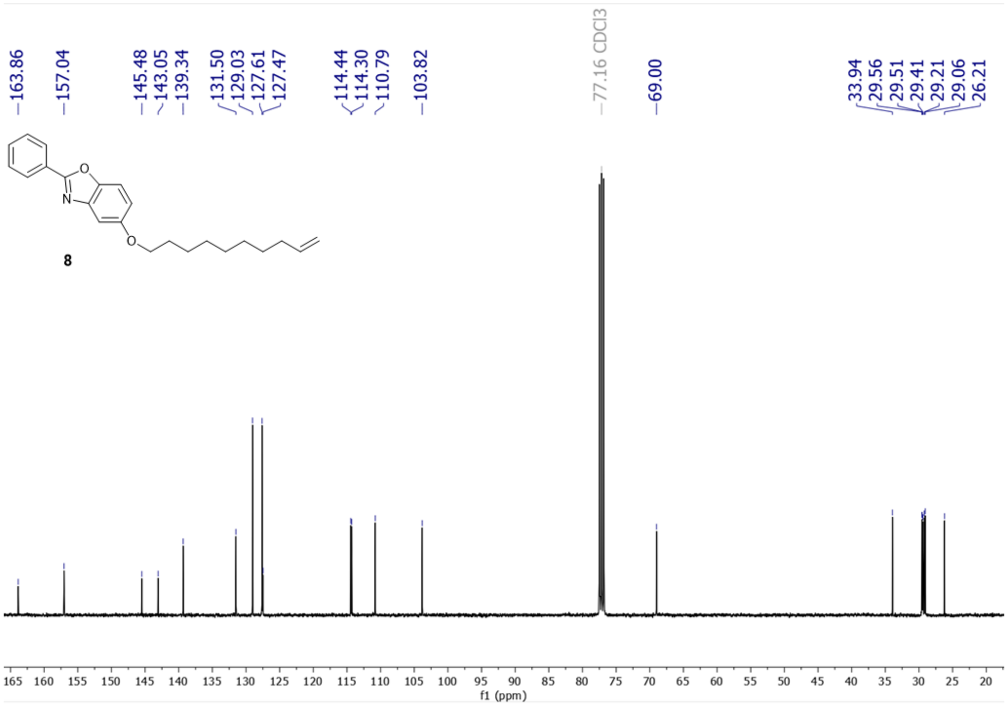

Figure S20. ^{13}C NMR spectrum of ligand **8,** $CDCl_3$, 101 MHz, 298 K.

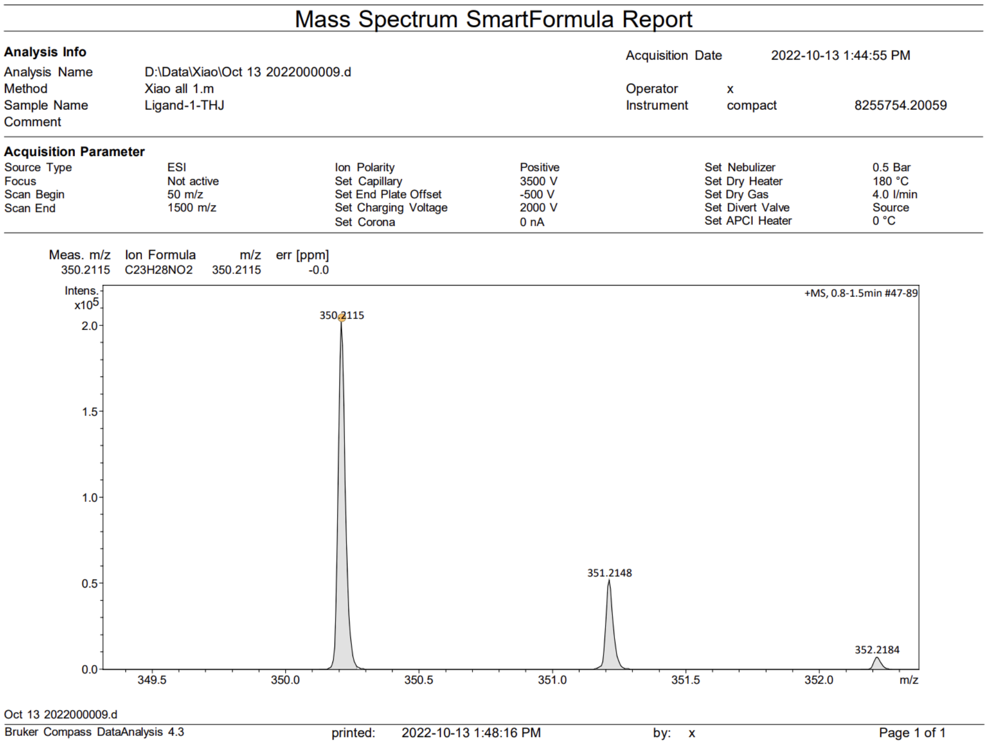

Mass Spectrum SmartFormula Report

Analysis Info

Analysis Name	D:\Data\Xiao\Oct 13 2022000009.d	Acquisition Date	2022-10-13 1:44:55 PM	
Method	Xiao all 1.m	Operator	x	
Sample Name	Ligand-1-THJ	Instrument	compact	8255754.20059
Comment				

Acquisition Parameter

Source Type	ESI	Ion Polarity	Positive	Set Nebulizer	0.5 Bar
Focus	Not active	Set Capillary	3500 V	Set Dry Heater	180 °C
Scan Begin	50 m/z	Set End Plate Offset	-500 V	Set Dry Gas	4.0 l/min
Scan End	1500 m/z	Set Charging Voltage	2000 V	Set Divert Valve	Source
		Set Corona	0 nA	Set APCI Heater	0 °C

Meas. m/z	Ion Formula	m/z	err [ppm]
350.2115	C23H28NO2	350.2115	-0.0

Oct 13 2022000009.d

Bruker Compass DataAnalysis 4.3 printed: 2022-10-13 1:48:16 PM by: x Page 1 of 1

Figure S21. Mass spectrum of ligand **8**. HMRS [ESI+] ion $[C_{23}H_{28}NO_2]^+$ m/z calculated: 350.2115 Found: 350.2115 [M+].

SV. Cyclic Voltammetry

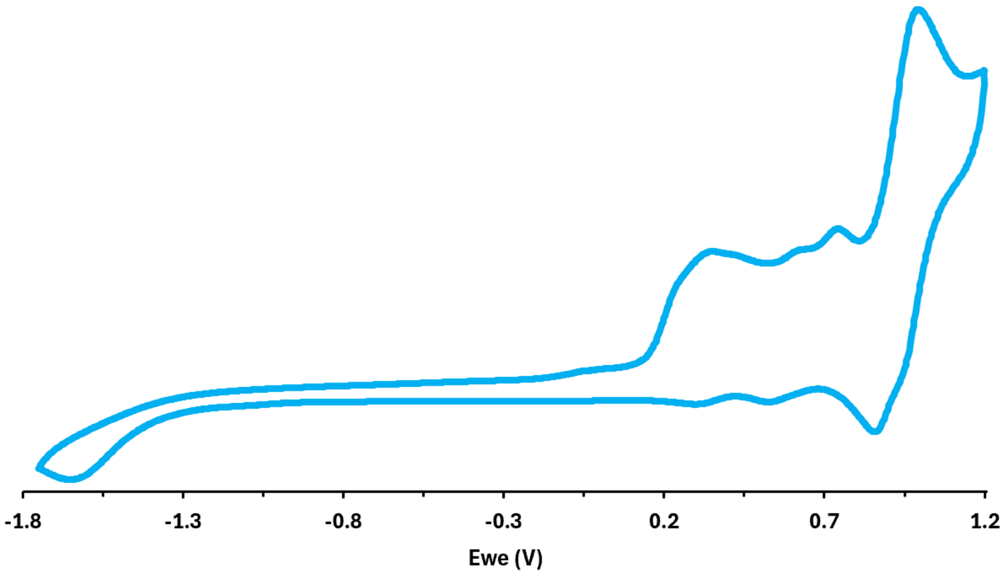

Figure S22. Cyclic voltammetry of complex **1**, the sample was 5mM in dry degassed CH_3CN and normalised to a ferrocene standard under inert argon conditions.

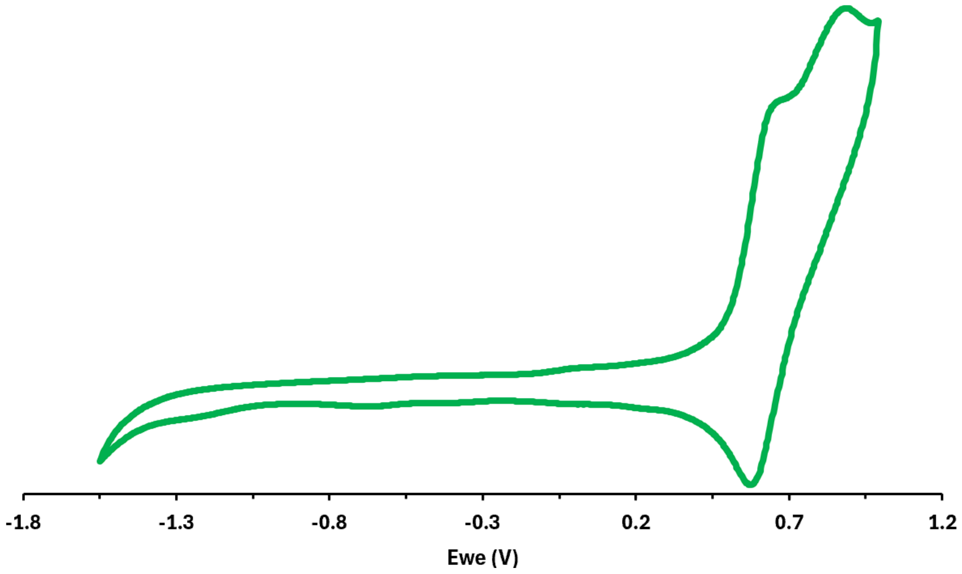

Figure S23. Cyclic voltammetry of complex **2**, the sample was 5mM in dry degassed CH_3CN and normalised to a ferrocene standard under inert argon conditions.

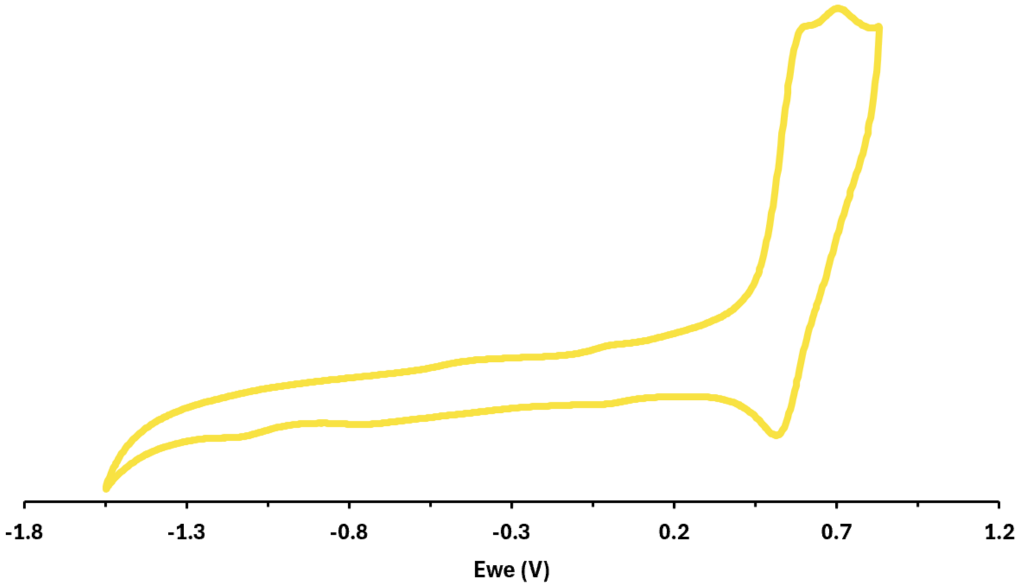

Figure S24. Cyclic voltammetry of complex **3**, the sample was 5mM in dry degassed CH_3CN and normalised to a ferrocene standard under inert argon conditions.

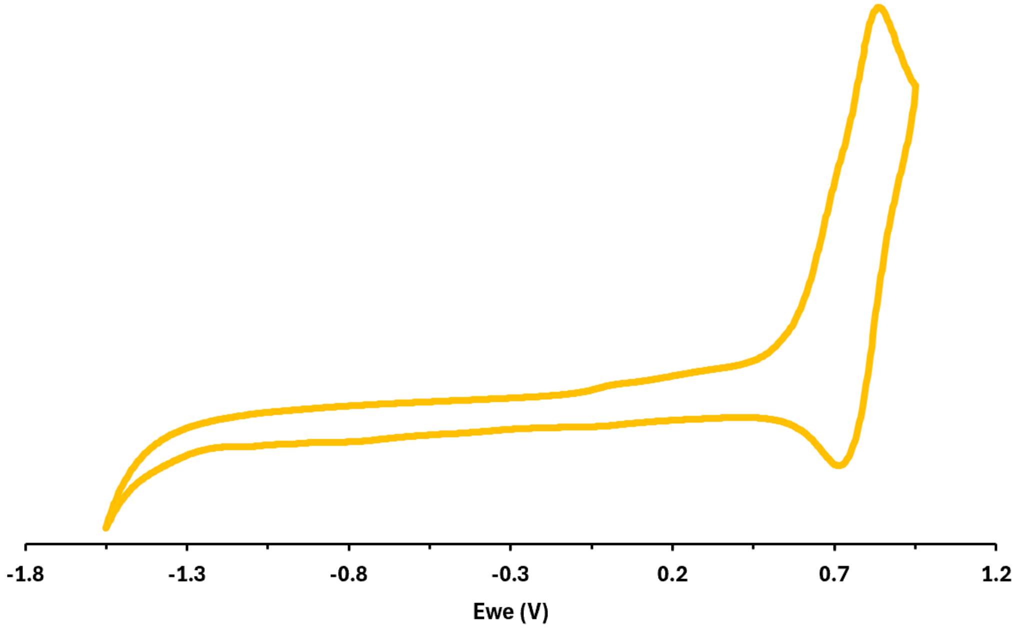

Figure S25. Cyclic voltammetry of complex **4**, the sample was 5mM in dry degassed CH_3CN and normalised to a ferrocene standard under inert argon conditions.

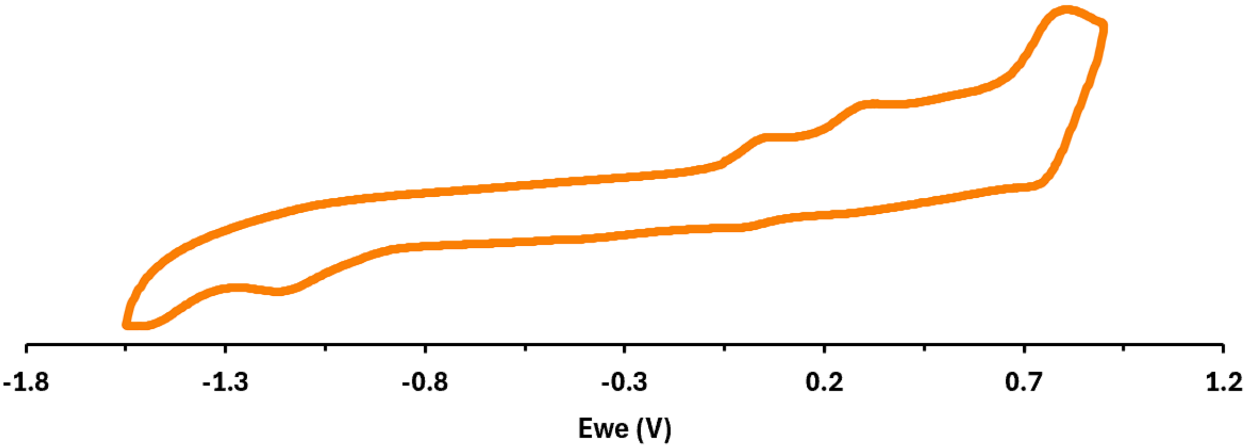

Figure S26. Cyclic voltammetry of complex **5**, the sample was 5mM in dry degassed CH_3CN and normalised to a ferrocene standard under inert argon conditions.

Supplementary Electro-chemical discussion

In the main body of the paper, the first major oxidation and reduction peaks are discussed. It is worth noting that there are additional minor peaks present in these CVs which may interfere with our major oxidations and reductions. These iridium complexes are heteroleptic with our guanidine ligand comprising the ancillary. As the guanidine ligand is asymmetric, we do obtain two isomers. Although we purify our mixes to isolate one isomer, studies have shown that ligands in iridium complexes are able to switch their binding when excited by external stimuli. [10-12]

All complexes show minor peaks proximal to the major peaks, with **1** and **5** having the largest of these. These additional sub-peaks are caused by contamination of the alternate isomer, showing during sample preparation and analysis some level of photoisomerization took place.

SVI. UV-Vis, Excitation and Emission data

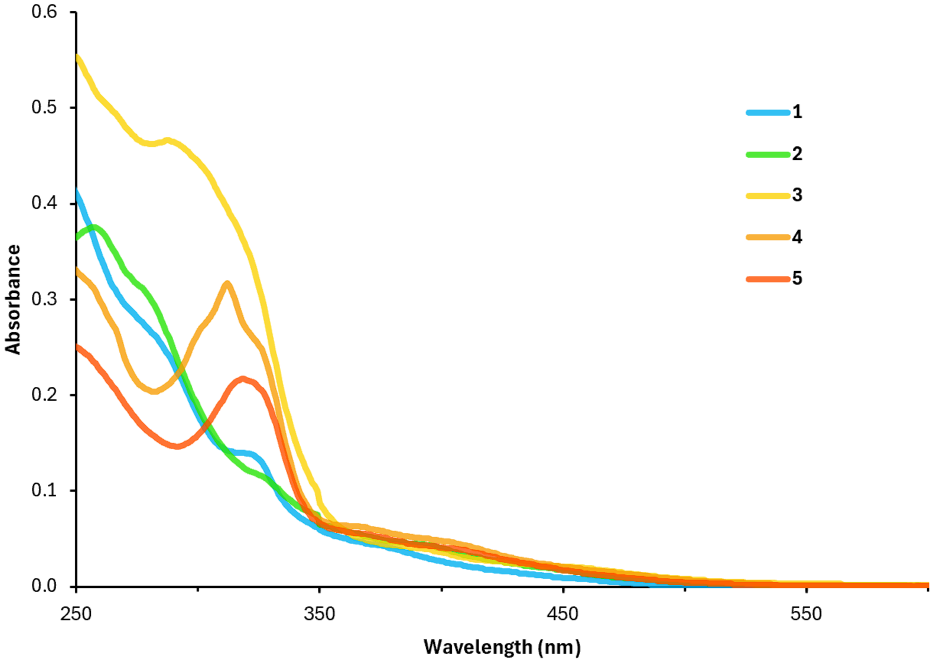

Figure S27. UV-vis absorption spectra of complexes **1** (blue line), **2** (green line), **3** (yellow line), **4** (orange line) and **5** (red line) in CH_3CN, ($1x10^{-5}$ M).

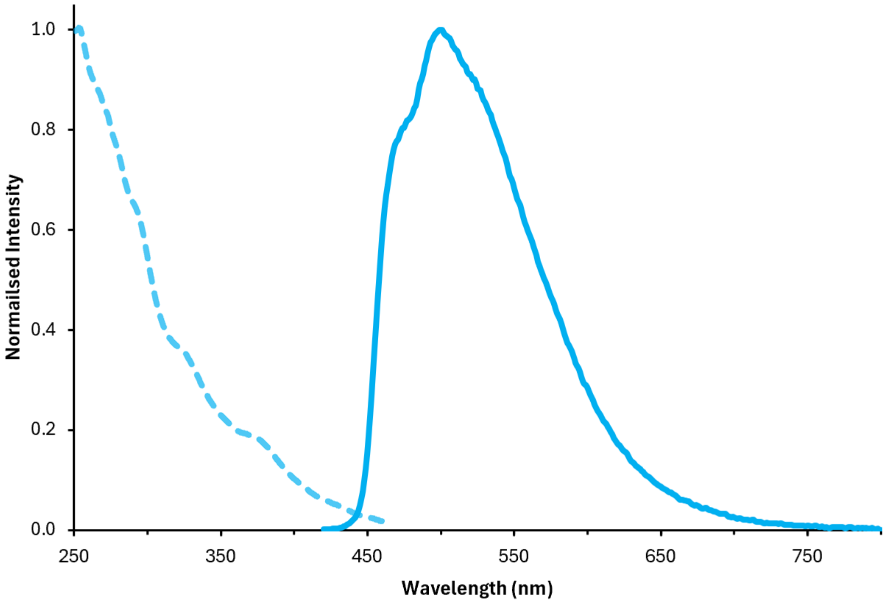

Figure S28. Normalized absorption-emission spectra of iridium complex **1** ($1x10^{-5}$ M) measured in CH_3CN solution, excited at 300 nm.

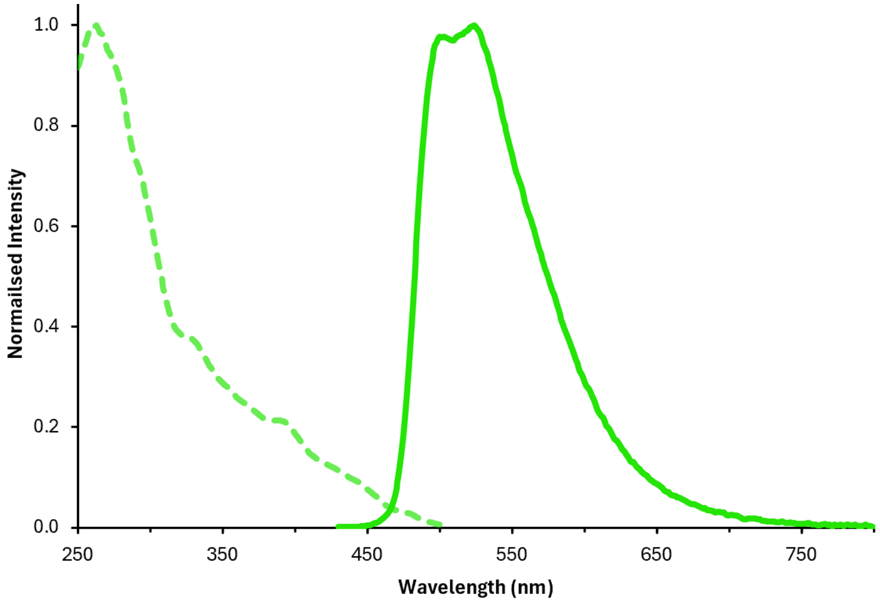

Figure S29. Normalized absorption-emission spectra of iridium complex **2** ($1x10^{-5}$ M) measured in CH_3CN solution, excited at 300 nm.

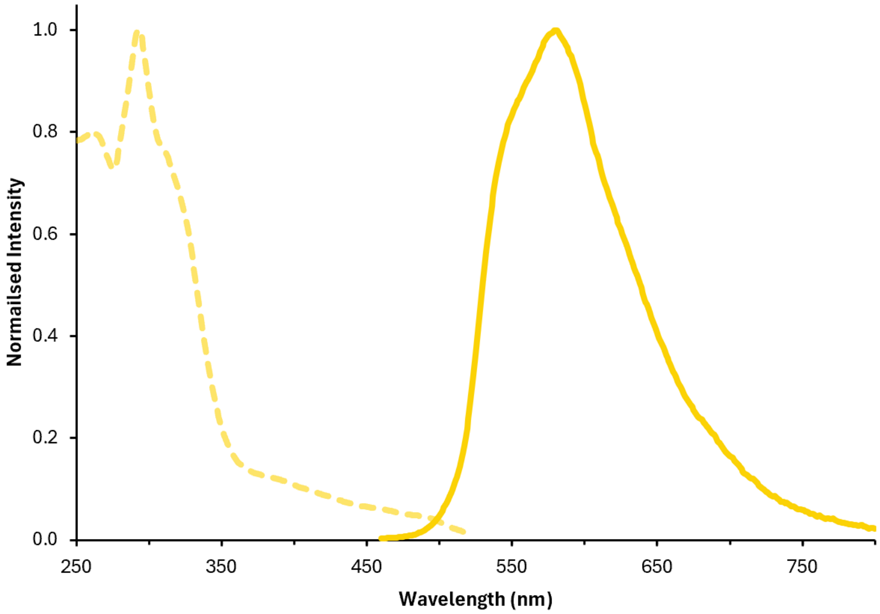

Figure S30. Normalized absorption-emission spectra of iridium complex **3** ($1x10^{-5}$ M) measured in CH_3CN solution, excited at 300 nm.

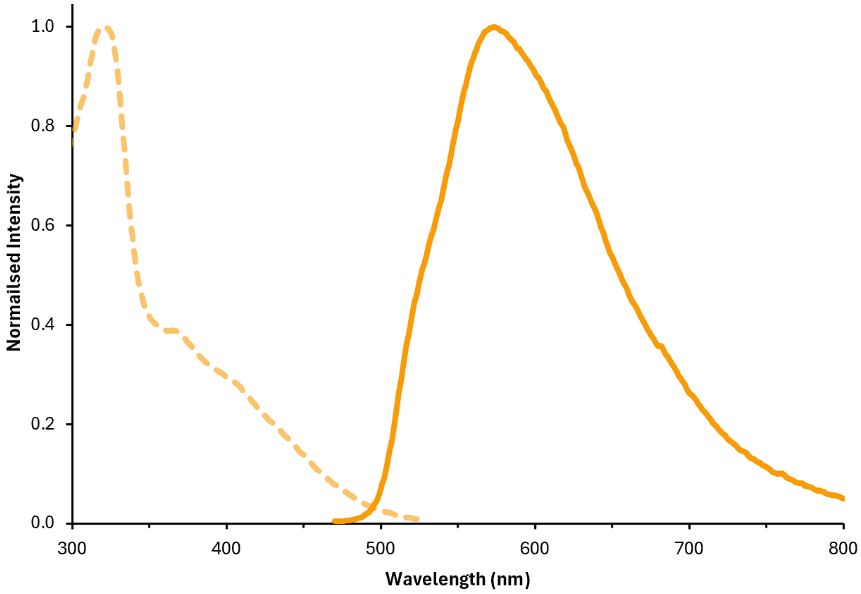

Figure S31. Normalized absorption-emission spectra of iridium complex **4** ($1x10^{-5}$ M) measured in CH_3CN solution, excited at 300 nm.

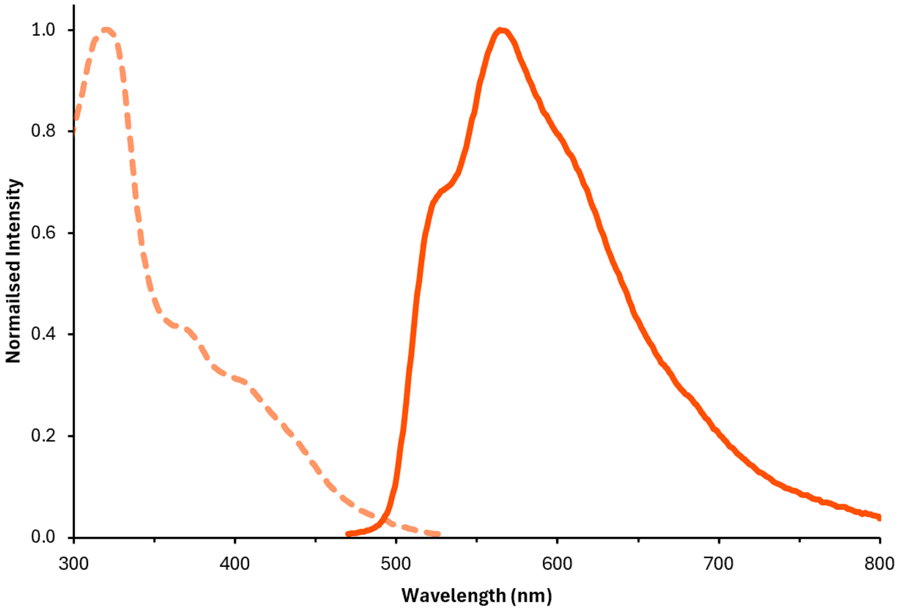

Figure S32. Normalized absorption-emission spectra of iridium complex **5** ($1x10^{-5}$ M) measured in CH_3CN solution, excited at 300 nm.

SVII: Stern-Volmer and photo-stability analysis

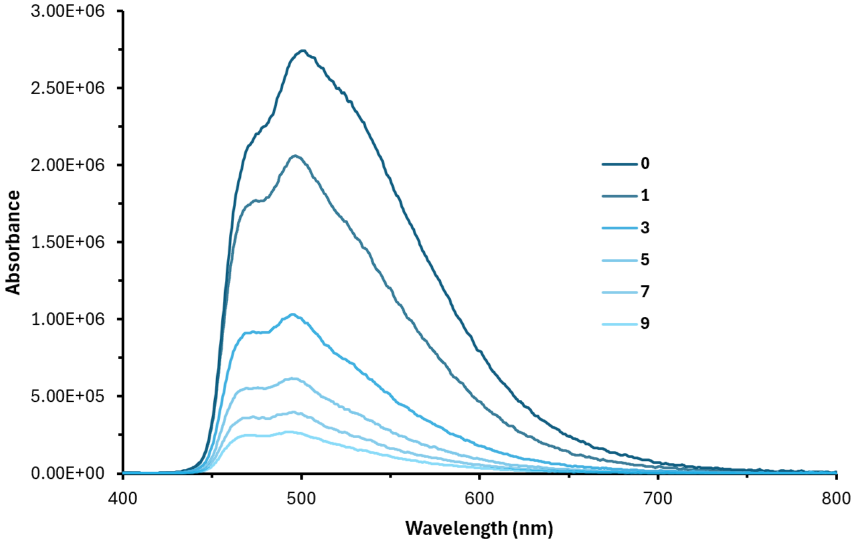

Figure S33. Emission titration of iridium complex **1** ($1\text{x}10^{-5}$ M) with $[Co(BPy)_3]^{2+}$ measured in argon degassed CH_3CN solution, excited at 300 nm. Number of molar equivalents indicated in graph legend.

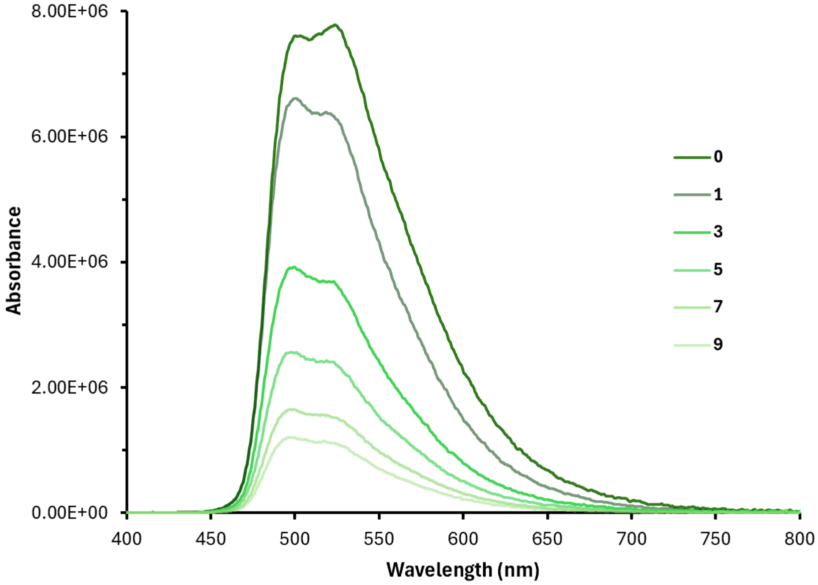

Figure S34. Emission titration of iridium complex **2** ($1\text{x}10^{-5}$ M) with $[Co(BPy)_3]^{2+}$ measured in argon degassed CH_3CN solution, excited at 300 nm. Number of molar equivalents indicated in graph legend.

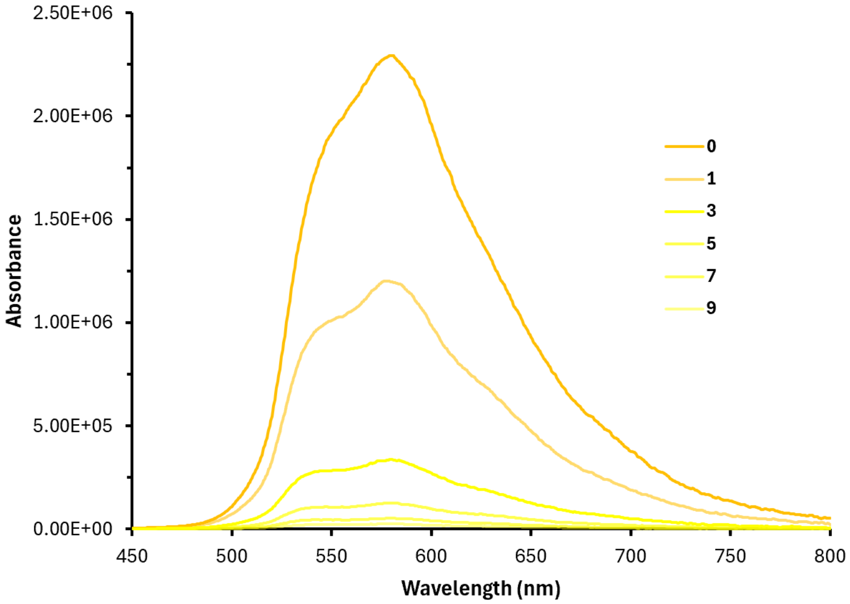

Figure S35. Emission titration of iridium complex **3** ($1x10^{-5}$ M) with $[Co(BPy)_3]^{2+}$ measured in argon degassed CH_3CN solution, excited at 300 nm. Number of molar equivalents indicated in graph legend.

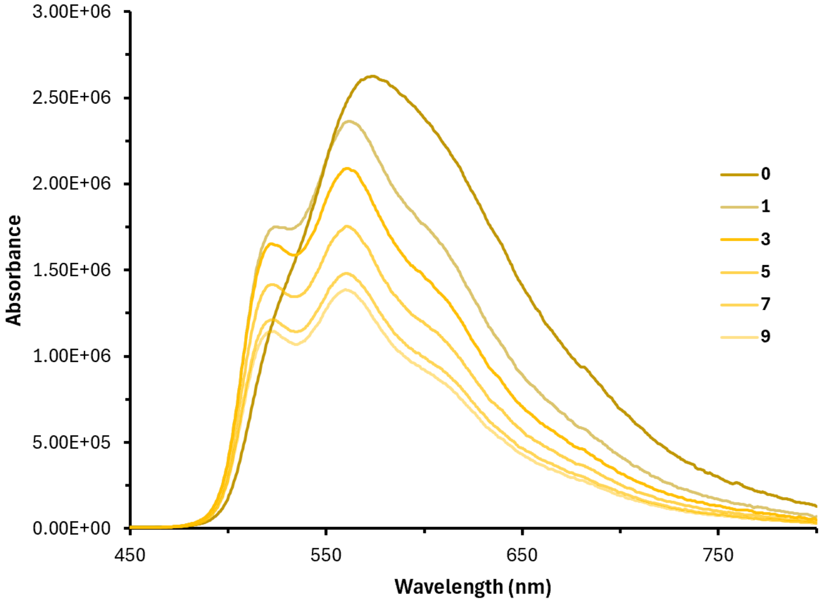

Figure S36. Emission titration of iridium complex **4** ($1x10^{-5}$ M) with $[Co(BPy)_3]^{2+}$ measured in argon degassed CH_3CN solution, excited at 300 nm. Number of molar equivalents indicated in graph legend.

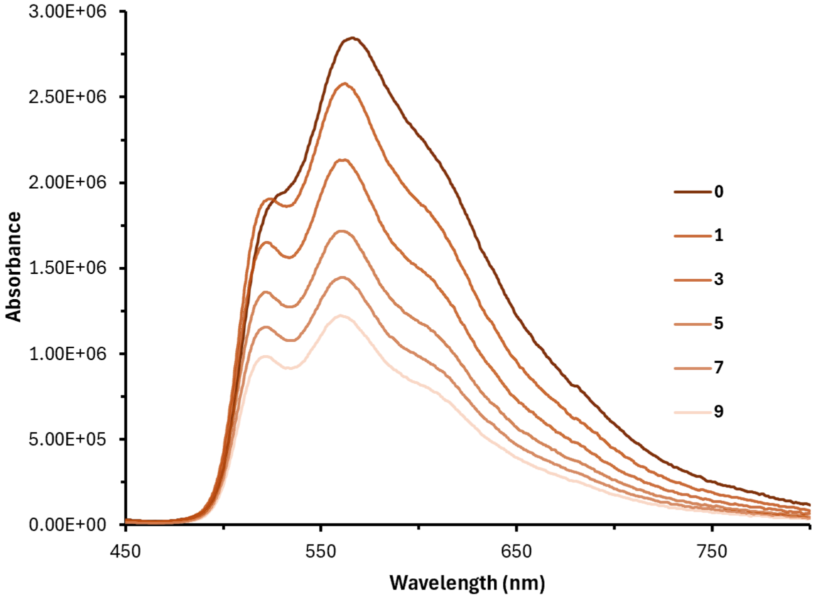

Figure S37. Emission titration of iridium complex **5** ($1x10^{-5}$ M) with $[Co(BPy)_3]^{2+}$ measured in argon degassed CH_3CN solution, excited at 300 nm. Number of molar equivalents indicated in graph legend.

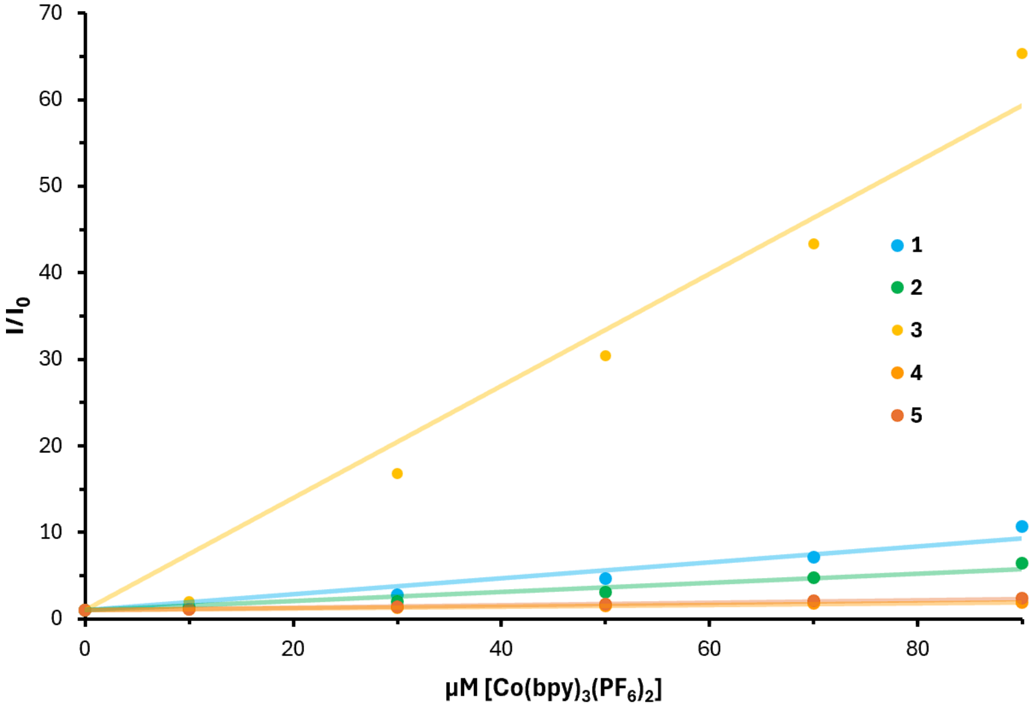

Figure S38. Stern-Volmer plot for emission quenching of complexes **1-5** with $[Co(BPy)_3]^{2+}$.

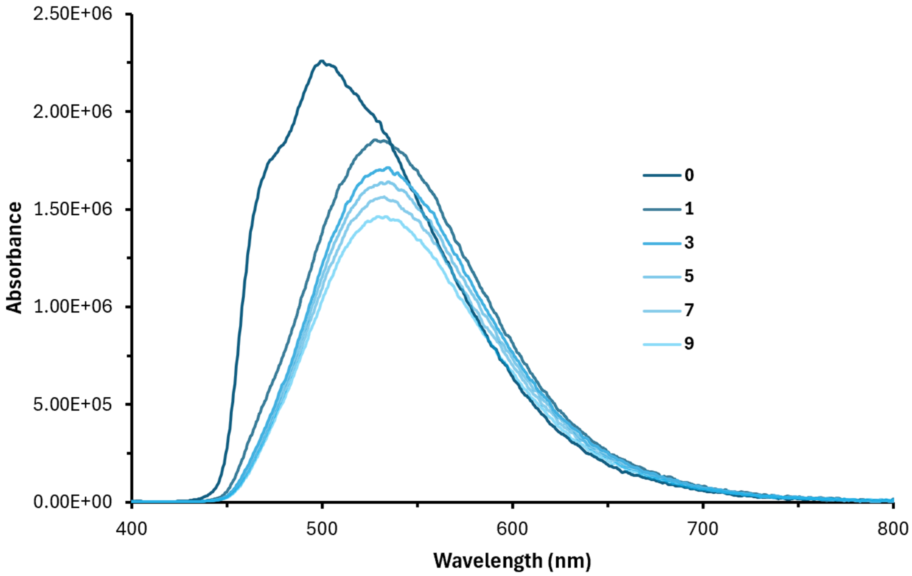

Figure S39. Emission titration of iridium complex **1** ($1x10^{-5}$ M) with NEt_3 measured in argon degassed CH_3CN solution, excited at 300 nm. Number of molar equivalents indicated in graph legend.

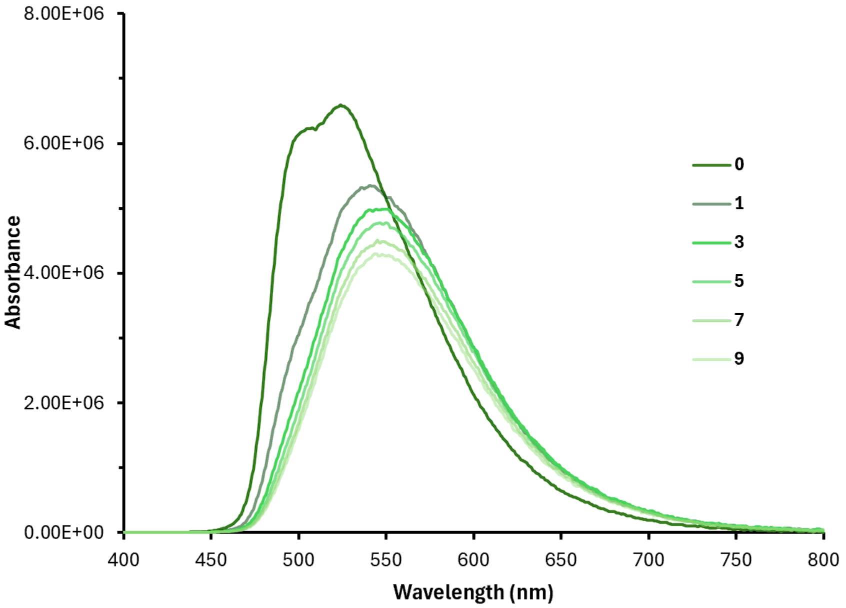

Figure S40. Emission titration of iridium complex **2** ($1x10^{-5}$ M) with NEt_3 measured in argon degassed CH_3CN solution, excited at 300 nm. Number of molar equivalents indicated in graph legend.

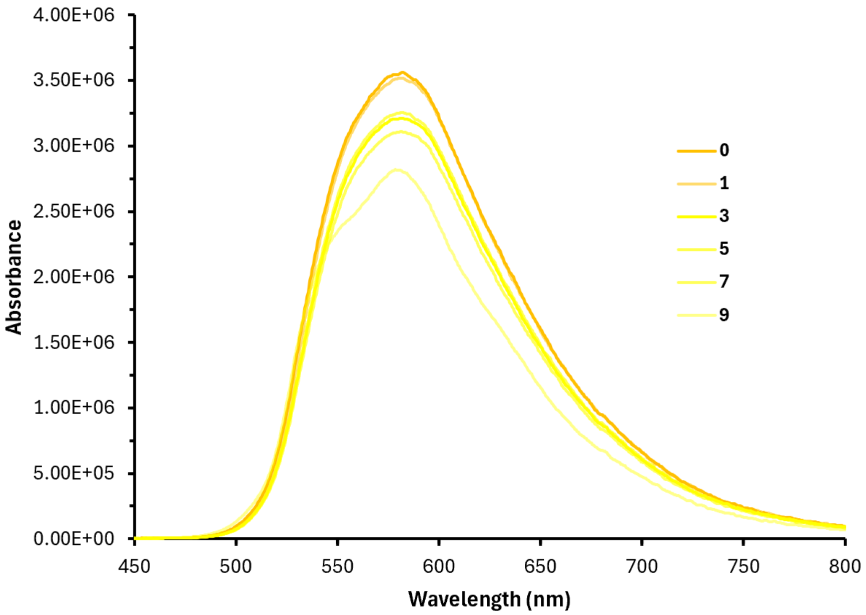

Figure S41. Emission titration of iridium complex **3** (1×10^{-5} M) with NEt_3 measured in argon degassed CH_3CN solution, excited at 300 nm. Number of molar equivalents indicated in graph legend.

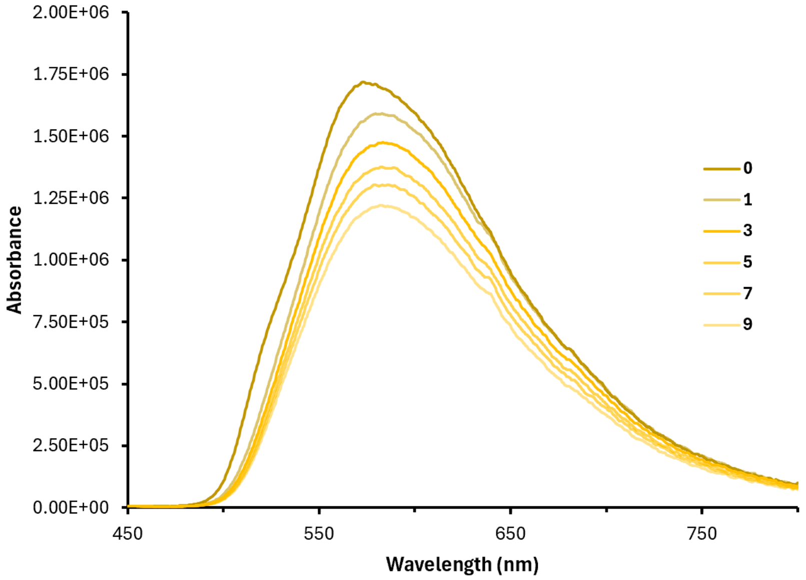

Figure S42. Emission titration of iridium complex **4** (1×10^{-5} M) with NEt_3 measured in argon degassed CH_3CN solution, excited at 300 nm. Number of molar equivalents indicated in graph legend.

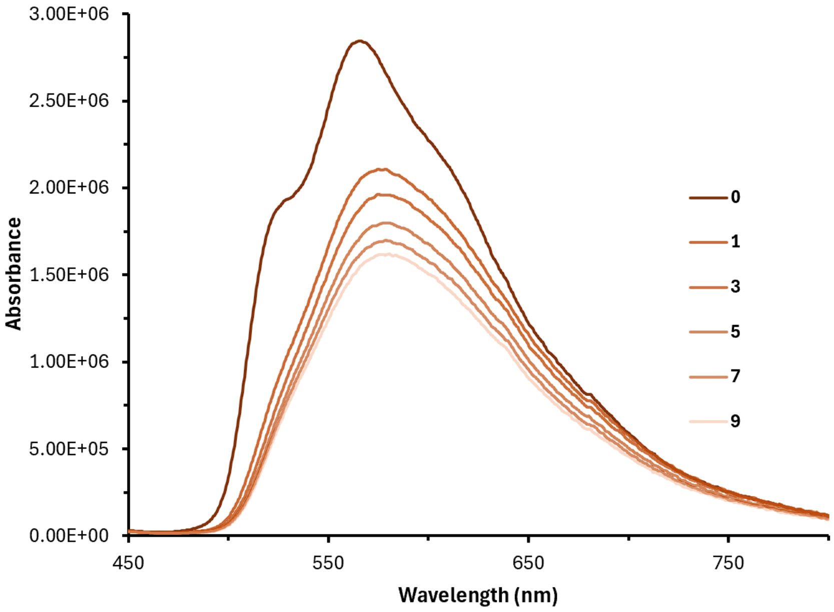

Figure S43. Emission titration of iridium complex **5** ($1x10^{-5}$ M) with NEt_3 measured in argon degassed CH_3CN solution, excited at 300 nm. Number of molar equivalents indicated in graph legend.

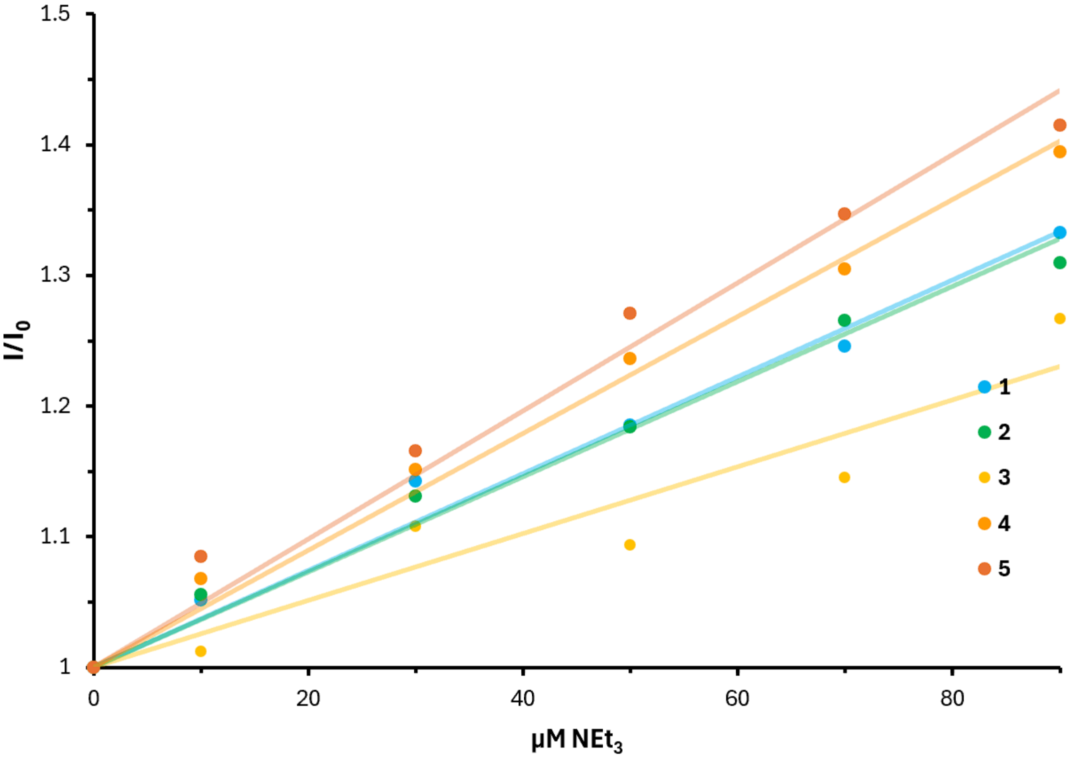

Figure S44. Stern-Volmer plot for emission quenching of complexes **1-5** with NEt_3.

Table S2. Quenching kinetics (K_q) of complexes **1-5**.

Complex	K_q [Co(BPy)$_3$]$^{2+}$ (M^{-1}s^{-1})	K_q NEt$_3$ (M^{-1}s^{-1})
1	5.04×10^{10}	2.02×10^{9}
2	7.84×10^{10}	5.36×10^{9}
3	3.42×10^{13}	1.68×10^{11}
4	5.83×10^{9}	2.56×10^{9}
5	7.65×10^{9}	2.56×10^{9}

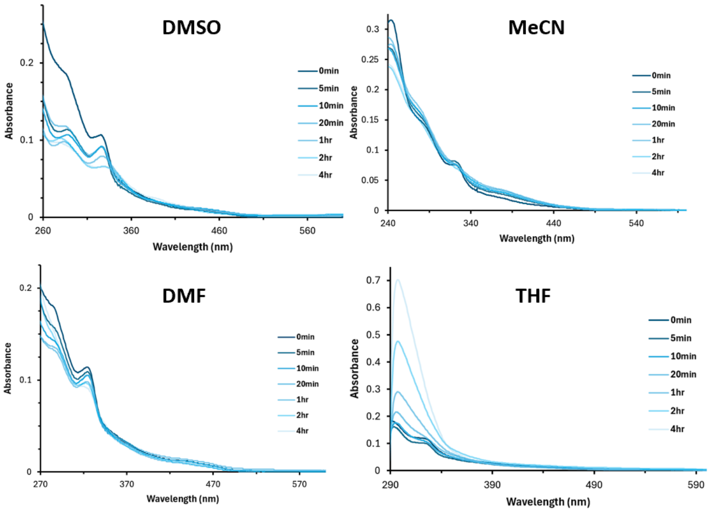

Figure S45. UV-vis spectra of complex **1** in a series of degassed solvents, the mixtures were excited by an array of UV LEDs (365 nm) for 4 hours, UV-vis profile was remeasured at specified time intervals to measure stability to UV light.

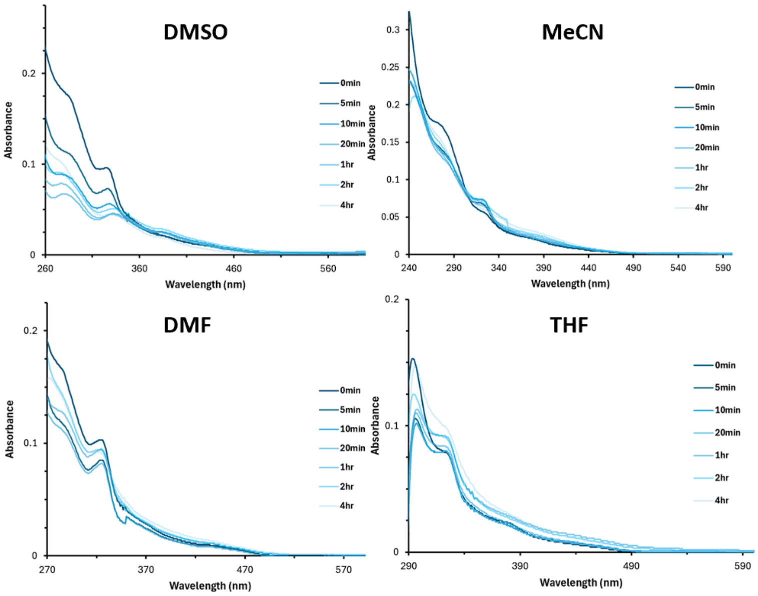

Figure S46. UV-vis spectra of complex **1** in a series of degassed solvents, the mixtures were excited by an array of Blue light LEDs (465 nm) for 4 hours, UV-vis profile was remeasured at specified time intervals to measure stability to UV light.

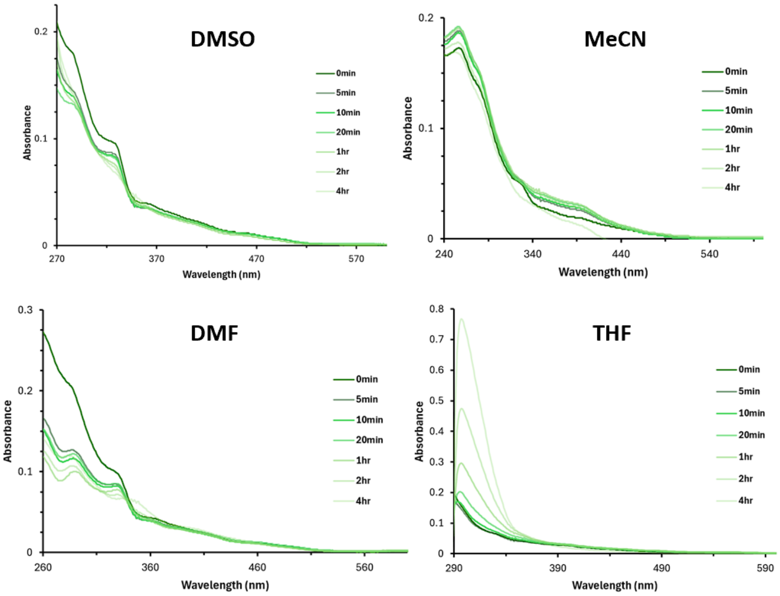

Figure S47. UV-vis spectra of complex **2** in a series of degassed solvents, the mixtures were excited by an array of UV LEDs (365 nm) for 4 hours, UV-vis profile was remeasured at specified time intervals to measure stability to UV light.

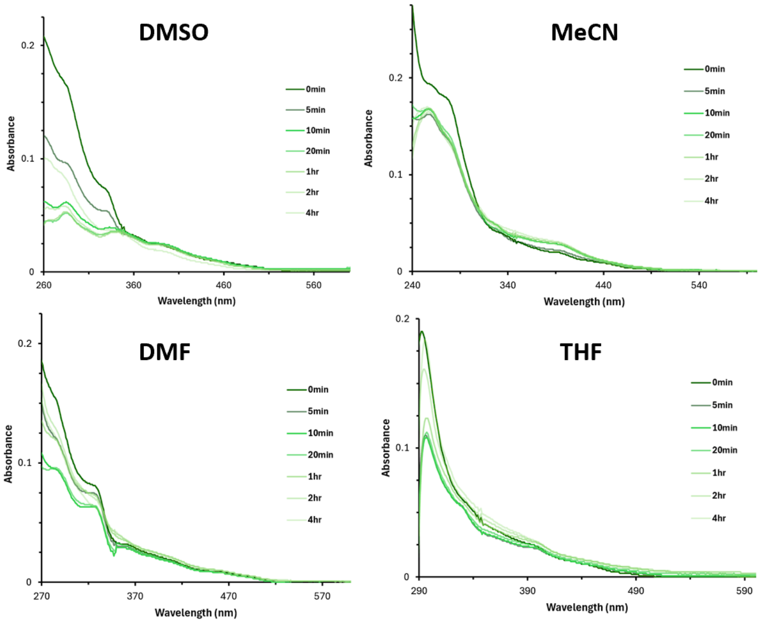

Figure S48. UV-vis spectra of complex **2** in a series of degassed solvents, the mixtures were excited by an array of Blue light LEDs (465 nm) for 4 hours, UV-vis profile was remeasured at specified time intervals to measure stability to UV light.

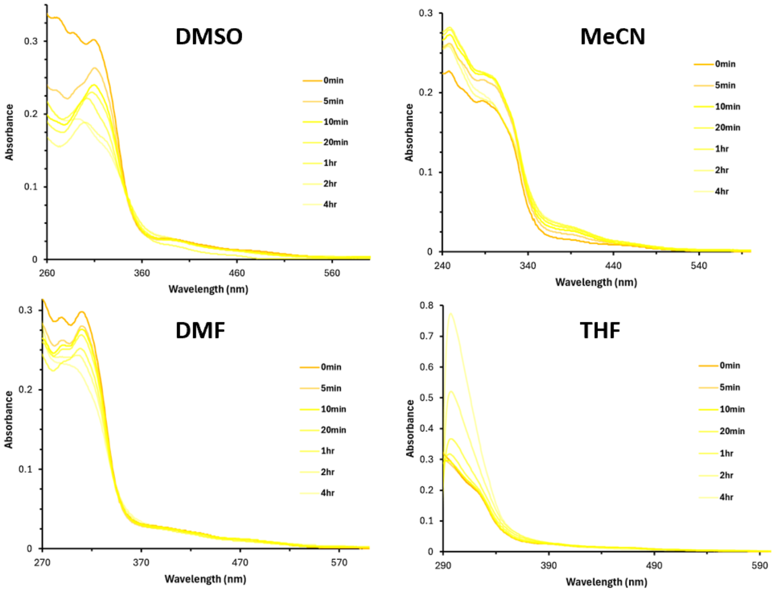

Figure S49. UV-vis spectra of complex **3** in a series of degassed solvents, the mixtures were excited by an array of UV LEDs (365 nm) for 4 hours, UV-vis profile was remeasured at specified time intervals to measure stability to UV light.

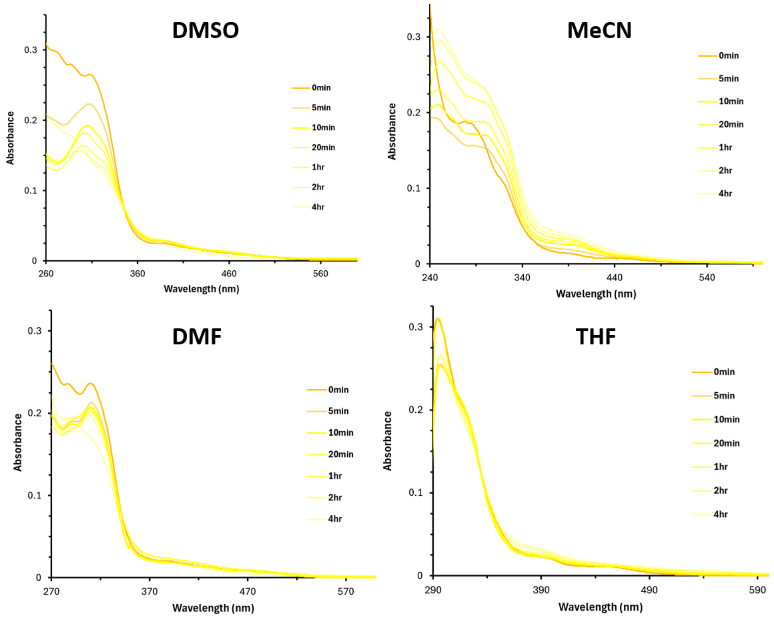

Figure S50. UV-vis spectra of complex **3** in a series of degassed solvents, the mixtures were excited by an array of Blue light LEDs (465 nm) for 4 hours, UV-vis profile was remeasured at specified time intervals to measure stability to UV light.

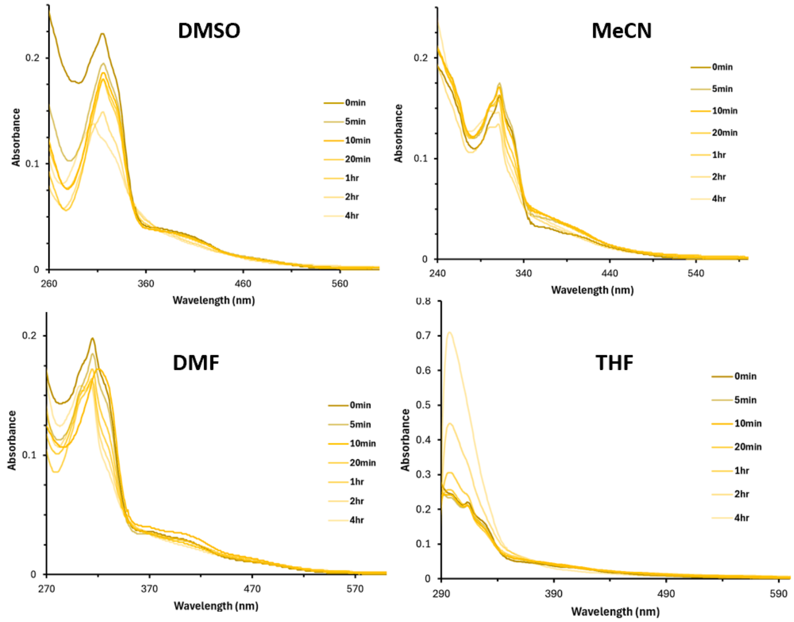

Figure S51. UV-vis spectra of complex **4** in a series of degassed solvents, the mixtures were excited by an array of UV LEDs (365 nm) for 4 hours, UV-vis profile was remeasured at specified time intervals to measure stability to UV light.

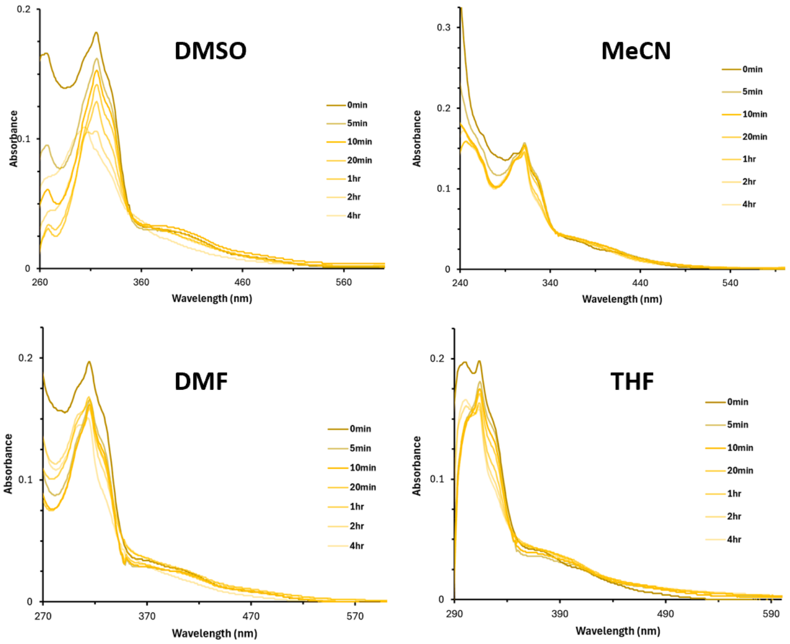

Figure S52. UV-vis spectra of complex **4** in a series of degassed solvents, the mixtures were excited by an array of Blue light LEDs (465 nm) for 4 hours, UV-vis profile was remeasured at specified time intervals to measure stability to UV light.

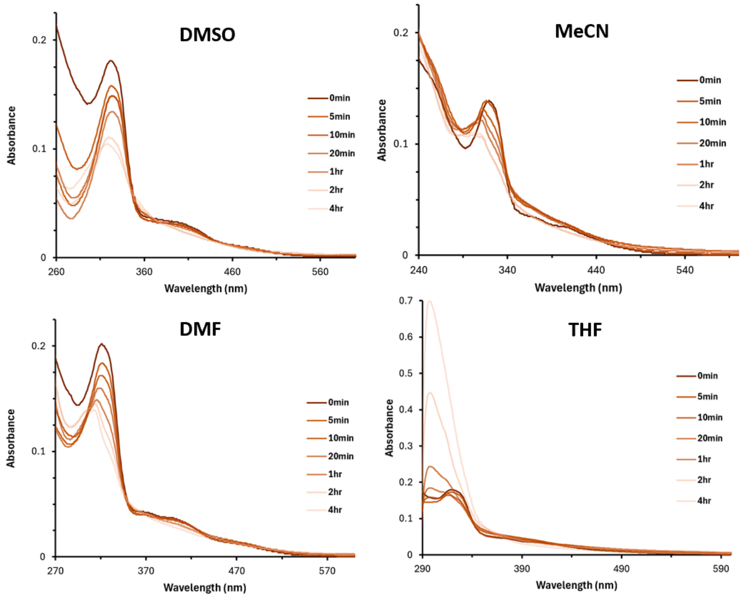

Figure S53. UV-vis spectra of complex **5** in a series of degassed solvents, the mixtures were excited by an array of UV LEDs (365 nm) for 4 hours, UV-vis profile was remeasured at specified time intervals to measure stability to UV light.

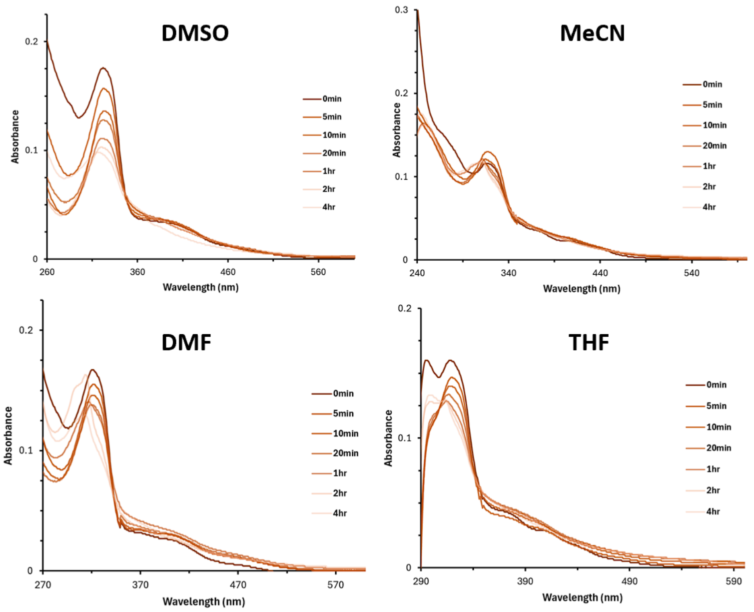

Figure S54. UV-vis spectra of complex **5** in a series of degassed solvents, the mixtures were excited by an array of Blue light LEDs (465 nm) for 4 hours, UV-vis profile was remeasured at specified time intervals to measure stability to UV light.

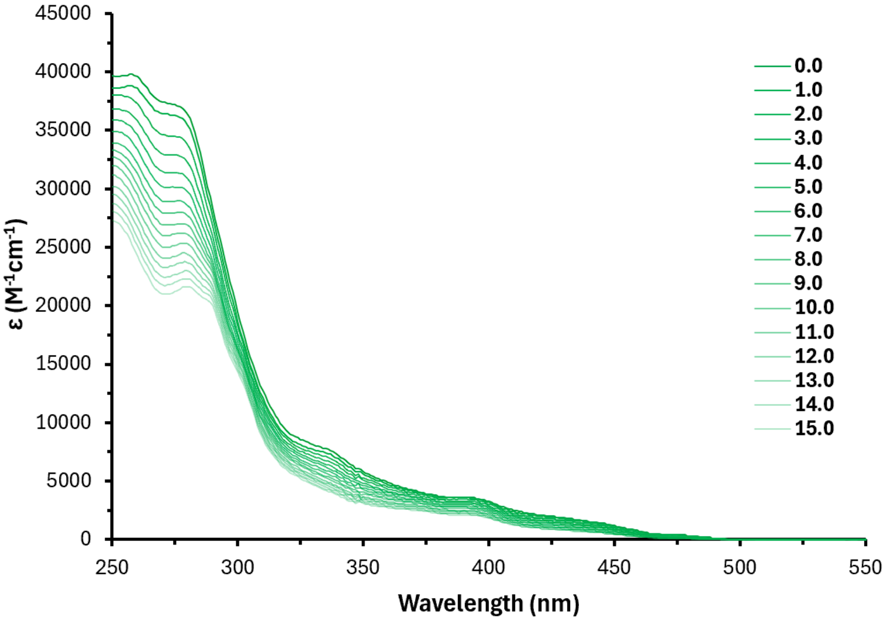

Figure S55. UV-vis titration of complex **2** in MeCN 1×10^{-5} M with molar additions of TFA in MeCN. The legend indicating how many molar equivalents are present in each scan.

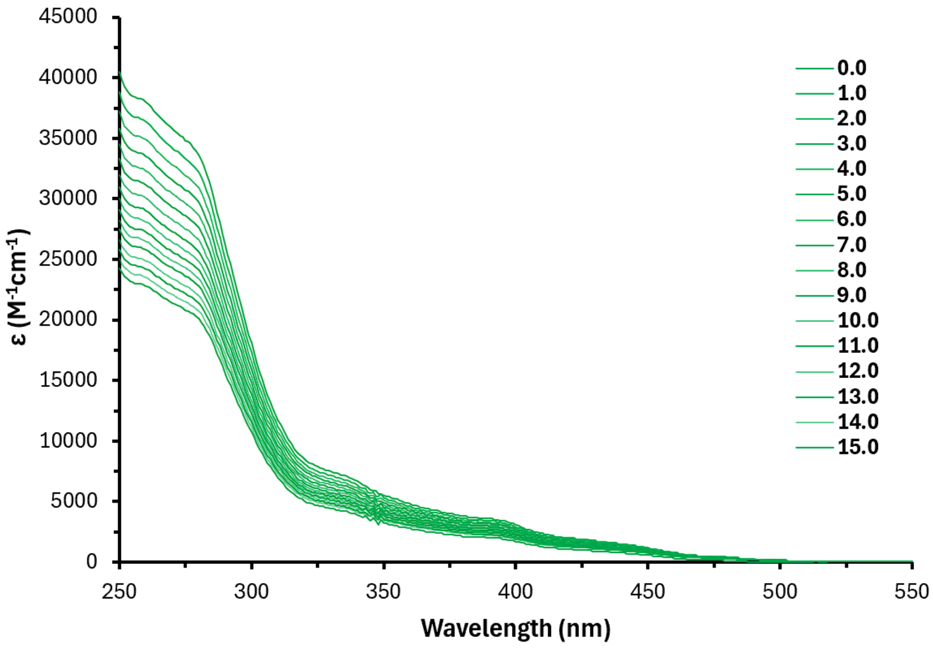

Figure S56. UV-vis dilution of complex **2** in MeCN 1×10^{-5} M with additions of MeCN without TFA. Volume of MeCN added was equal to the additions in the TFA titration of figure S55.

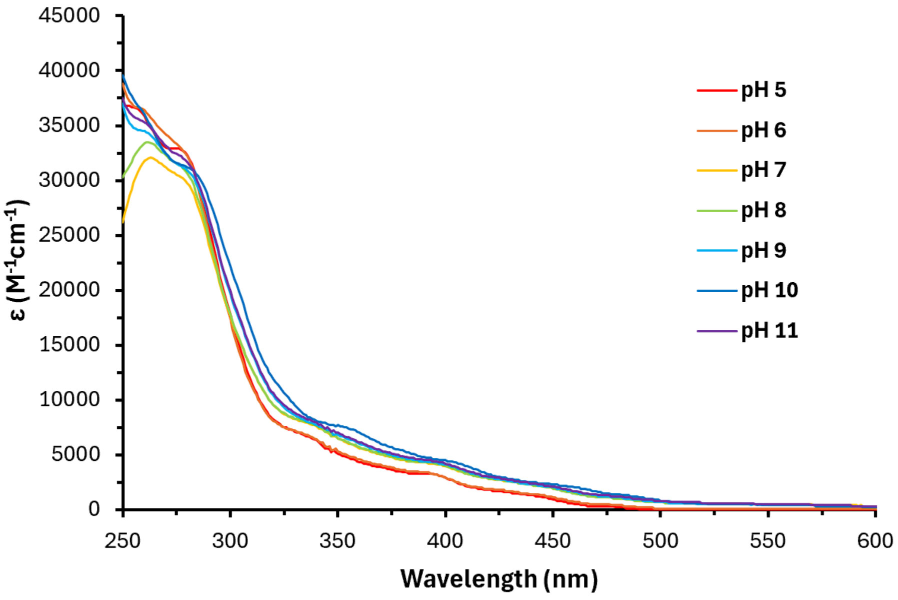

Figure S57. UV-vis spectra of complex **2** in DMSO:H_2O (1:1) 1×10^{-5} M in varying pH conditions.

SVIII. PLQYs and decay lifetimes

Table S2. a) Excitation and emission maxima for Ir(III) complexes **1**-**5**; in CH_3CN degassed for 1 min (N_2) at 298 K. **b)** PLQYs for Ir(III) complexes **1**-**5**; in CH_3CN degassed for 20 mins (Ar) at 298 K using a FS5 SC-30 integrating sphere module. **c)** decay lifetimes using TCSPC excited at 365 nm and their corresponding chi-squared values for Ir(III) complexes **1**-**5**; in CH_3CN degassed for 20 mins (Ar) at 298 K. Complexes decay biexponentially. **d)** the radiative (k_r) and nonradiative (k_{nr}) rate constants were calculated as $k_r = \phi_{PL}/\tau_{PL}$ and $k_{nr} = (1-\phi_{PL})/\tau_{PL}$.

Ir(III) Complex	**Excitation Maxima (nm)**[a]	**Emission Maxima (nm)**[a]	**PLQY (%)**[b]	**Lifetime (μs) (τ_{PL}, χ^2)**[c]	**k_r (x 10^5 s^{-1})**[d]	**k_{nr} (x 10^5 s^{-1})**[d]
1	266, 320, 368	473, 498	89	1.84	4.8	0.6
2	264, 335, 391	500, 522	67	0.68	9.9	4.9
3	294, 382, 450	547, 583	12	0.02	60.0	440.0
4	316, 363, 401	534, 576	30	1.75	1.7	4.0
5	316, 365, 399	530, 568	34	1.92	1.8	3.4

Decay Lifetime Measurement of Ir(III) complex 1

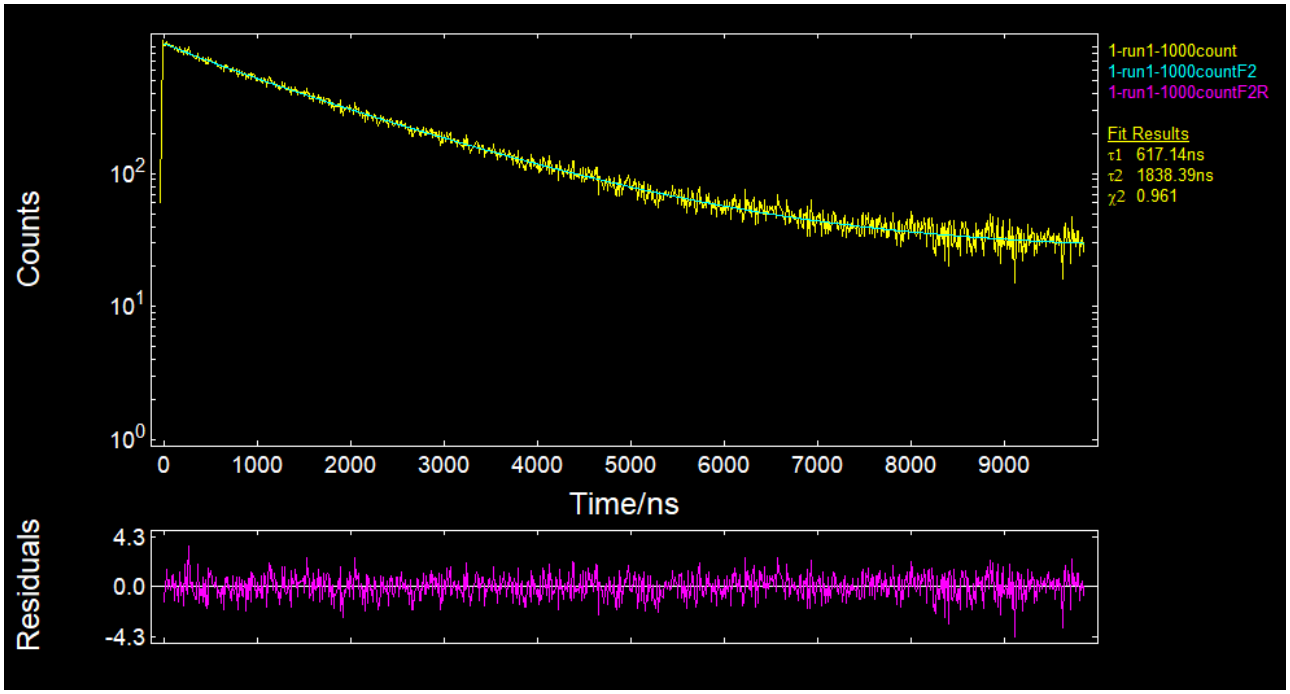

Figure S58. Biexponential lifetime decay of Ir(III) complex **1**, ~1·10^{-5} M (Absorbance of 0.065 from UV-Vis) in CHCl$_3$ degassed for 20 mins (Ar) at 298 K after excitation at 365 nm. Data collected at λ_{max} = 470 nm.

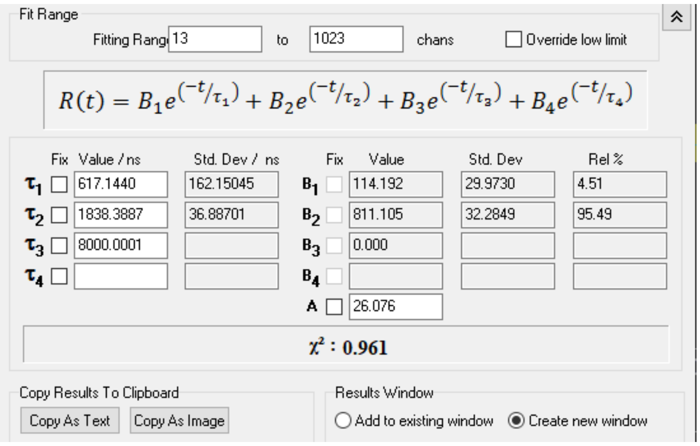

Fit Range

Fitting Rang 13 to 1023 chans ☐ Override low limit

$$R(t) = B_1 e^{(-t/\tau_1)} + B_2 e^{(-t/\tau_2)} + B_3 e^{(-t/\tau_3)} + B_4 e^{(-t/\tau_4)}$$

	Fix	Value / ns	Std. Dev / ns		Fix	Value	Std. Dev	Rel %
τ_1	☐	617.1440	162.15045	B_1	☐	114.192	29.9730	4.51
τ_2	☐	1838.3887	36.88701	B_2	☐	811.105	32.2849	95.49
τ_3	☐	8000.0001		B_3	☐	0.000		
τ_4	☐			B_4	☐			
				A	☐	26.076		

χ^2 : 0.961

Copy Results To Clipboard

Results Window

○ Add to existing window ● Create new window

Figure S59. Fit result of Ir(III) complex **1**, ~1·10^{-5} M (Absorbance of 0.065 from UV-Vis) in CHCl$_3$ degassed for 20 mins (Ar) at 298 K after excitation at 365 nm. Data collected at λ_{max} = 470 nm.

Decay Lifetime Measurement of Ir(III) complex 2

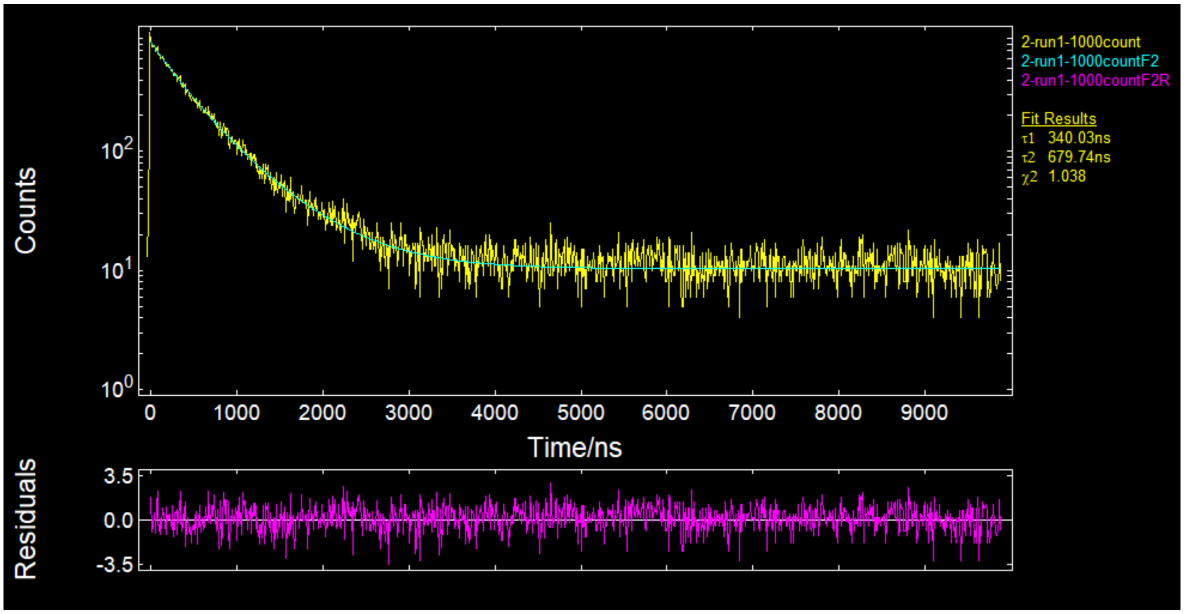

Figure S60. Monoexponential lifetime decay of Ir(III) complex **2**, ~$1{\cdot}10^{-5}$ M (Absorbance of 0.081 from UV-Vis) in $CHCl_3$ degassed for 20 mins (Ar) at 298 K after excitation at 365 nm. Data collected at λ_{max} = 540 nm.

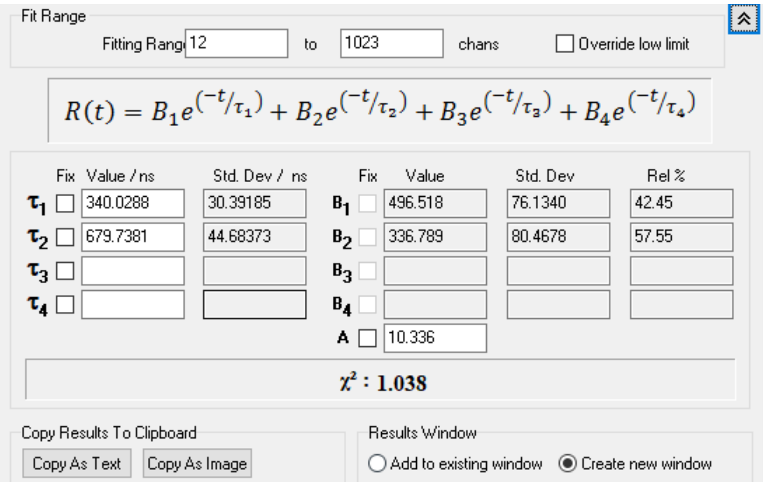

Fit Range

Fitting Rang 12 to 1023 chans ☐ Override low limit

$$R(t) = B_1 e^{\left(-t/\tau_1\right)} + B_2 e^{\left(-t/\tau_2\right)} + B_3 e^{\left(-t/\tau_3\right)} + B_4 e^{\left(-t/\tau_4\right)}$$

	Fix	Value / ns	Std. Dev / ns		Fix	Value	Std. Dev	Rel %
τ_1	☐	340.0288	30.39185	B_1	☐	496.518	76.1340	42.45
τ_2	☐	679.7381	44.68373	B_2	☐	336.789	80.4678	57.55
τ_3	☐			B_3	☐			
τ_4	☐			B_4	☐			
				A	☐	10.336		

χ^2 : 1.038

Copy Results To Clipboard

Results Window ○ Add to existing window ● Create new window

Figure S61. Fit result of Ir(III) complex **2**, ~$1{\cdot}10^{-5}$ M (Absorbance of 0.081 from UV-Vis) in $CHCl_3$ degassed for 20 mins (Ar) at 298 K after excitation at 365 nm. Data collected at λ_{max} = 540 nm.

Decay Lifetime Measurement of Ir(III) complex 3

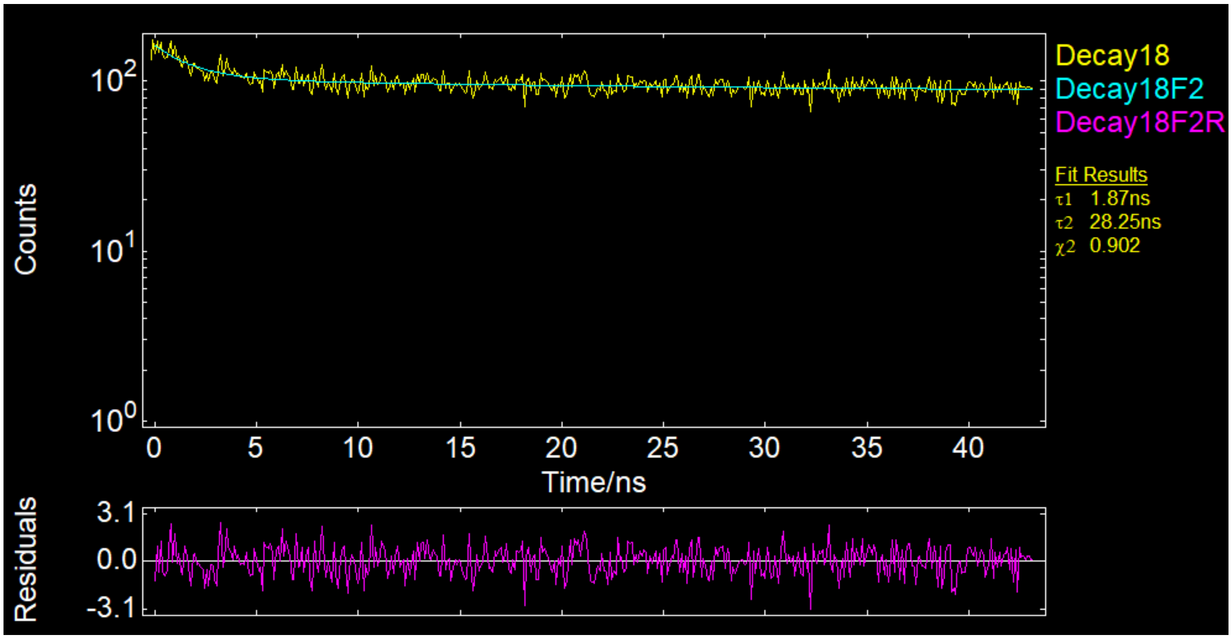

Figure S62. Biexponential lifetime decay of Ir(III) complex **3,** ~$1{\cdot}10^{-5}$ M (Absorbance of 0.079 from UV-Vis) in $CHCl_3$ degassed for 20 mins (Ar) at 298 K after excitation at 365 nm. Data collected at λ_{max} = 540 nm.

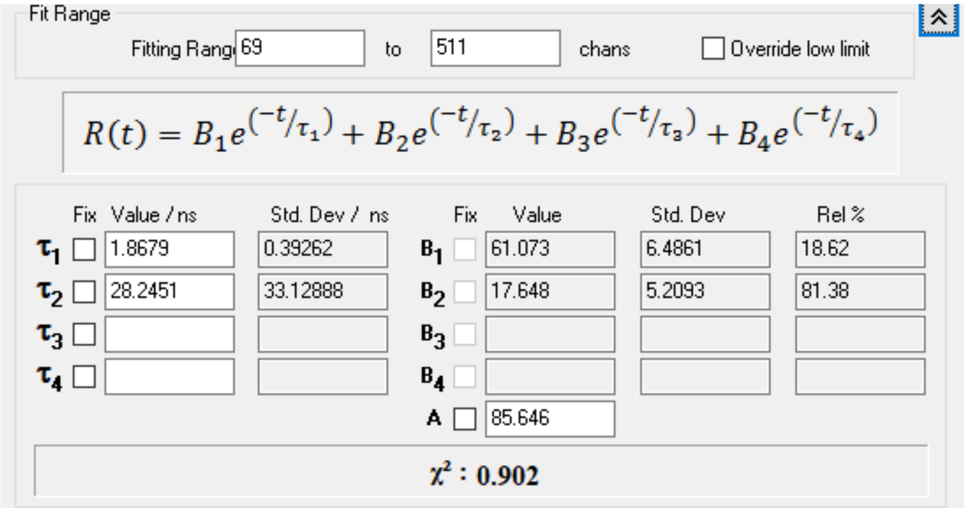

Fit Range

Fitting Rang 69 to 511 chans ☐ Override low limit

$$R(t) = B_1 e^{\left(-t/\tau_1\right)} + B_2 e^{\left(-t/\tau_2\right)} + B_3 e^{\left(-t/\tau_3\right)} + B_4 e^{\left(-t/\tau_4\right)}$$

	Fix	Value / ns	Std. Dev / ns		Fix	Value	Std. Dev	Rel %
τ_1	☐	1.8679	0.39262	B_1	☐	61.073	6.4861	18.62
τ_2	☐	28.2451	33.12888	B_2	☐	17.648	5.2093	81.38
τ_3	☐			B_3	☐			
τ_4	☐			B_4	☐			
				A	☐	85.646		

χ^2 : 0.902

Figure S63. Fit result of Ir(III) complex **3**, ~$1{\cdot}10^{-5}$ M (Absorbance of 0.079 from UV-Vis) in $CHCl_3$ degassed for 20 mins (Ar) at 298 K after excitation at 365 nm. Data collected at λ_{max} = 540 nm.

Decay Lifetime Measurement of Ir(III) complex 4

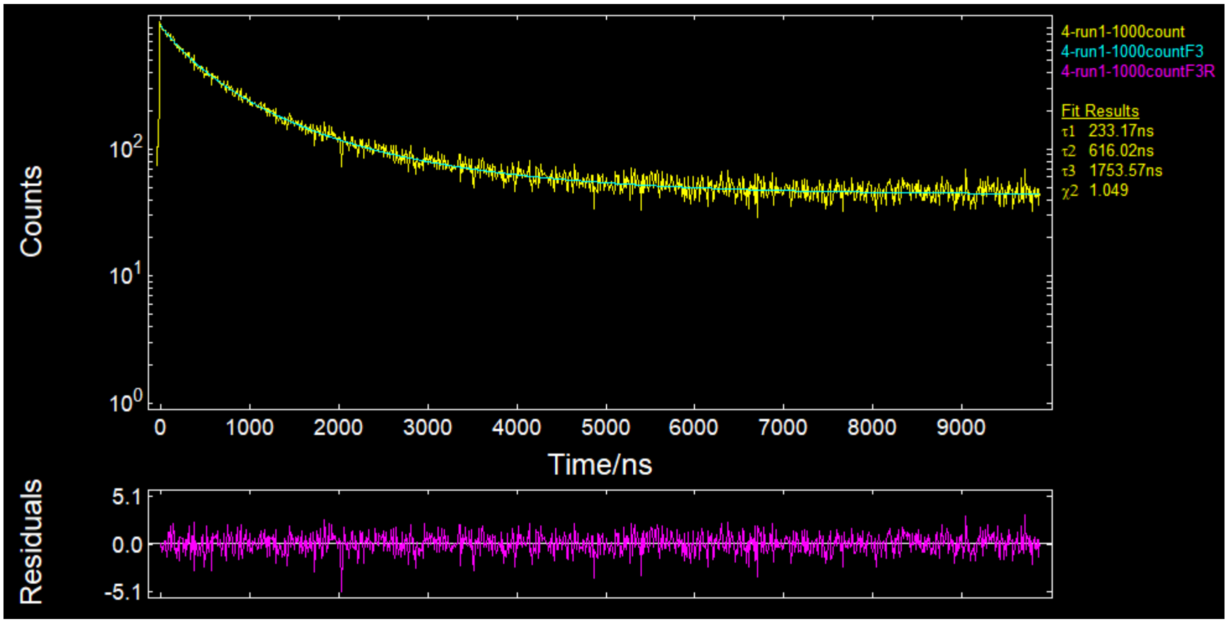

Figure S64. Biexponential lifetime decay of Ir(III) complex **4,** ~1·10^{-6} M (Absorbance of ? from UV-Vis) in CHCl$_3$ degassed for 20 mins (Ar) at 298 K after excitation at 365 nm. Data collected at λ_{max} = 540 nm.

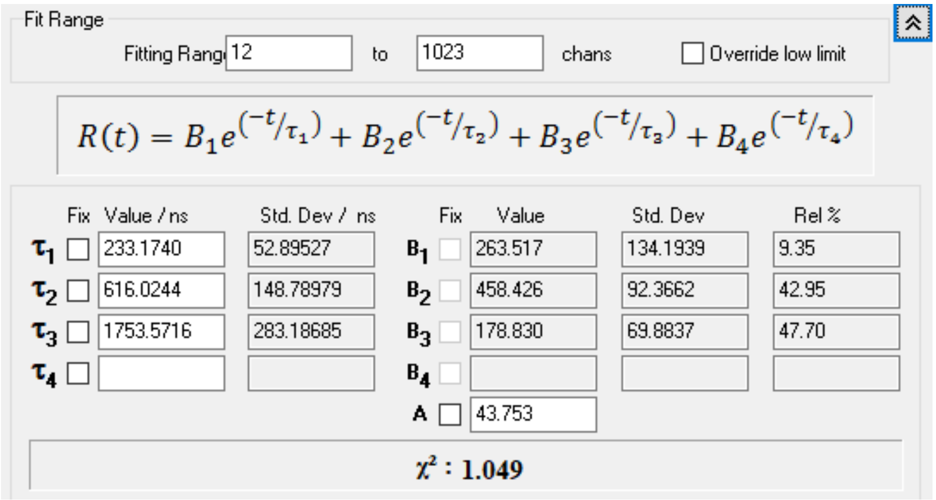

Fit Range

Fitting Range 12 to 1023 chans ☐ Override low limit

$$R(t) = B_1e^{(-t/\tau_1)} + B_2e^{(-t/\tau_2)} + B_3e^{(-t/\tau_3)} + B_4e^{(-t/\tau_4)}$$

	Fix	Value / ns	Std. Dev / ns		Fix	Value	Std. Dev	Rel %
τ_1	☐	233.1740	52.89527	B_1	☐	263.517	134.1939	9.35
τ_2	☐	616.0244	148.78979	B_2	☐	458.426	92.3662	42.95
τ_3	☐	1753.5716	283.18685	B_3	☐	178.830	69.8837	47.70
τ_4	☐			B_4	☐			
				A	☐	43.753		

χ^2 : 1.049

Figure S65. Fit result of Ir(III) complex **4**, ~1·10^{-6} M (Absorbance of ? from UV-Vis) in CHCl$_3$ degassed for 20 mins (Ar) at 298 K after excitation at 365 nm. Data collected at λ_{max} = 540 nm.

Decay Lifetime Measurement of Ir(III) complex 5

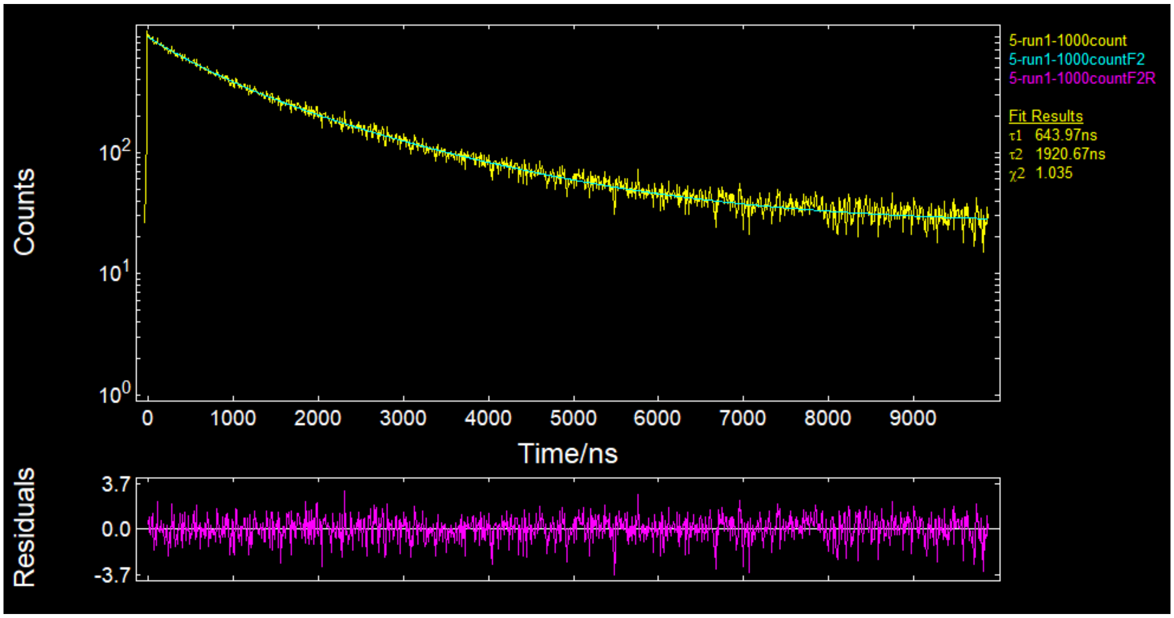

Figure S66. Biexponential lifetime decay of Ir(III) complex **5,** ~1·10^{-6} M (Absorbance of ? from UV-Vis) in $CHCl_3$ degassed for 20 mins (Ar) at 298 K after excitation at 365 nm. Data collected at λ_{max} = 540 nm.

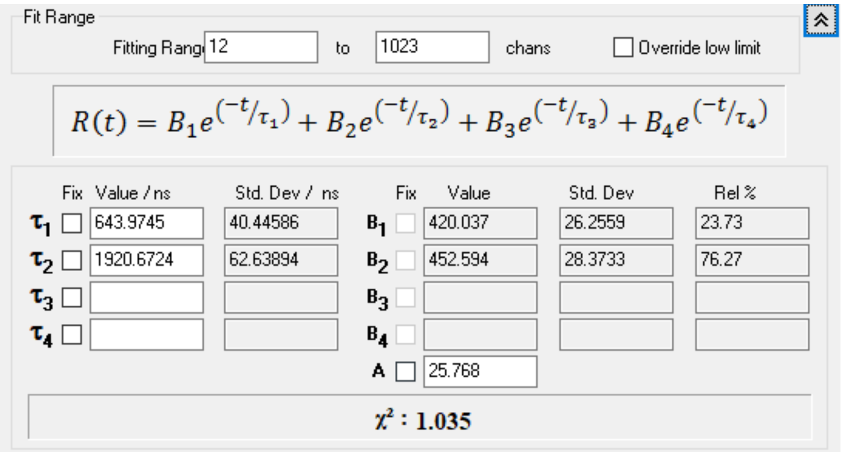

Fit Range

Fitting Rang 12 to 1023 chans ☐ Override low limit

$$R(t) = B_1 e^{\left(-t/\tau_1\right)} + B_2 e^{\left(-t/\tau_2\right)} + B_3 e^{\left(-t/\tau_3\right)} + B_4 e^{\left(-t/\tau_4\right)}$$

	Fix	Value / ns	Std. Dev / ns		Fix	Value	Std. Dev	Rel %
τ_1	☐	643.9745	40.44586	B_1	☐	420.037	26.2559	23.73
τ_2	☐	1920.6724	62.63894	B_2	☐	452.594	28.3733	76.27
τ_3	☐			B_3	☐			
τ_4	☐			B_4	☐			
				A	☐	25.768		

χ^2 : 1.035

Figure S67. Fit result of Ir(III) complex **5**, ~1·10^{-6} M (Absorbance of ? from UV-Vis) in $CHCl_3$ degassed for 20 mins (Ar) at 298 K after excitation at 365 nm. Data collected at λ_{max} = 540 nm.

SIX. High throughput hydrogen evolution condition screening

Table S3. Screening conditions for photocatalytic hydrogen generation with complex **2**. All variables were changed individually (varying condition highlighted in red), while all other conditions were consistent with the initial conditions. Initial conditions were determined from review of existing literature. Solvents are 5 mL 1:1 ratio unless specified otherwise, all screens were run for 5 hours before hydrogen evolution was measured. Hydrogen generation rate was calculated relative to time mols of H_2 and mass of PS.

Trial	**PS** (μmol)	**Co-Cat.** (mM)	**Solvent**	**LiCl** (M)	**pH**	**Electron donor** (M)	**Rate of H_2** (μmolg^{-1}hr^{-1}) **Run 1**	**Rate of H_2** (μmolg^{-1}hr^{-1}) **Run 2**
Initial	0.10	0.50	DMSO/H_2O	0.2	10	NEt_3 (0.3)	340.7	330.6
1	0.00	0.50	DMSO/H_2O	0.2	10	NEt_3 (0.3)	0	0
2	0.01	0.50	DMSO/H_2O	0.2	10	NEt_3 (0.3)	126.5	145.7
3	0.20	0.50	DMSO/H_2O	0.2	10	NEt_3 (0.3)	43.5	60.3
4	0.50	0.50	DMSO/H_2O	0.2	10	NEt_3 (0.3)	58.8	44.8
5	1.0	0.50	DMSO/H_2O	0.2	10	NEt_3 (0.3)	20.5	22.5
6	2.0	0.50	DMSO/H_2O	0.2	10	NEt_3 (0.3)	11.4	8.1
7	0.10	0.00	DMSO/H_2O	0.2	10	NEt_3 (0.3)	3.5	2.0
8	0.10	0.1	DMSO/H_2O	0.2	10	NEt_3 (0.3)	5.0	7.5
9	0.10	0.25	DMSO/H_2O	0.2	10	NEt_3 (0.3)	122.7	159.3
10	0.10	1.0	DMSO/H_2O	0.2	10	NEt_3 (0.3)	173.4	191.1
11	0.10	2.5	DMSO/H_2O	0.2	10	NEt_3 (0.3)	117.0	127.0
12	0.10	5.00	DMSO/H_2O	0.2	10	NEt_3 (0.3)	81.5	113.9
13	0.10	0.50	DMSO/H_2O 1:4	0.2	10	NEt_3 (0.3)	203.4	207.1
14	0.10	0.50	DMSO/H_2O 1:2	0.2	10	NEt_3 (0.3)	112.1	127.6

15	0.10	0.50	DMSO/H_2O 2:1	0.2	10	NEt_3 (0.3)	73.1	60.0
16	0.10	0.50	DMSO/H_2O 4:1	0.2	10	NEt_3 (0.3)	31.3	41.9
17	0.10	0.50	THF/H_2O	0.2	10	NEt_3 (0.3)	174.1	170.6
18	0.10	0.50	DMF/H_2O	0.2	10	NEt_3 (0.3)	450.2	444.4
19	0.10	0.50	MeCN/H_2O	0.2	10	NEt_3 (0.3)	279.5	298.7
20	0.10	0.50	H_2O	0.2	10	NEt_3 (0.3)	16.6	20.5
21	0.10	0.50	DMSO/H_2O	0.0	10	NEt_3 (0.3)	13.8	10.3
22	0.10	0.50	DMSO/H_2O	0.02	10	NEt_3 (0.3)	17.8	14.9
23	0.10	0.50	DMSO/H_2O	0.08	10	NEt_3 (0.3)	30.4	37.3
24	0.10	0.50	DMSO/H_2O	0.16	10	NEt_3 (0.3)	99.0	127.6
25	0.10	0.50	DMSO/H_2O	0.40	10	NEt_3 (0.3)	266.5	279.5
26	0.10	0.50	DMSO/H_2O	0.6	10	NEt_3 (0.3)	148.2	158.0
27	0.10	0.50	DMSO/H_2O	0.2	11	NEt_3 (0.3)	162.8	180.4
28	0.10	0.50	DMSO/H_2O	0.2	9	NEt_3 (0.3)	112.7	125.4
29	0.10	0.50	DMSO/H_2O	0.2	8	NEt_3 (0.3)	113.0	115.7
30	0.10	0.50	DMSO/H_2O	0.2	7	NEt_3 (0.3)	17.6	13.8
31	0.10	0.50	DMSO/H_2O	0.2	6	NEt_3 (0.3)	2.6	1.9
32	0.10	0.50	DMSO/H_2O	0.2	5	NEt_3 (0.3)	0	0
33	0.10	0.50	DMSO/H_2O	0.2	10	EDTA (0.3)	14.6	12.5
34	0.10	0.50	DMSO/H_2O	0.2	10	Na^+ ascorbate (0.3)	238.1	250.8
35	0.10	0.50	DMSO/H_2O	0.2	10	DMA (0.3)	5.8	11.5
36	0.10	0.50	DMSO/H_2O	0.2	10	TEOA (0.3)	40.5	13.2
37	0.10	0.50	DMSO/H_2O	0.2	10	MeOH (0.3)	0	0
38	0.10	0.50	DMSO/H_2O	0.2	10	NEt_3 (0.00)	0	0
39	0.10	0.50	DMSO/H_2O	0.2	10	NEt_3 (0.03)	7.9	11.4
40	0.10	0.50	DMSO/H_2O	0.2	10	NEt_3 (0.06)	15.5	18.5
41	0.10	0.50	DMSO/H_2O	0.2	10	NEt_3 (0.10)	152.1	160.3
42	0.10	0.50	DMSO/H_2O	0.2	10	NEt_3 (0.40)	190.7	200.1
43	0.10	0.50	DMSO/H_2O	0.2	10	NEt_3 (0.60)	165.2	157.9

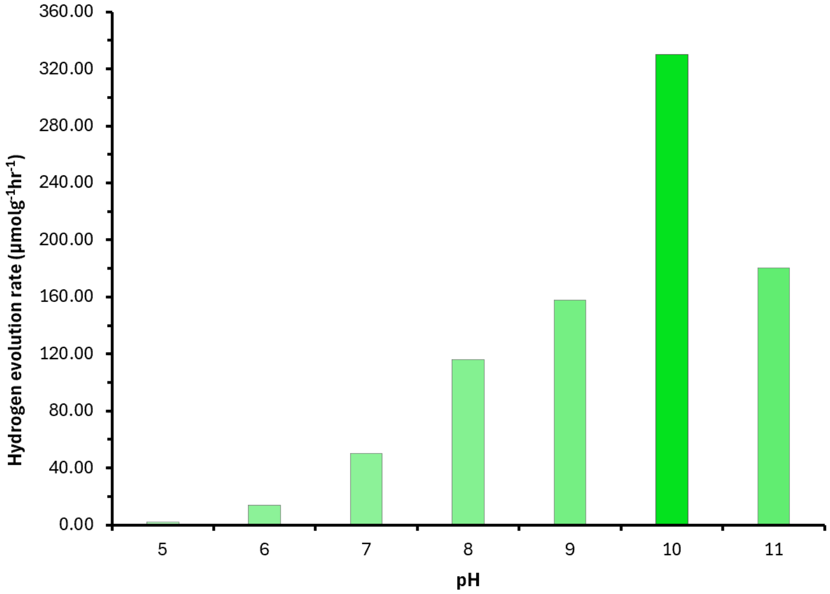

Figure S68. Hydrogen generation rate of complex **2** under different pH's, pH was adjusted using 36% HCl. All other conditions were kept consistent with initial conditions in the screen.

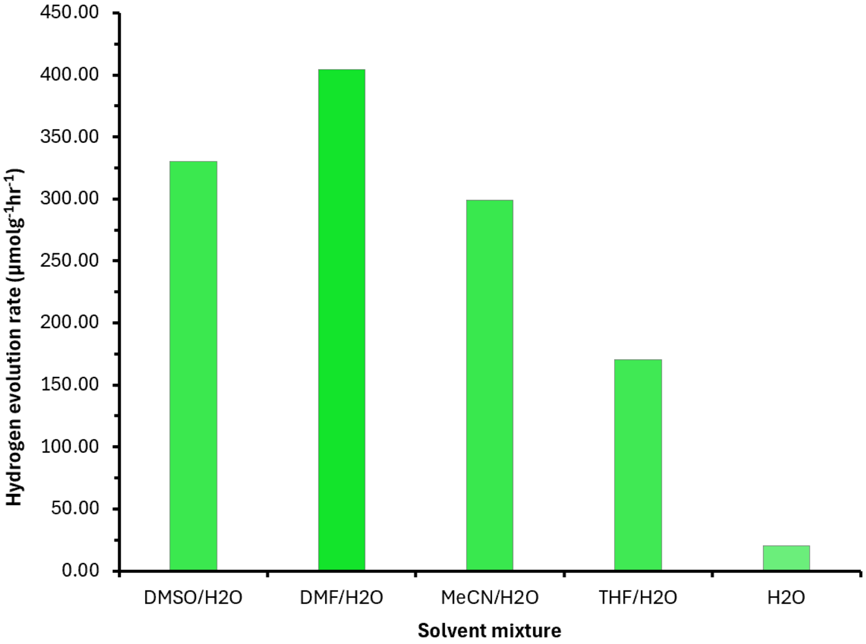

Figure S69. Hydrogen generation rate of complex **2** in different solvent systems, all other conditions were kept consistent with initial conditions in the screen.

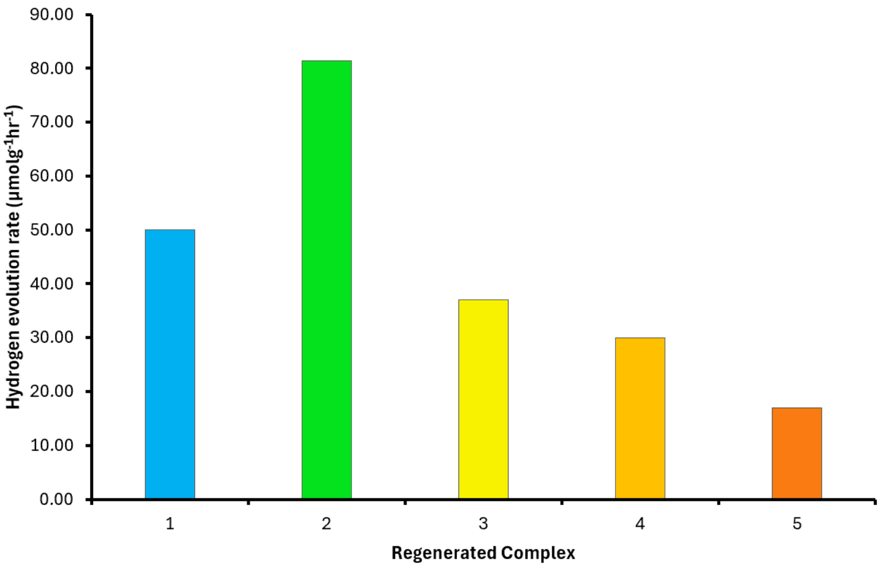

Figure S70. Hydrogen generation rate of complexes in the optimum conditions after the PS has been recycled. Regeneration runs were performed by correcting pH, degassing reaction solutions and adding an additional 0.1 M of sacrificial electron donor (NEt_3).

SX. DFT studies

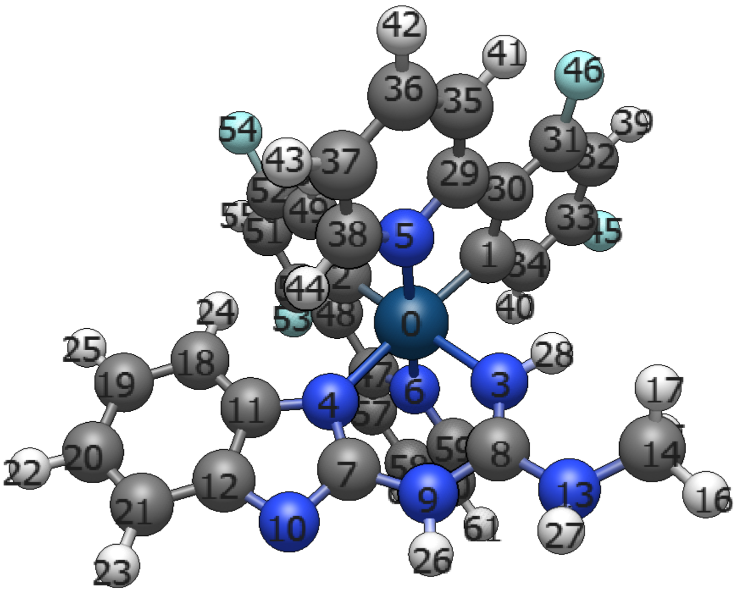

Figure S71. Optimised geometry model used for complex **1**. TD-DFT inputs and energy calculations were based upon this optimised input model.

Table S4. Cartesian coordinates for optimised compound **1**.

Center Number	Atomic Number	Atomic Type	Coordinates (Angstroms) X	Y	Z
0	77	0	-0.171892	-0.246907	0.141685
1	6	0	-2.101241	0.335505	0.327697
2	6	0	0.307171	1.624229	-0.442612
3	7	0	-0.747764	-2.211789	0.922212
4	7	0	1.809573	-1.176799	-0.136696
5	7	0	-0.902319	-0.860888	-1.695000
6	7	0	0.523247	0.520961	1.937096
7	6	0	2.176930	-2.376032	0.383076
8	6	0	-0.020860	-3.251195	1.223959
9	7	0	1.331791	-3.242753	1.102524
10	7	0	3.426802	-2.779592	0.214664
11	6	0	2.993070	-0.740846	-0.741047
12	6	0	3.980140	-1.741991	-0.508346
13	7	0	-0.534217	-4.416927	1.770080

14	6	0	-1.966385	-4.600716	1.944096
15	1	0	-2.366495	-3.822170	2.601560
16	1	0	-2.132159	-5.564339	2.430836
17	1	0	-2.528401	-4.587357	0.997855
18	6	0	3.301742	0.408201	-1.480547
19	6	0	4.602145	0.540022	-1.965901
20	6	0	5.581989	-0.444111	-1.729438
21	6	0	5.282729	-1.592109	-1.002308
22	1	0	6.585146	-0.303326	-2.124528
23	1	0	6.028348	-2.360731	-0.817936
24	1	0	2.559898	1.173608	-1.671851
25	1	0	4.864156	1.425403	-2.540001
26	1	0	1.850919	-4.027327	1.474074
27	1	0	-0.024794	-5.255191	1.520965
28	1	0	-1.746224	-2.378167	0.972876
29	6	0	-2.240887	-0.661785	-1.908874
30	6	0	-2.924769	-0.013295	-0.787413
31	6	0	-4.293032	0.295144	-0.738184
32	6	0	-4.885161	0.926717	0.342819
33	6	0	-4.056044	1.258683	1.410964
34	6	0	-2.695583	0.978008	1.422875
35	6	0	-2.810912	-1.061595	-3.128764
36	6	0	-2.017151	-1.646075	-4.108661
37	6	0	-0.654724	-1.832451	-3.869859
38	6	0	-0.136835	-1.426366	-2.647339
39	1	0	-5.944205	1.152646	0.349294
40	1	0	-2.113071	1.272504	2.289388
41	1	0	-3.865748	-0.902636	-3.296742
42	1	0	-2.459917	-1.948836	-5.053355
43	1	0	0.001177	-2.277926	-4.609864
44	1	0	0.910805	-1.536015	-2.395154
45	9	0	-4.610527	1.875672	2.474490
46	9	0	-5.109195	-0.028421	-1.774272
47	6	0	1.014909	1.799457	1.891207
48	6	0	0.879541	2.434486	0.584102
49	6	0	0.097211	2.197890	-1.705714
50	6	0	1.238809	3.756960	0.280710
51	6	0	1.051071	4.321954	-0.968878
52	6	0	0.468477	3.514425	-1.942240
53	9	0	1.792625	4.553320	1.229961
54	9	0	0.263188	4.044724	-3.165304
55	1	0	1.337288	5.346461	-1.170875
56	1	0	-0.343069	1.633838	-2.520409
57	6	0	1.567008	2.368685	3.052112
58	6	0	1.606695	1.642706	4.234317
59	6	0	0.562938	-0.174652	3.088643

```
  60         6         0       1.091558    0.344934    4.260390
  61         1         0       1.100766   -0.257063    5.162579
  62         1         0       2.036351    2.086067    5.128011
  63         1         0       0.147254   -1.172894    3.040856
  64         1         0       1.959758    3.373435    3.009604
---------------------------------------------------------------------
```

Energy

E(RB3LYP) = -2081.92244351 Hartree

Zero point corrected free energy = -2081.483288 Hartree

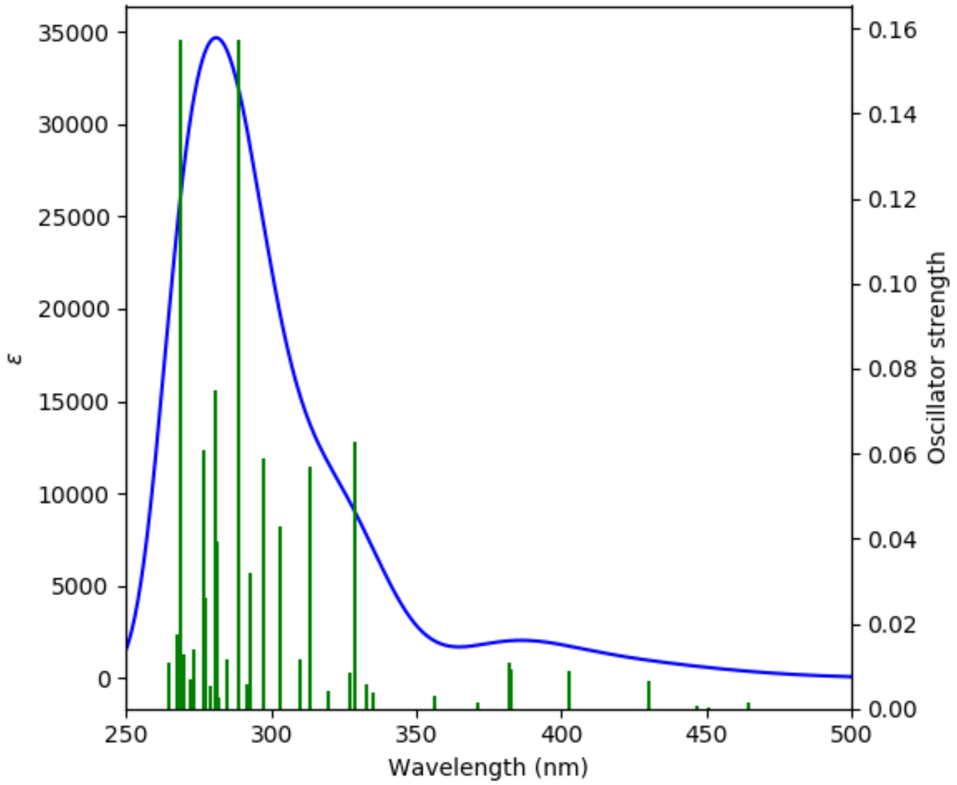

Figure S72. Calculated UV/vis spectrum for complex **1**.

Table S5. Calculated energy levels of ten highly contributing singlet states and first five triplet states for complex **1**.

Spin State	**Transition configurations**	**Excitation energy (eV, nm)**	**Oscillator strength**

S_5	HOMO-2→LUMO (95.7%)	3.0768, 402.97	0.0089
S_7	HOMO-2→LUMO+1 (72.5%) HOMO→LUMO+2 (22.9%)	3.2440, 382.19	0.0107
S_{13}	HOMO-4→LUMO (45.5%) HOMO-4→LUMO+1 (12.4%) HOMO-3→LUMO (8.9%) HOMO-2→LUMO+2 (27.2%)	3.7690, 328.96	0.0627
S_{16}	HOMO-5→LUMO (5.2%) HOMO-5→LUMO+1 (2.9%) HOMO-4→LUMO+1 (3.9%) HOMO-3→LUMO (3.3%) HOMO-3→LUMO+1 (68.6%) HOMO-2→LUMO+3 (7.9%)	3.9595, 313.13	0.0568
S_{18}	HOMO-7→LUMO (4.8%) HOMO-6→LUMO (68.2%) HOMO-5→LUMO (4.7%) HOMO-4→LUMO+2 (13.2%)	4.0933, 302.89	0.0430
S_{19}	HOMO-6→LUMO+1 (4.4%) HOMO-5→LUMO+1 (61.2%) HOMO-3→LUMO+1 (5.0%) HOMO-3→LUMO+2 (4.4%) HOMO-3→LUMO+3 (15.7%) HOMO-2→LUMO+3 (2.3%)	4.1691, 297.39	0.0590
S_{22}	HOMO-1→LUMO+4 (25.2%) HOMO→LUMO+4 (63.2%)	4.2957, 288.63	0.1574

S_{26}	HOMO-7→LUMO (3.2%) HOMO-6→LUMO (3.5%) HOMO-5→LUMO (2.1%) HOMO-5→LUMO+2 (5.7%) HOMO-4→LUMO+2 (25.4%) HOMO-4→LUMO+3 (35.2%) HOMO-3→LUMO+2 (5.8%) HOMO-1→LUMO+4 (5.3%) HOMO→LUMO+4 (3.2%)	4.4191, 280.56	0.0748
S_{29}	HOMO-6→LUMO (4.2%) HOMO-5→LUMO+2 (5.0%) HOMO-4→LUMO+2 (9.4%) HOMO-4→LUMO+3 (37.1%) HOMO-1→LUMO+5 (26.4%) HOMO-1→LUMO+6 (2.2%)	4.4833, 276.55	0.0610
S_{33}	HOMO-8→LUMO+1 (2.6%) HOMO-6→LUMO+1 (4.8%) HOMO-5→LUMO+1 (6.3%) HOMO-5→LUMO+2 (16.2%) HOMO-5→LUMO+3 (10.0%) HOMO-3→LUMO+3 (40.5%) HOMO-2→LUMO+5 (5.1%)	4.6138, 268.73	0.1575
T_1	HOMO-4→LUMO (3.5%) HOMO-2→LUMO (6.5%) HOMO-1→LUMO (13.2%)	2.6327, 470.94	0.0000

	HOMO→LUMO (72.5%)		
T_2	HOMO-1→LUMO (74.9%) HOMO→LUMO (19.7%)	2.7310, 453.98	0.0000
T_3	HOMO-2→LUMO+1 (7.9%) HOMO-1→LUMO+1 (15.3%) HOMO→LUMO+1 (74.3%)	2.7533, 450.31	0.0000
T_4	HOMO-3→LUMO+1 (10.1%) HOMO-2→LUMO+1 (4.4%) HOMO-1→LUMO+1 (70.0%) HOMO→LUMO+1 (8.1%)	2.7977, 443.16	0.0000
T_5	HOMO-6→LUMO (4.8%) HOMO-5→LUMO (8.4%) HOMO-4→LUMO (6.2%) HOMO-2→LUMO (52.9%) HOMO-1→LUMO (7.9%) HOMO-1→LUMO+1 (3.0%) HOMO→LUMO (6.0%)	2.8349, 437.34	0.0000

Table S6. Calculated MO energies of orbitals involved in transitions for **1**.

Orbital	**Energy/ eV**		**Orbital**	**Energy/ eV**
LUMO+6	0.38		HOMO	-4.75
LUMO+5	0.11		HOMO-1	-4.90
LUMO+4	0.09		HOMO-2	-5.42
LUMO+3	-0.84		HOMO-3	-5.98

LUMO+2	-1.00		HOMO-4	-6.03
LUMO+1	-1.42		HOMO-5	-6.20
LUMO	-1.59		HOMO-6	-6.27
			HOMO-7	-6.48
			HOMO-8	-6.65

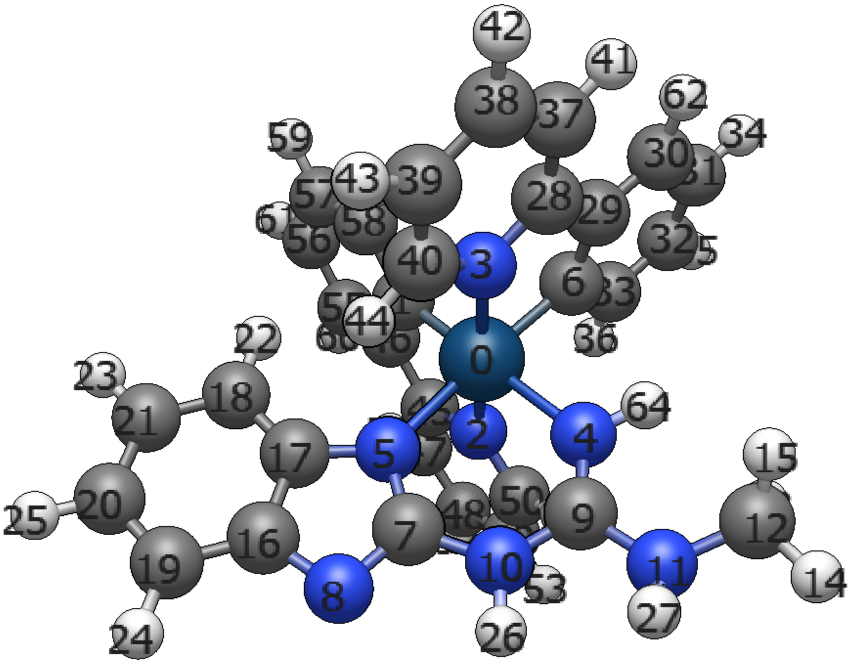

Figure S73. Optimised geometry model used for complex **2**. TD-DFT inputs and energy calculations were based upon this optimised input model.

Table S7. Cartesian coordinates for optimised compound **2**.

```
---------------------------------------------------------------------
 Center     Atomic      Atomic             Coordinates (Angstroms)
 Number     Number       Type             X           Y           Z
---------------------------------------------------------------------
      0         77           0       -0.350798    0.032475    0.115016
      1          6           0        0.171735    1.782974   -0.750275
      2          7           0        0.369842    1.051162    1.770233
```

3	7	0	-1.101281	-0.840399	-1.605580
4	7	0	-0.968881	-1.774459	1.202526
5	7	0	1.609986	-0.991124	-0.023415
6	6	0	-2.269852	0.676979	0.207922
7	6	0	1.942142	-2.117074	0.657057
8	7	0	3.175873	-2.586525	0.537731
9	6	0	-0.271309	-2.781986	1.643763
10	7	0	1.078342	-2.843196	1.499870
11	7	0	-0.809978	-3.836972	2.367730
12	6	0	-2.244788	-3.943550	2.579463
13	1	0	-2.609250	-3.064574	3.120771
14	1	0	-2.435756	-4.820489	3.202192
15	1	0	-2.820335	-4.046143	1.646753
16	6	0	3.755024	-1.681998	-0.329025
17	6	0	2.799622	-0.688309	-0.692087
18	6	0	3.137237	0.335496	-1.586780
19	6	0	5.055204	-1.649108	-0.850614
20	6	0	5.383474	-0.625195	-1.734125
21	6	0	4.434854	0.351253	-2.096998
22	1	0	2.419423	1.094427	-1.872860
23	1	0	4.719812	1.138897	-2.790437
24	1	0	5.777001	-2.410358	-0.566848
25	1	0	6.385596	-0.577061	-2.153728
26	1	0	1.577056	-3.582857	1.976328
27	1	0	-0.337338	-4.720827	2.226117
28	6	0	-2.436632	-0.648078	-1.834179
29	6	0	-3.108806	0.178099	-0.828425
30	6	0	-4.481159	0.481019	-0.870397
31	6	0	-5.047553	1.288167	0.109450
32	6	0	-4.237931	1.796333	1.132869
33	6	0	-2.875768	1.494792	1.177095
34	1	0	-6.107559	1.524712	0.076720
35	1	0	-4.674971	2.434995	1.897743
36	1	0	-2.271822	1.909297	1.980354
37	6	0	-3.032095	-1.216312	-2.969934
38	6	0	-2.269986	-1.962467	-3.860035
39	6	0	-0.906793	-2.137770	-3.609624
40	6	0	-0.361427	-1.560768	-2.470240
41	1	0	-4.089567	-1.061862	-3.151884
42	1	0	-2.731447	-2.398193	-4.741819
43	1	0	-0.271264	-2.705529	-4.280530
44	1	0	0.688079	-1.653102	-2.218306
45	6	0	0.885315	2.294163	1.518440
46	6	0	0.763280	2.729359	0.130808
47	6	0	1.455751	3.032048	2.567822
48	6	0	1.494072	2.510915	3.852758

49	6	0	0.955353	1.242654	4.088482
50	6	0	0.407464	0.549941	3.019272
51	1	0	1.870889	4.012055	2.363375
52	1	0	1.938992	3.082991	4.661968
53	1	0	0.962561	0.793853	5.075936
54	1	0	-0.025204	-0.435567	3.135911
55	6	0	1.176878	3.994658	-0.321406
56	6	0	0.998540	4.353342	-1.651511
57	6	0	0.394706	3.444923	-2.530262
58	6	0	-0.012044	2.187270	-2.084611
59	1	0	0.242824	3.722829	-3.571170
60	1	0	1.635389	4.704786	0.362270
61	1	0	1.318322	5.330553	-2.002347
62	1	0	-5.111539	0.092123	-1.666592
63	1	0	-0.471384	1.505362	-2.795094
64	1	0	-1.971413	-1.890892	1.297244

Energy

E(RB3LYP) = -1684.98688716 Hartree

Zero point corrected free energy = -1684.512942 Hartree

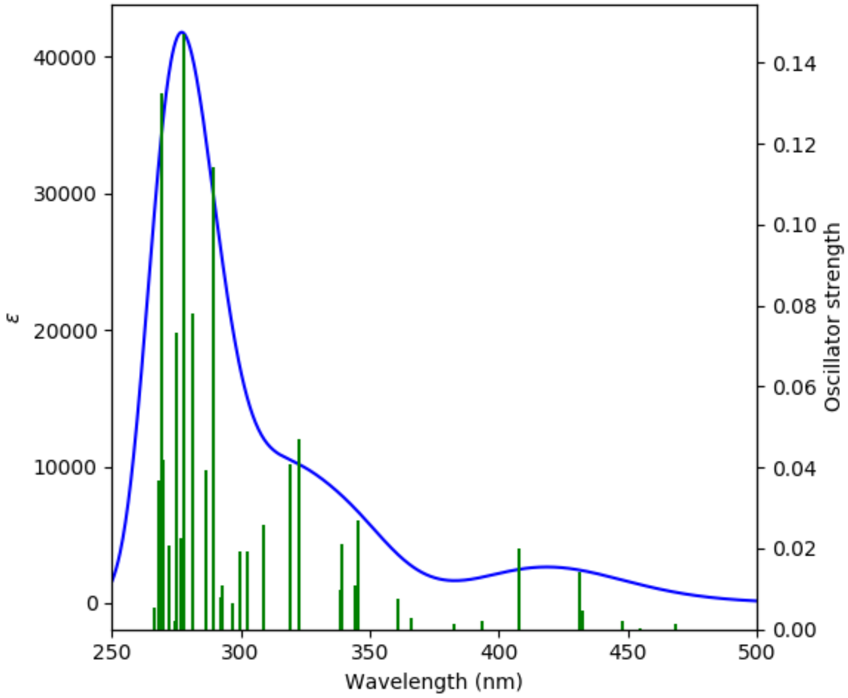

Figure S74. Calculated UV/vis spectrum for complex **2**.

Table S8. Calculated energy levels of ten highly contributing singlet states and first five triplet states for complex **2**.

Spin State	**Transition configurations**	**Excitation energy (eV, nm)**	**Oscillator strength**
S_5	HOMO-2→LUMO (90.7%) HOMO→LUMO (4.6%)	2.8732, 531.51	0.0141
S_6	HOMO-2→LUMO+1 (92.4%) HOMO-1→LUMO+1 (2.2%)	408.15	0.0200
S_{12}	HOMO-4→LUMO (2.3%) HOMO-3→LUMO (19.5%) HOMO-2→LUMO+3 (73.2%)	3.5871, 345.63	0.0269
S_{14}	HOMO-4→LUMO (46.4%) HOMO-3→LUMO (25.7%) HOMO-3→LUMO+1 (18.5%) HOMO-2→LUMO+3 (2.0%)	3.6541, 339.30	0.0212
S_{16}	HOMO-5→LUMO (80.2%) HOMO-4→LUMO (5.6%) HOMO-4→LUMO+1 (2.3%) HOMO-3→LUMO+2 (6.4%)	3.8447, 322.48	0.0471
S_{17}	HOMO-6→LUMO+1 (2.1%) HOMO-4→LUMO+1 (84.4%)	3.8864, 319.02	0.0409
S_{24}	HOMO-7→LUMO (3.6%) HOMO-5→LUMO+2 (3.2%) HOMO-1→LUMO+4 (27.9%)	4.2862, 289.26	0.1142

	HOMO→LUMO+4 (57.3%)		
S_{26}	HOMO-1→LUMO+4 (61.1%) HOMO→LUMO+4 (30.1%)	4.4046, 281.49	0.0781
S_{27}	HOMO-7→LUMO (19.4%) HOMO-7→LUMO+1 (7.7%) HOMO-6→LUMO+1 (7.3%) HOMO-5→LUMO+2 (11.8%) HOMO-5→LUMO+3 (20.6%) HOMO-4→LUMO+3 (10.6%) HOMO-3→LUMO+2 (4.6%) HOMO-2→LUMO+5 (3.9%)	4.4604, 277.96	0.1472
S_{33}	HOMO-6→LUMO+1 (8.4%) HOMO-5→LUMO+3 (12.1%) HOMO-4→LUMO+3 (14.5%) HOMO-4→LUMO+9 (3.1%) HOMO-2→LUMO+4 (6.7%) HOMO-2→LUMO+5 (3.2%) HOMO-1→LUMO+6 (11.2%) HOMO-1→LUMO+7 (3.2%) HOMO-1→LUMO+8 (5.1%) HOMO-1→LUMO+9 (9.5%)	4.6044, 269.27	0.1326
T_1	HOMO-5→LUMO (3.6%) HOMO-3→LUMO (5.0%) HOMO-2→LUMO (34.0%) HOMO-1→LUMO (13.8%)	2.5568, 484.91	0.0000

	HOMO→LUMO (36.0%)		
T$_2$	HOMO-5→LUMO+1 (2.9%) HOMO-4→LUMO+1 (4.9%) HOMO-2→LUMO+1 (59.9%) HOMO-1→LUMO+1 (6.0%) HOMO→LUMO+1 (18.8%)	2.6455, 468.66	0.0000
T$_3$	HOMO-2→LUMO (18.9%) HOMO-1→LUMO (14.8%) HOMO→LUMO (60.0%)	2.7061, 458.17	0.0000
T$_4$	HOMO-5→LUMO (3.4%) HOMO-2→LUMO (24.1%) HOMO-1→LUMO (60.7%) HOMO-1→LUMO+1 (5.9%)	2.7147, 456.72	0.0000
T$_5$	HOMO-4→LUMO+1 (11.1%) HOMO-2→LUMO (2.4%) HOMO-2→LUMO+1 (6.6%) HOMO-1→LUMO (5.0%) HOMO-1→LUMO+1 (62.6%) HOMO→LUMO+1 (6.3%)	2.7508, 450.71	0.0000

Table S9. Calculated MO energies of orbitals involved in transitions for **2**.

Orbital	**Energy/ eV**		**Orbital**	**Energy/ eV**
LUMO+9	1.12		HOMO	-4.55
LUMO+8	1.05		HOMO-1	-4.68
LUMO+7	0.80		HOMO-2	-4.99

LUMO+6	0.76		HOMO-3	-5.71
LUMO+5	0.51		HOMO-4	-5.74
LUMO+4	0.30		HOMO-5	-5.84
LUMO+3	-0.72		HOMO-6	-6.08
LUMO+2	-0.88		HOMO-7	-6.26
LUMO+1	-1.22			
LUMO	-1.39			

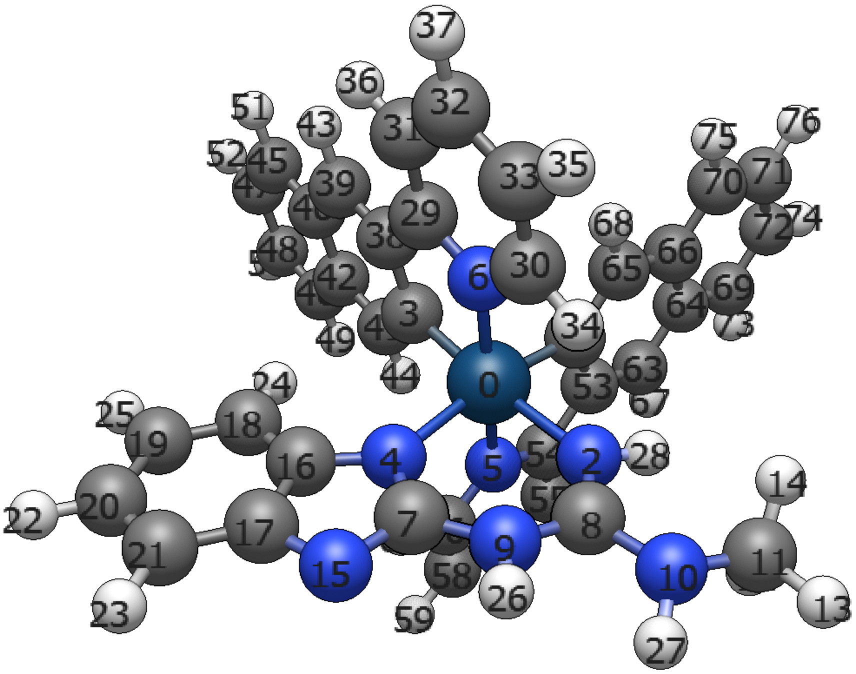

Figure S75. Optimised geometry model used for complex **3**. TD-DFT inputs and energy calculations were based upon this optimised input model.

Table S10. Cartesian coordinates for optimised compound **3**.

Center Number	Atomic Number	Atomic Type	Coordinates (Angstroms) X	Y	Z
0	77	0	-0.044514	-0.547528	0.020287
1	6	0	1.943088	-0.150632	-0.049437
2	7	0	0.452295	-2.687304	0.067019
3	6	0	-0.408302	1.441331	0.117759
4	7	0	-2.142416	-1.258989	-0.092066
5	7	0	0.238260	-0.587128	-2.027543
6	7	0	-0.288742	-0.341750	2.067465
7	6	0	-2.528566	-2.548923	0.078131
8	6	0	-0.312806	-3.737997	0.155381
9	7	0	-1.662044	-3.641126	0.277812
10	7	0	0.166764	-5.039454	0.215627
11	6	0	1.582807	-5.323884	0.045013
12	1	0	1.976561	-5.020824	-0.937200
13	1	0	1.733099	-6.399541	0.161453
14	1	0	2.162917	-4.820645	0.825223
15	7	0	-3.824213	-2.827886	0.061432
16	6	0	-3.366967	-0.603296	-0.251797
17	6	0	-4.392408	-1.587967	-0.149514
18	6	0	-3.686247	0.739575	-0.491408
19	6	0	-5.033907	1.075543	-0.614739
20	6	0	-6.049972	0.105581	-0.506046
21	6	0	-5.741896	-1.231646	-0.274483
22	1	0	-7.089444	0.408569	-0.607518
23	1	0	-6.516708	-1.989349	-0.193475
24	1	0	-2.915181	1.495084	-0.577777
25	1	0	-5.304564	2.112541	-0.798260
26	1	0	-2.186109	-4.482810	0.477314
27	1	0	-0.453698	-5.728905	-0.189623
28	1	0	1.430083	-2.899326	-0.095507
29	6	0	-0.613177	0.913308	2.503438
30	6	0	-0.200143	-1.354933	2.949972
31	6	0	-0.856455	1.132408	3.867843
32	6	0	-0.765763	0.085708	4.773977
33	6	0	-0.427035	-1.187461	4.307976
34	1	0	0.065966	-2.315111	2.526951
35	1	0	-0.344603	-2.036888	4.977487
36	1	0	-1.121612	2.126736	4.207545
37	1	0	-0.957920	0.257212	5.829202
38	6	0	-0.661659	1.928159	1.451249
39	6	0	-0.915844	3.267158	1.702089

40	6	0	-0.924165	4.215837	0.654936
41	6	0	-0.400033	2.379298	-0.901098
42	6	0	-0.653097	3.759082	-0.677816
43	1	0	-1.110117	3.622820	2.711546
44	1	0	-0.205778	2.069574	-1.925462
45	6	0	-1.181831	5.596679	0.878928
46	6	0	-0.652895	4.714943	-1.731344
47	6	0	-1.174077	6.494067	-0.164125
48	6	0	-0.906276	6.045422	-1.483120
49	1	0	-0.448798	4.373654	-2.743822
50	1	0	-0.902712	6.760976	-2.301507
51	1	0	-1.386500	5.932061	1.893585
52	1	0	-1.372943	7.546856	0.017145
53	6	0	2.492659	-0.157554	-1.384774
54	6	0	1.519364	-0.382324	-2.459407
55	6	0	1.796508	-0.388927	-3.833771
56	6	0	-0.753188	-0.786326	-2.917661
57	6	0	0.775320	-0.597925	-4.752194
58	6	0	-0.526531	-0.799121	-4.287666
59	1	0	-1.356812	-0.958458	-4.967110
60	1	0	-1.738362	-0.927816	-2.490297
61	1	0	2.811828	-0.221527	-4.174643
62	1	0	0.990126	-0.598551	-5.817087
63	6	0	3.845372	0.035494	-1.615770
64	6	0	4.743289	0.252921	-0.545162
65	6	0	2.827667	0.065742	0.992830
66	6	0	4.219962	0.269364	0.790644
67	1	0	4.251118	0.025599	-2.625322
68	1	0	2.461637	0.089662	2.017373
69	6	0	6.136692	0.453596	-0.748628
70	6	0	5.123086	0.490007	1.866888
71	6	0	6.467555	0.681952	1.638096
72	6	0	6.982487	0.663498	0.316568
73	1	0	6.523658	0.440817	-1.765527
74	1	0	8.045144	0.817748	0.150068
75	1	0	4.729910	0.507502	2.880971
76	1	0	7.142366	0.850907	2.473401

Energy

E(RB3LYP) = -1992.26001155 Hartree

Zero point corrected free energy = -1991.700311 Hartree

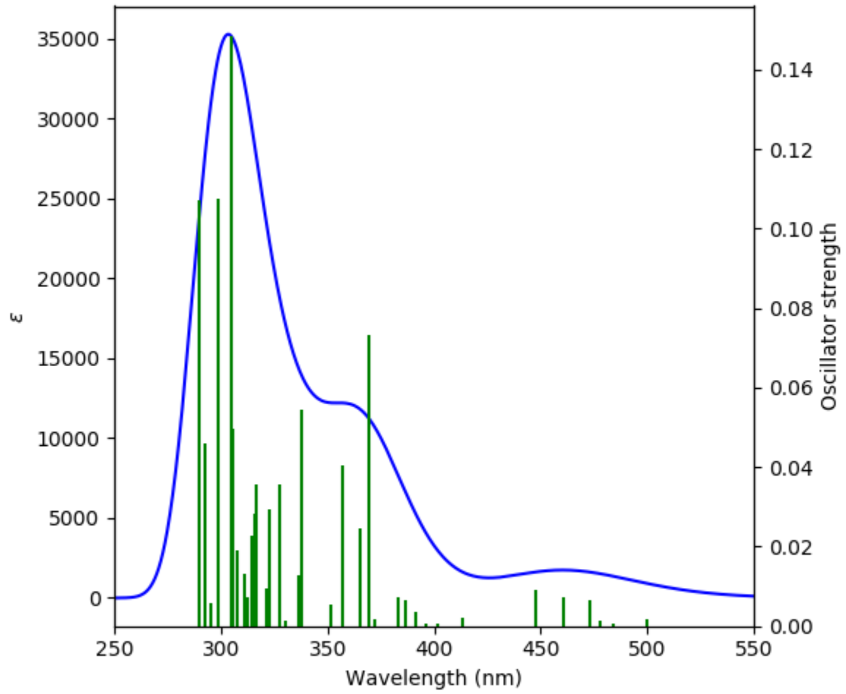

Figure S76. Calculated UV/vis spectrum for complex **3**.

Table S11. Calculated energy levels of ten highly contributing singlet states and first five triplet states for complex **3**.

Spin State	Transition configurations	Excitation energy (eV, nm)	Oscillator strength
S_6	HOMO-2→LUMO+1 (94.7%)	2.7698, 447.64	0.0090
S_{14}	HOMO-6→LUMO (6.6%) HOMO-5→LUMO (5.3%) HOMO-4→LUMO (73.1%) HOMO-3→LUMO (4.0%) HOMO-2→LUMO+3 (3.4%)	3.3556, 369.48	0.0733
S_{16}	HOMO-6→LUMO+1 (5.2%)	3.4763, 356.65	0.0403

	HOMO-5→LUMO (2.0%) HOMO-5→LUMO+1 (16.8%) HOMO-4→LUMO+1 (56.8%) HOMO-3→LUMO+1 (9.3%)		
S_{18}	HOMO-7→LUMO+1 (3.4%) HOMO-6→LUMO (15.3%) HOMO-6→LUMO+1 (5.9%) HOMO-5→LUMO (3.7%) HOMO-5→LUMO+1 (50.7%) HOMO-4→LUMO (2.3%) HOMO-4→LUMO+1 (10.1%) HOMO-2→LUMO+5 (2.5%)	3.6696, 337.86	0.0545
S_{21}	HOMO-7→LUMO (35.4%) HOMO-6→LUMO (2.2%) HOMO-5→LUMO+2 (7.8%) HOMO-4→LUMO+2 (34.3%) HOMO-3→LUMO+2 (4.6%) HOMO-2→LUMO+4 (7.1%)	3.7832, 327.72	0.0355
S_{24}	HOMO-7→LUMO (17.4%) HOMO-7→LUMO+1 (3.7%) HOMO-6→LUMO+2 (2.5%) HOMO-4→LUMO+2 (30.1%) HOMO-4→LUMO+3 (10.0%) HOMO-3→LUMO+3 (13.0%) HOMO-2→LUMO+4 (6.0%)	3.9220, 316.12	0.0357

	HOMO-1→LUMO+4 (6.5%)		
S_{26}	HOMO-7→LUMO (2.9%) HOMO-7→LUMO+1 (2.0%) HOMO-6→LUMO+1 (4.1%) HOMO-4→LUMO+2 (3.7%) HOMO-1→LUMO+4 (72.3%) HOMO→LUMO+4 (5.2%)	3.9410, 314.60	0.0226
S_{30}	HOMO-7→LUMO (2.7%) HOMO-5→LUMO+2 (2.6%) HOMO-2→LUMO+4 (19.1%) HOMO-2→LUMO+5 (2.4%) HOMO-1→LUMO+5 (66.6%)	4.0581, 305.52	0.0495
S_{31}	HOMO-7→LUMO (3.9%) HOMO-7→LUMO+1 (19.4%) HOMO-5→LUMO+3 (7.1%) HOMO-2→LUMO+4 (37.7%) HOMO-1→LUMO+5 (15.3%)	4.0659, 304.93	0.1486
S_{34}	HOMO-6→LUMO+2 (36.4%) HOMO-5→LUMO+3 (11.5%) HOMO-4→LUMO+2 (3.0%) HOMO-2→LUMO+5 (29.8%) HOMO→LUMO+6 (7.2%)	4.2359, 292.70	0.0459
T_1	HOMO-4→LUMO+1 (5.6%) HOMO-3→LUMO+1 (18.1%) HOMO-3→LUMO+3 (2.6%)	2.2827, 543.14	0.0000

	HOMO-3→LUMO+5 (2.6%) HOMO-2→LUMO (9.5%) HOMO-2→LUMO+1 (36.6%) HOMO-2→LUMO+3 (3.0%) HOMO-2→LUMO+5 (5.3%) HOMO-1→LUMO+1 (4.8%)		
T_2	HOMO-7→LUMO (3.8%) HOMO-4→LUMO (16.2%) HOMO-3→LUMO (28.8%) HOMO-3→LUMO+2 (3.4%) HOMO-3→LUMO+4 (4.6%) HOMO-2→LUMO (21.7%) HOMO-2→LUMO+1 (4.6%)	2.3250, 533.28	0.0000
T_3	HOMO-5→LUMO (2.2%) HOMO-4→LUMO (4.2%) HOMO-2→LUMO (11.1%) HOMO-1→LUMO (14.9%) HOMO→LUMO (61.2%)	2.4445, 507.19	0.0000
T_4	HOMO-2→LUMO (5.3%) HOMO-1→LUMO (52.9%) HOMO→LUMO (30.9%) HOMO→LUMO+1 (3.3%)	2.5492, 486.36	0.0000
T_5	HOMO-4→LUMO+1 (3.9%) HOMO-3→LUMO+1 (2.5%) HOMO-2→LUMO (2.5%) HOMO-1→LUMO (7.8%) HOMO-1→LUMO+1 (6.1%)	2.5830, 480.01	0.0000

	HOMO→LUMO+1 (71.7%)		

Table S12. Calculated MO energies of orbitals involved in transitions for **3**.

Orbital	**Energy/ eV**		**Orbital**	**Energy/ eV**
LUMO+6	0.28		HOMO	-4.57
LUMO+5	-0.09		HOMO-1	-4.70
LUMO+4	-0.29		HOMO-2	-4.86
LUMO+3	-0.91		HOMO-3	-5.35
LUMO+2	-1.05		HOMO-4	-5.53
LUMO+1	-1.45		HOMO-5	-5.78
LUMO	-1.62		HOMO-6	-5.91
			HOMO-7	-5.97

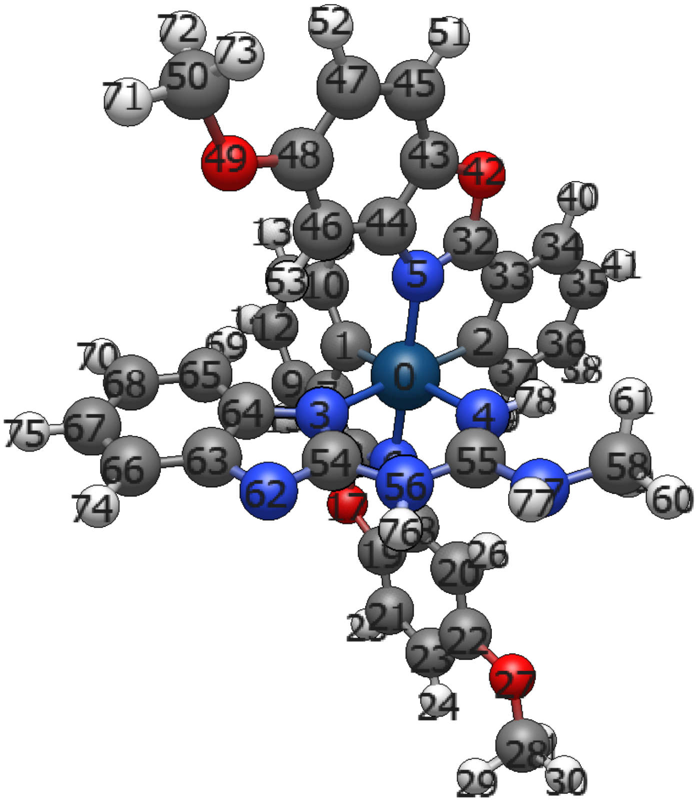

Figure S77. Optimised geometry model used for complex **4**. TD-DFT inputs and energy calculations were based upon this optimised input model.

Table S13. Cartesian coordinates for optimised compound **4**.

Center Number	Atomic Number	Atomic Type	Coordinates (Angstroms)		
			X	Y	Z
0	77	0	-0.073521	0.518463	0.191790
1	6	0	0.220205	0.369534	2.202812
2	6	0	-0.365663	2.530604	0.415895
3	7	0	0.324831	-1.587367	-0.321740
4	7	0	-0.517715	0.747770	-1.931518
5	7	0	1.832508	1.223836	-0.225640
6	7	0	-1.971918	-0.061071	0.808921
7	6	0	-0.913882	-0.062161	2.951395
8	6	0	-2.049024	-0.290637	2.110943
9	6	0	-0.907396	-0.222145	4.346447
10	6	0	1.367325	0.666820	2.959889

11	6	0	1.384005	0.518056	4.348021
12	6	0	0.254007	0.068222	5.048631
13	1	0	2.293099	0.750817	4.898588
14	1	0	0.287298	-0.047663	6.128047
15	1	0	-1.801131	-0.566206	4.860191
16	1	0	2.271512	1.002925	2.459888
17	8	0	-3.267017	-0.714821	2.516598
18	6	0	-3.230652	-0.349880	0.285195
19	6	0	-4.031469	-0.759024	1.363653
20	6	0	-3.759745	-0.288396	-0.998969
21	6	0	-5.354061	-1.126003	1.225257
22	6	0	-5.103471	-0.657111	-1.161137
23	6	0	-5.890343	-1.071126	-0.067471
24	1	0	-6.925472	-1.354096	-0.212656
25	1	0	-5.951821	-1.442388	2.072983
26	1	0	-3.175262	0.027363	-1.852363
27	8	0	-5.570487	-0.577619	-2.443858
28	6	0	-6.912541	-0.953715	-2.701652
29	1	0	-7.097128	-2.003631	-2.437871
30	1	0	-7.058382	-0.822503	-3.775575
31	1	0	-7.624247	-0.315548	-2.160579
32	6	0	1.924825	2.542122	-0.198901
33	6	0	0.777365	3.338155	0.136139
34	6	0	0.767130	4.740973	0.192212
35	6	0	-0.412239	5.388847	0.537471
36	6	0	-1.556625	4.628201	0.819550
37	6	0	-1.533288	3.232157	0.760402
38	1	0	-2.479134	5.136488	1.092471
39	1	0	-2.442743	2.682159	0.988050
40	1	0	1.670350	5.303788	-0.029214
41	1	0	-0.447204	6.473280	0.590468
42	8	0	3.158101	3.007777	-0.500169
43	6	0	3.918295	1.871753	-0.736469
44	6	0	3.098110	0.744606	-0.566408
45	6	0	5.252682	1.787262	-1.077650
46	6	0	3.606656	-0.538305	-0.733213
47	6	0	5.772505	0.498807	-1.252634
48	6	0	4.962569	-0.644176	-1.081400
49	8	0	5.417416	-1.920015	-1.236938
50	6	0	6.781560	-2.126711	-1.558355
51	1	0	5.870810	2.669669	-1.202286
52	1	0	6.816595	0.392949	-1.520164
53	1	0	3.002531	-1.425607	-0.589259
54	6	0	0.009956	-2.156129	-1.512536
55	6	0	-0.630417	-0.143824	-2.873785
56	7	0	-0.486998	-1.471963	-2.636613

57	7	0	-0.978692	0.161038	-4.182128
58	6	0	-1.116291	1.540344	-4.620759
59	1	0	-1.899011	2.041451	-4.042274
60	1	0	-1.428464	1.537701	-5.667533
61	1	0	-0.186117	2.123151	-4.535883
62	7	0	0.179055	-3.463169	-1.651943
63	6	0	0.668967	-3.832678	-0.416520
64	6	0	0.771955	-2.683576	0.421426
65	6	0	1.273504	-2.795694	1.724788
66	6	0	1.049995	-5.097586	0.050980
67	6	0	1.536181	-5.199877	1.350626
68	6	0	1.648299	-4.061667	2.173013
69	1	0	1.372400	-1.930744	2.368361
70	1	0	2.037761	-4.169774	3.182517
71	1	0	6.912223	-3.208704	-1.615523
72	1	0	7.446795	-1.722544	-0.783324
73	1	0	7.043270	-1.679556	-2.527215
74	1	0	0.965666	-5.966260	-0.596542
75	1	0	1.839231	-6.169941	1.737700
76	1	0	-0.746209	-2.120071	-3.368360
77	1	0	-0.585082	-0.465526	-4.872581
78	1	0	-0.566541	1.705036	-2.259676

Energy

E(RB3LYP) = -2216.87109386 Hartree

Zero point corrected free energy = -2216.318169 Hartree

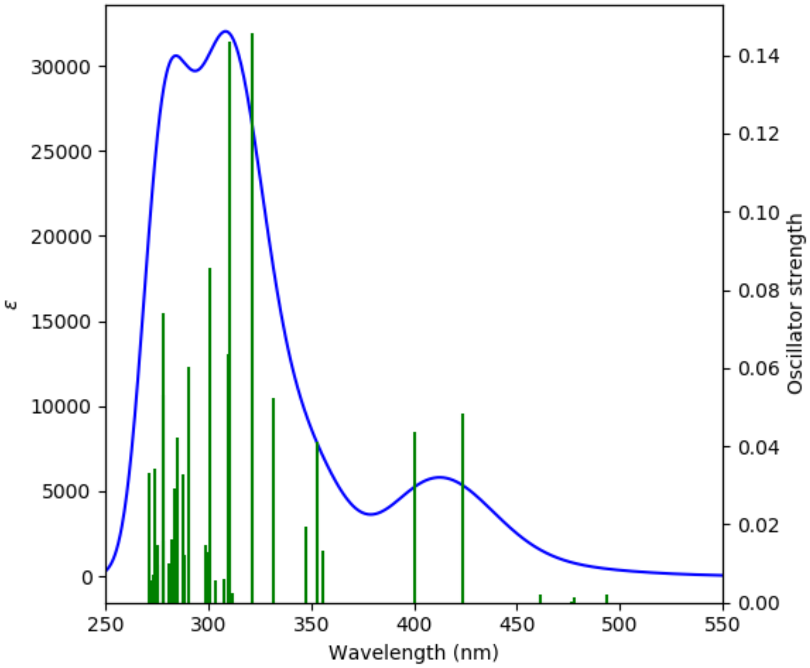

Figure S78. Calculated UV/vis spectrum for complex **4**.

Table S14. Calculated energy levels of ten highly contributing singlet states and first five triplet states for complex **4**.

Spin State	**Transition configurations**	**Excitation energy (eV, nm)**	**Oscillator strength**
S_5	HOMO-2→LUMO (96.5%)	2.9249, 423.89	0.0482
S_6	HOMO-2→LUMO+1 (96.4%)	3.0958, 400.49	0.0438
S_8	HOMO-4→LUMO (68.4%) HOMO-4→LUMO+1 (4.6%) HOMO-3→LUMO (11.1%) HOMO-3→LUMO+1 (11.1%)	3.5130, 352.93	0.0411
S_{10}	HOMO-6→LUMO+1 (3.6%) HOMO-4→LUMO+1 (61.6%)	3.7378, 331.70	0.0523

	HOMO-3→LUMO+1 (25.9%)		
S_{11}	HOMO-7→LUMO (2.9%) HOMO-6→LUMO (2.1%) HOMO-5→LUMO (83.4%) HOMO-3→LUMO (5.3%)	3.8599, 321.21	0.1458
S_{13}	HOMO-7→LUMO (3.2%) HOMO-6→LUMO (70.1%) HOMO-5→LUMO (2.5%) HOMO-5→LUMO+1 (13.7%)	3.9996, 309.99	0.1435
S_{17}	HOMO-7→LUMO (33.2%) HOMO-6→LUMO (2.3%) HOMO-6→LUMO+1 (49.7%) HOMO-5→LUMO+1 (6.3%)	4.1274, 300.39	0.0855
S_{20}	HOMO-7→LUMO+1 (2.5%) HOMO-1→LUMO+4 (10.2%) HOMO-1→LUMO+5 (6.8%) HOMO-1→LUMO+10 (2.1%) HOMO→LUMO+4 (47.2%) HOMO→LUMO+5 (16.7%)	4.2750, 290.02	0.0602
S_{29}	HOMO-9→LUMO (45.8%) HOMO-2→LUMO+2 (3.8%) HOMO-2→LUMO+4 (5.0%) HOMO-2→LUMO+10 (2.7%) HOMO-1→LUMO+4 (2.1%) HOMO-1→LUMO+5 (8.6%)	4.4633, 277.79	0.0739

	HOMO-1→LUMO+10 (2.7%) HOMO→LUMO+5 (3.7%) HOMO→LUMO+6 (8.6%)		
S_{32}	HOMO-10→LUMO+1 (5.1%) HOMO-9→LUMO (2.8%) HOMO-2→LUMO+2 (61.1%) HOMO-2→LUMO+3 (2.3%) HOMO→LUMO+7 (15.6%)	4.5279, 273.82	0.0342
T_1	HOMO-3→LUMO (7.5%) HOMO-2→LUMO (11.5%) HOMO-1→LUMO (12.5%) HOMO→LUMO (63.4%)	2.4595, 504.11	0.0000
T_2	HOMO-3→LUMO (3.4%) HOMO-2→LUMO+1 (8.2%) HOMO-1→LUMO (42.0%) HOMO-1→LUMO+1 (2.5%) HOMO→LUMO (12.7%) HOMO→LUMO+1 (26.1%)	2.5630, 483.74	0.0000
T_3	HOMO-1→LUMO (20.4%) HOMO-1→LUMO+1 (17.5%) HOMO→LUMO+1 (54.9%)	2.5825, 480.10	0.0000
T_4	HOMO-4→LUMO+1 (2.9%) HOMO-3→LUMO+1 (9.7%) HOMO-2→LUMO (7.6%) HOMO-2→LUMO+1 (11.8%) HOMO-1→LUMO (9.6%)	2.6091, 475.19	0.0000

	HOMO-1→LUMO+1 (39.4%) HOMO→LUMO (11.3%)		
T_5	HOMO-5→LUMO (4.0%) HOMO-3→LUMO (6.8%) HOMO-2→LUMO (46.2%) HOMO-1→LUMO (10.9%) HOMO-1→LUMO+1 (13.2%) HOMO→LUMO (9.8%)	2.6573, 466.58	0.0000

Table S15. Calculated MO energies of orbitals involved in transitions for **4**.

Orbital	**Energy/ eV**		**Orbital**	**Energy/ eV**
LUMO+10	1.02		HOMO	-4.45
LUMO+9	0.86		HOMO-1	-4.59
LUMO+8	0.63		HOMO-2	-5.09
LUMO+7	0.57		HOMO-3	-5.57
LUMO+6	0.52		HOMO-4	-5.66
LUMO+5	0.40		HOMO-5	-5.83
LUMO+4	0.32		HOMO-6	-5.93
LUMO+3	0.08		HOMO-7	-6.17
LUMO+2	0.03		HOMO-8	-6.33
LUMO+1	-1.36		HOMO-9	-6.43
LUMO	-1.45		HOMO-10	-6.45

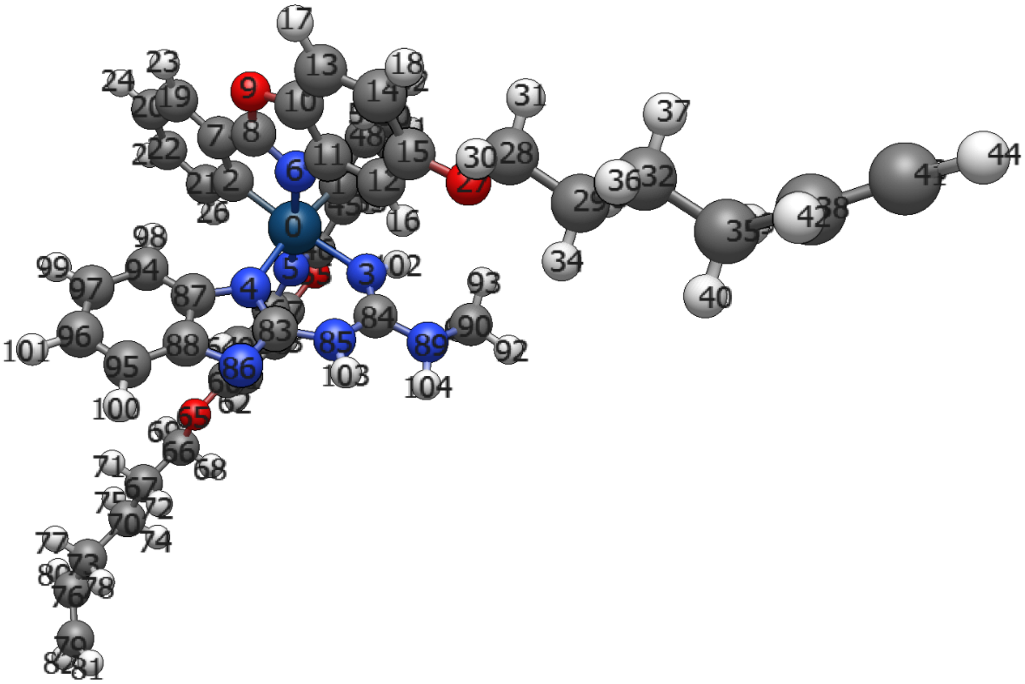

Figure S79. Optimised geometry model used for complex **5**. TD-DFT inputs and energy calculations were based upon this optimised input model.

Table S16. Cartesian coordinates for optimised compound **5**.

Center Number	Atomic Number	Atomic Type	Coordinates (Angstroms)		
			X	Y	Z
0	77	0	-0.113038	-1.298130	-0.125255
1	6	0	-0.715352	-2.860251	-1.300991
2	6	0	0.502000	-2.638747	1.280402
3	7	0	-0.909412	0.062655	-1.633327
4	7	0	0.568745	0.535561	0.889733
5	7	0	1.555798	-1.521072	-1.337748
6	7	0	-1.765204	-1.307132	1.135519
7	6	0	-0.416493	-2.863145	2.347697
8	6	0	-1.607009	-2.083733	2.196478
9	8	0	-2.656493	-2.060227	3.048344
10	6	0	-3.562244	-1.185008	2.474081
11	6	0	-3.015296	-0.706458	1.272764
12	6	0	-3.729138	0.187300	0.482510
13	6	0	-4.803227	-0.805381	2.942133
14	6	0	-5.523986	0.099367	2.152600

15	6	0	-4.993614	0.587175	0.940572
16	1	0	-3.341458	0.572276	-0.450879
17	1	0	-5.203776	-1.185806	3.875373
18	1	0	-6.501315	0.419944	2.490818
19	6	0	-0.173344	-3.753808	3.405634
20	6	0	1.013995	-4.472554	3.416880
21	6	0	1.682951	-3.400592	1.327879
22	6	0	1.933167	-4.293950	2.371282
23	1	0	-0.907866	-3.873578	4.197611
24	1	0	1.228182	-5.167578	4.223582
25	1	0	2.862048	-4.860437	2.377363
26	1	0	2.431424	-3.284457	0.548836
27	8	0	-5.649198	1.467077	0.126093
28	6	0	-6.926271	1.961038	0.521736
29	6	0	-7.398276	2.935173	-0.550052
30	1	0	-6.848971	2.464334	1.496870
31	1	0	-7.636630	1.127520	0.628050
32	6	0	-8.772540	3.536922	-0.230397
33	1	0	-7.431119	2.408469	-1.512615
34	1	0	-6.651030	3.732764	-0.651945
35	6	0	-9.258138	4.521546	-1.311920
36	1	0	-8.731801	4.055746	0.738337
37	1	0	-9.515961	2.735782	-0.118991
38	6	0	-10.585059	5.148000	-0.978025
39	1	0	-9.325633	4.004114	-2.278033
40	1	0	-8.499908	5.311021	-1.430647
41	6	0	-11.697912	5.026101	-1.702918
42	1	0	-10.614047	5.734657	-0.057689
43	1	0	-11.717790	4.450669	-2.626697
44	1	0	-12.630457	5.498681	-1.406060
45	6	0	0.214225	-3.241782	-2.314489
46	6	0	1.419820	-2.463383	-2.254526
47	6	0	-0.032365	-4.261719	-3.247131
48	6	0	-1.922742	-3.578529	-1.284935
49	6	0	-1.241796	-4.943040	-3.190635
50	6	0	-2.180579	-4.595729	-2.208005
51	1	0	-1.457221	-5.737935	-3.898998
52	1	0	-3.126454	-5.131598	-2.162916
53	1	0	0.715261	-4.510468	-3.995980
54	1	0	-2.677714	-3.342938	-0.539371
55	8	0	2.493879	-2.593011	-3.065640
56	6	0	2.820321	-0.962119	-1.528275
57	6	0	3.396728	-1.641597	-2.613536
58	6	0	4.659704	-1.359606	-3.092929
59	6	0	3.514173	0.046107	-0.869220
60	6	0	4.801049	0.348151	-1.342831

```
   61         6           0        5.364330   -0.342143   -2.437959
   62         1           0        6.359091   -0.093130   -2.785904
   63         1           0        5.089192   -1.897134   -3.931323
   64         1           0        3.101811    0.573694   -0.018078
   65         8           0        5.442283    1.343403   -0.668646
   66         6           0        6.768814    1.704411   -1.042842
   67         6           0        7.225963    2.812955   -0.103470
   68         1           0        6.785561    2.048975   -2.088005
   69         1           0        7.432585    0.830068   -0.965874
   70         6           0        8.652177    3.287548   -0.408871
   71         1           0        7.160677    2.445807    0.928478
   72         1           0        6.522093    3.651045   -0.183064
   73         6           0        9.118533    4.414573    0.533152
   74         1           0        8.716074    3.642520   -1.446836
   75         1           0        9.348774    2.439952   -0.330430
   76         6           0       10.533857    4.850342    0.266108
   77         1           0        9.034298    4.058443    1.571358
   78         1           0        8.442190    5.274514    0.441901
   79         6           0       10.905521    6.076433   -0.104767
   80         1           0       11.297366    4.078370    0.382024
   81         1           0       10.180769    6.878315   -0.233422
   82         1           0       11.946407    6.329460   -0.288701
   83         6           0        0.212384    1.791840    0.522026
   84         6           0       -0.971693    1.362980   -1.653600
   85         7           0       -0.534372    2.127431   -0.621682
   86         7           0        0.592396    2.805136    1.287335
   87         6           0        1.292782    0.764319    2.063508
   88         6           0        1.291296    2.171593    2.293582
   89         7           0       -1.549886    2.088482   -2.686357
   90         6           0       -2.006989    1.431028   -3.899986
   91         1           0       -1.203425    0.919294   -4.451779
   92         1           0       -2.448605    2.186689   -4.553557
   93         1           0       -2.788030    0.702295   -3.660472
   94         6           0        1.964819   -0.098793    2.938990
   95         6           0        1.945939    2.717424    3.405954
   96         6           0        2.601004    1.850540    4.275000
   97         6           0        2.611117    0.461627    4.040049
   98         1           0        1.989204   -1.167925    2.770956
   99         1           0        3.136167   -0.192272    4.732317
  100         1           0        1.936219    3.791480    3.571312
  101         1           0        3.116792    2.248415    5.145864
  102         1           0       -1.194875   -0.378822   -2.499347
  103         1           0       -0.761399    3.112901   -0.626252
  104         1           0       -1.138675    3.001978   -2.830354
 ---------------------------------------------------------------------
```

Energy

E(RB3LYP) = -2607.52600633 Hartree

Zero point corrected free energy = -2606.747417 Hartree

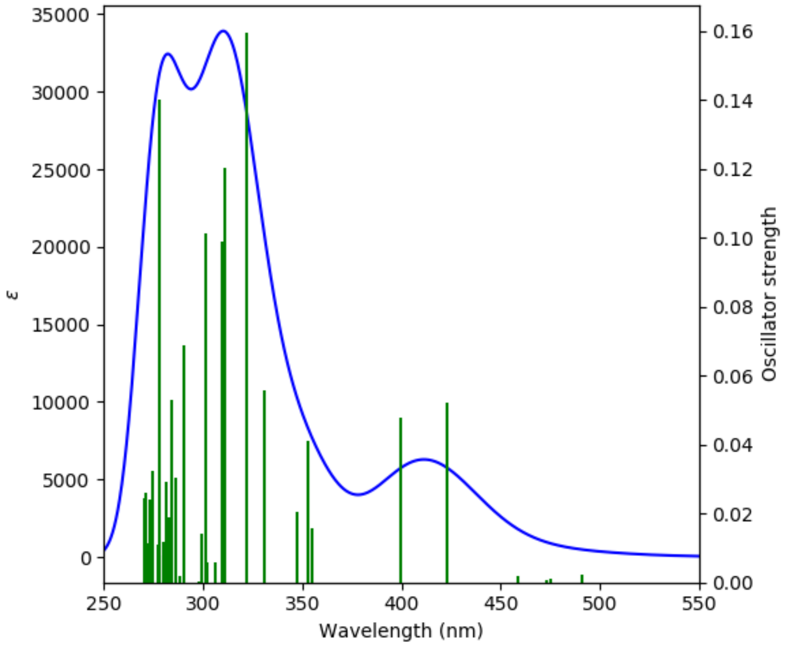

Figure S80. Calculated UV/vis spectrum for complex **5**.

Table S17. Calculated energy levels of ten highly contributing singlet states and first five triplet states for complex **5**.

Spin State	**Transition configurations**	**Excitation energy (eV, nm)**	**Oscillator strength**
S_5	HOMO-2→LUMO (96.4%)	2.9305, 423.08	0.0521
S_6	HOMO-2→LUMO+1 (96.3%)	3.1042, 399.41	0.0478
S_8	HOMO-4→LUMO (72.3%) HOMO-4→LUMO+1 (3.5%) HOMO-3→LUMO (9.3%) HOMO-3→LUMO+1 (10.2%)	3.5110, 353.13	0.0409

S_{10}	HOMO-6→LUMO+1 (3.8%) HOMO-5→LUMO+1 (2.4%) HOMO-4→LUMO+1 (62.2%) HOMO-3→LUMO+1 (24.3%)	3.7447, 331.09	0.0559
S_{11}	HOMO-7→LUMO (2.6%) HOMO-5→LUMO (83.6%) HOMO-3→LUMO (5.7%)	3.8519, 321.88	0.1596
S_{12}	HOMO-7→LUMO (3.4%) HOMO-6→LUMO (76.2%) HOMO-5→LUMO (2.1%) HOMO-5→LUMO+1 (8.0%) HOMO→LUMO+2 (2.4%)	3.9878, 310.91	0.1203
S_{14}	HOMO-7→LUMO+1 (4.2%) HOMO-6→LUMO (5.6%) HOMO-6→LUMO+1 (9.4%) HOMO-5→LUMO+1 (60.7%) HOMO-3→LUMO+1 (6.1%) HOMO→LUMO+2 (10.0%)	4.0043, 309.63	0.0990
S_{17}	HOMO-7→LUMO (20.1%) HOMO-6→LUMO+1 (60.1%) HOMO-5→LUMO+1 (9.9%)	4.1182, 301.06	0.1011
S_{23}	HOMO-3→LUMO+12 (2.4%) HOMO-1→LUMO+4 (38.2%) HOMO-1→LUMO+11 (2.5%) HOMO-1→LUMO+12 (9.7%)	4.3591, 284.42	0.0531

	HOMO→LUMO+4 (4.1%) HOMO→LUMO+5 (23.1%)		
S_{28}	HOMO-10→LUMO (15.8%) HOMO-9→LUMO (50.8%) HOMO-2→LUMO+2 (3.6%) HOMO-2→LUMO+4 (9.9%) HOMO-1→LUMO+5 (4.2%)	4.4603, 277.97	0.1400
T_1	HOMO-3→LUMO (8.6%) HOMO-2→LUMO (12.4%) HOMO-1→LUMO (11.5%) HOMO→LUMO (62.0%)	2.4707, 501.82	0.0000
T_2	HOMO-3→LUMO (3.0%) HOMO-3→LUMO+1 (3.0%) HOMO-2→LUMO+1 (10.0%) HOMO-1→LUMO (45.8%) HOMO-1→LUMO+1 (8.3%) HOMO→LUMO (10.7%) HOMO→LUMO+1 (14.0%)	2.5741, 481.66	0.0000
T_3	HOMO-2→LUMO (3.7%) HOMO-1→LUMO (8.8%) HOMO-1→LUMO+1 (18.0%) HOMO→’LUMO+1 (64.0%)	2.5989, 477.06	0.0000
T_4	HOMO-4→LUMO+1 (2.7%) HOMO-3→LUMO+1 (8.4%) HOMO-2→LUMO (6.1%) HOMO-2→LUMO+1 (13.9%) HOMO-1→LUMO (19.7%)	2.6171, 473.74	0.0000

	HOMO-1→LUMO+1 (25.7%) HOMO→LUMO (14.5%) HOMO→LUMO+1 (3.6%)		
T_5	HOMO-5→LUMO (3.7%) HOMO-3→LUMO (7.3%) HOMO-2→LUMO (43.2%) HOMO-1→LUMO (9.5%) HOMO-1→LUMO+1 (13.2%) HOMO→LUMO (11.7%) HOMO→LUMO+1 (2.9%)	2.6610, 465.94	0.0000

Table S18. Calculated MO energies of orbitals involved in transitions for **5**.

Orbital	**Energy/ eV**		**Orbital**	**Energy/ eV**
LUMO+12	1.02		HOMO	-4.45
LUMO+11	0.86		HOMO-1	-4.59
LUMO+10	0.66		HOMO-2	-5.09
LUMO+9	0.65		HOMO-3	-5.56
LUMO+8	0.59		HOMO-4	-5.65
LUMO+7	0.53		HOMO-5	-5.81
LUMO+6	0.49		HOMO-6	-5.90
LUMO+5	0.41		HOMO-7	-6.15
LUMO+4	0.33		HOMO-8	-6.34
LUMO+3	0.10		HOMO-9	-6.41

LUMO+2	0.05		HOMO-10	-6.42
LUMO+1	-1.29		HOMO-11	-6.83
LUMO	-1.44		HOMO-12	-6.84

SXI: Bibliography

[1]- Brouwer, A. M.; Standards for photoluminescence quantum yield measurements in solution (IUPAC technical report). *Pure and Applied Chemistry* 2011, *83* (**12**), 2213–2228.

[2]- Gaussian 16, Revision C.01, M. J. Frisch, G. W. Trucks, H. B. Schlegel, G. E. Scuseria, M. A. Robb, J. R. Cheeseman, G. Scalmani, V. Barone, G. A. Petersson, H. Nakatsuji, X. Li, M. Caricato, A. V. Marenich, J. Bloino, B. G. Janesko, R. Gomperts, B. Mennucci, H. P. Hratchian, J. V. Ortiz, A. F. Izmaylov, J. L. Sonnenberg, D. Williams-Young, F. Ding, F. Lipparini, F. Egidi, J. Goings, B. Peng, A. Petrone, T. Henderson, D. Ranasinghe, V. G. Zakrzewski, J. Gao, N. Rega, G. Zheng, W. Liang, M. Hada, M. Ehara, K. Toyota, R. Fukuda, J. Hasegawa, M. Ishida, T. Nakajima, Y. Honda, O. Kitao, H. Nakai, T. Vreven, K. Throssell, J. A. Montgomery, Jr., J. E. Peralta, F. Ogliaro, M. J. Bearpark, J. J. Heyd, E. N. Brothers, K. N. Kudin, V. N. Staroverov, T. A. Keith, R. Kobayashi, J. Normand, K. Raghavachari, A. P. Rendell, J. C. Burant, S. S. Iyengar, J. Tomasi, M. Cossi, J. M. Millam, M. Klene, C. Adamo, R. Cammi, J. W. Ochterski, R. L. Martin, K. Morokuma, O. Farkas, J. B. Foresman, and D. J. Fox, Gaussian, Inc., Wallingford CT, 2016.

[3]- Y. Yang, M. N. Weaver and K. M. Merz, *The Journal of Physical Chemistry A*, 2009, **113**, 9843–9851.

[4]- J. Tirado-Rives and W. L. Jorgensen, *Journal of Chemical Theory and Computation*, 2008, **4**, 297–306.

[5]- M. D. Hanwell, D. E. Curtis, D. C. Lonie, T. Vandermeersch, E. Zurek and G. R. Hutchison, *Journal of Cheminformatics* **17** (2012)

[6]- N. M. O'boyle, A. L. Tenderholt and K. M. Langner, *Journal of Computational Chemistry*, 2008, **29**, 839–845.

[7]- B. Balónová, D. R. Martir, E. R. Clark, H. J. Shepherd, E. Zysman-Colman and B. A. Blight, *Inorganic Chemistry*, 2018, **57**, 8581–8587.

[8]- B Balónová, T. H. Jones, A. E. True, S. M. Hetherington and B. A. Blight, *RSC Advances*, 2024, **14**, 34288–34297.

[9]- M. Nonoyama, *Bulletin of the Chemical Society of Japan*, 1974, **47**, 767–768.

[10]- D. Escudero, *ChemPhotoChem*, 2019, **3**, 697–701.

[11]- K. Tsuchiya, E. Ito, S. Yagai, A. Kitamura and T. Karatsu, *European Journal of Inorganic Chemistry*, 2009, **2009**, 2104–2109.

[12]- Y. Zheng, A. S. Batsanov, R. M. Edkins, A. Beeby and M. R. Bryce, *Inorganic Chemistry*, 2011, **51**, 290–297.